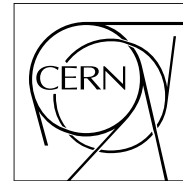


The Compact Muon Solenoid Experiment  
**Analysis Note**

The content of this note is intended for CMS internal use and distribution only



**12 November 2013 (v4, 20 January 2014)**

# Search for a BSM resonance decaying to W vector bosons in the semileptonic final state (update of EXO-12-021 using 22Jan2013 rereco)

C. Bernardes, A. Bonato, A. Carvalho, A. Hinzmann, Q. Li, S. Liu, M. Mozer, P. Mercadante, S. Novaes, M. Pierini, F. Santanastasio, A. Spiezia, T. Tomei, Z. Xu, Nhan Viet Tran, R. Gerosa, P. Govoni

## Abstract

A search for new particles decaying to two W bosons with subsequent decay to a final state containing two leptons and two quarks, X to WW to lν qqbar, is presented. Results are based on data corresponding to an integrated luminosity of 19.7 fb<sup>-1</sup> of proton-proton collisions at sqrt(s)=8 TeV and collected with the CMS detector at the CERN LHC. Jet sub-structure techniques are exploited for separating the signal from the SM background when the boost of the W causes the two quarks to merge into the same jet reconstructed in the detector. A model-independent statistical interpretation is applied to the selected dataset, setting limits on the cross section of a narrow resonance decaying to WW (or WZ) as a function of its mass.

# CMS Draft Analysis Note

*The content of this note is intended for CMS internal use and distribution only*

2014/01/20

Head Id: 223654

<https://svn.cern.ch/repos/tdr2/notes/AN-13-381/trunk/AN-13-381.tex> Archive Id: 219546:223654

Archive Date: 2014/01/17

Archive Tag:

## Search for a BSM resonance decaying to W vector bosons in the semileptonic final state (update of EXO-12-021 using 22Jan2013 rereco)

C. Bernardes<sup>7</sup>, A. Bonato<sup>1</sup>, A. Hinzmann<sup>1</sup>, Q. Li<sup>5</sup>, S. Liu<sup>5</sup>, Z. Xu<sup>5</sup>, M. Mozer<sup>4</sup>, P. Mercadante<sup>7</sup>,  
S. Novaes<sup>6</sup>, M. Pierini<sup>1</sup>, F. Santanastasio<sup>1</sup>, A. Spiezia<sup>8</sup>, T. Tomei<sup>6</sup>, Nhan Viet Tran<sup>2</sup>, Raffaele  
Gerosa<sup>3</sup>, and Pietro Govoni<sup>3</sup>

<sup>1</sup> CERN

<sup>2</sup> Fermilab National Laboratory

<sup>3</sup> Universit di Milano Bicocca

<sup>4</sup> KIT

<sup>5</sup> Peking University

<sup>6</sup> SPRACE-UNESP

<sup>7</sup> SPRACE-UFABC

<sup>8</sup> Universit di Perugia

### Abstract

A search for new particles decaying to two W bosons with subsequent decay to a final state containing two leptons and two quarks,  $X \rightarrow WW \rightarrow q\bar{q}\ell\nu$ , is presented. Results are based on data corresponding to an integrated luminosity of  $19.7 \text{ fb}^{-1}$  of proton-proton collisions at  $\sqrt{s} = 8 \text{ TeV}$  and collected with the CMS detector at the CERN LHC. Jet sub-structure techniques are exploited for separating the signal from the SM background when the boost of the W causes the two quarks to merge into the same jet reconstructed in the detector. A model-independent statistical interpretation is applied to the selected dataset, setting limits on the cross section of a narrow resonance decaying to WW as a function of its mass.

This box is only visible in draft mode. Please make sure the values below make sense.

PDFAuthor:

EXO-VV analysis team

PDFTitle:

Search for a BSM resonance decaying to vector bosons in the semileptonic final state Xto WWto "(lv+)"(qbarq")

PDFSubject:

CMS

PDFKeywords:

CMS, physics, exotica, graviton, boosted jets

Please also verify that the abstract does not use any user defined symbols

DRAFT

## 1 Contents

2	1	Preface . . . . .	2
3	2	Monte Carlo Samples and Data Sets . . . . .	2
4	2.1	Signal MC . . . . .	2
5	2.2	Background MC and cross-sections . . . . .	7
6	2.3	Data samples . . . . .	8
7	3	Event Reconstruction and Selection . . . . .	9
8	3.1	Control plots in the hadronic W mass sideband . . . . .	11
9	3.2	Data vs MC comparison in signal region . . . . .	18
10	4	Signal modeling: $m_{WW}$ shapes and efficiency . . . . .	22
11	4.1	Parametrization of the $m_{WW}$ signal shape (narrow resonances) . . . . .	22
12	4.2	Parametrization of the $m_{WW}$ signal shape (wide resonances) . . . . .	23
13	4.3	Signal efficiency . . . . .	25
14	5	Background estimate . . . . .	28
15	5.1	Main Method - $\alpha$ Method . . . . .	28
16	5.2	Cross-Check Method - $m_{WW}$ Smoothness Test . . . . .	39
17	6	Systematic Uncertainties . . . . .	40
18	7	Results . . . . .	41
19	7.1	Limits - Main Method $\alpha$ . . . . .	41
20	7.2	Limits - Cross-Check Method ( $m_{WW}$ smoothness test) . . . . .	43
21	7.3	Limits - Comparison between two methods . . . . .	45
22	7.4	Statistical combination with other analyses . . . . .	45
23	8	Model-independent Analysis . . . . .	51
24	8.1	Simplified Limits . . . . .	51
25	8.2	Wide Resonances . . . . .	52
26	8.3	Parametrized Selection Efficiencies . . . . .	56
27	8.4	Summary of Paramterized Efficiencies and Related Uncertainties . . . . .	66
28	8.5	Results . . . . .	66
29	9	Conclusions . . . . .	69

## 30 1 Preface

31 This note is an update of the EXO-12-021 [1] analysis (search for WW resonances in semi-  
 32 leptonic final states with electrons and muons) using the legacy 8 TeV 22Jan2013 rereco dataset.

33 The analysis was already approved in August 2013 using a combination of prompt reco and  
 34 rereco datasets produced in 2012. The results of this search are combined with those from a  
 35 complementary search for ZZ resonances in the semi-leptonic final state, EXO-12-022 [2], also  
 36 approved in August 2013. Both searches are described in the EXO-13-009 paper. The EXO-13-  
 37 009 also includes a statistical combination of the results with another complementary search  
 38 for VV resonances in the dijet final state, EXO-12-024 [3], approved in Spring 2013.

39 The approved EXO-12-021 search was performed by two different groups with different anal-  
 40 ysis tools working in close contact since January 2013 (i.e. group 1 = the authors of [4], and  
 41 group 2 = the authors of [5]). For this analysis update, and therefore for the final results in-  
 42 cluded in the EXO-13-009 paper, we proceed in the following way:

- 43 • use group 1 root-trees
- 44 • use  $\alpha$  method for main background estimation (the group 2 implementation)
- 45 • perform cross-check of the  $\alpha$  method using a smoothness test to  $m_{WW}$  distribution (a  
 46 la “dijet” fit), using group 1 implementation.

47 In this note, we do not describe the analysis methods in detail. For this we refer the reader to  
 48 the documentation provided for the approved EXO-12-021 PAS [1, 4, 5]. We highlight instead  
 49 the main differences with respect to the approved analysis, and show the new results that will  
 50 be included in the EXO-13-009 combined paper.

## 51 2 Monte Carlo Samples and Data Sets

### 52 2.1 Signal MC

53 The signal samples used in this analysis are reported in Tables 1, 2, 3, and 4 and divided in  
 54 three sets:

- 55 • Bulk graviton [6] decaying to a pair W bosons. Simulated samples were privately  
 56 produced using the full machinery available in CMSSW, following the conditions  
 57 used for the official Summer12 campaign. More details on the generation tools and  
 58 the validation can be found in Section 3.1 of [4]. For this update the samples were  
 59 reprocessed with inclusive W decays (in order to be useful also for the EXO-12-024  
 60 analysis [3] analysis). Due to a bug in the generator, the branching ratios of the  
 61  $W \rightarrow l\nu$  decays compared to  $W \rightarrow q\bar{q}'$  decays are wrong. We filter therefore the  
 62 events at generator level to select only semi-leptonic final states and we use these  
 63 samples to estimate the signal efficiency and signal  $m_{WW}$  shapes.  $W \rightarrow \tau\nu$  decays  
 64 were missing in the previous iteration of the analysis while they contribute ( 10%  
 65 of total signal efficiency) to the electron+neutrino+jet and muon+neutrino+jet final  
 66 states considered in this search. We generate both narrow and wide resonance sam-  
 67 ples with different intrinsic widths.
- 68 • RS1 graviton [7, 8] decaying to a pair W bosons. Half of these samples are pro-  
 69 duced in the official Summer12 campaign. The others using the same private pro-  
 70 duction discussed above. They are used mainly to calculate efficiencies and perform  
 71 cross-checks in the contest of the model-independent interpretation of the results  
 72 discussed in Section 8

- <sup>73</sup>    •  $W'$  decaying to  $WZ$ . They are used mainly to calculate efficiencies and perform  
<sup>74</sup>    cross-checks in the context of the model-independent interpretation of the results  
<sup>75</sup>    discussed in Section 8

DRAFT

Table 1: **The bulk graviton signal cross section should be multiplied by a factor 1/4, due to a bug recently found in the theoretical calculation. More details can be found in Section 3 of [9]. We don't plan to update this AN. The values in the EXO-13-009 will be correct.** Narrow Bulk Graviton to WW signal MC samples. The W decays are inclusive but relative branching ratios of hadronic and leptonic decays are wrong as described in the text. In the analysis we select at gen level only the semi-leptonic final states. The number of events and the cross-sections quoted are reported for the semi-leptonic decay chain  $pp \rightarrow X \rightarrow WW \rightarrow \ell\nu q\bar{q}$ , with  $\ell = e, \mu, \tau$ . The  $\tilde{k}$  parameter is shorthand for  $k/M_{Pl}$ . The dataset naming convention is sometimes weird and confusing. Still the information in the table is correct. The samples can be found at *cms dbs ph analysis 01* as well as in global DBS (in the latter case the dataset name is slightly different, i.e. for example need to change “shuai” with “StoreResults” since these datasets were promoted from local DBS to global DBS).

Sample	$N$	$\sigma$ [pb]	$\tilde{k}$	$M_G$ [TeV]
<b>Bulk graviton (narrow resonance)</b>				
/BulkG_WW_inclusive_c0p2_M600_GENSIM/shuai-BulkG_WW_inclusive_c0p2_M600_AODSIM-2c74483358b1f8805e5601fc325d256c/USER	11854	2.292e-02	0.2	0.6
/BulkG_WW_inclusive_c0p2_M700_GENSIM/shuai-BulkG_WW_inclusive_c0p2_M700_AODSIM-2c74483358b1f8805e5601fc325d256c/USER	12164	8.362e-03	0.2	0.7
/BulkG_WW_inclusive_c0p2_M800_GENSIM/shuai-BulkG_WW_inclusive_c0p2_M800_AODSIM-2c74483358b1f8805e5601fc325d256c/USER	11998	3.479e-03	0.2	0.8
/BulkG_WW_inclusive_c0p2_M900_GENSIM/shuai-BulkG_WW_inclusive_c0p2_M900_AODSIM-2c74483358b1f8805e5601fc325d256c/USER	11940	1.600e-03	0.2	0.9
/BulkG_WW_jjjj_c0p2_M1000_JHU_qili-BulkG_WW_jjjj_c0p2_M1000_JHU-AODSIM-c8f8ed334db8a7d6f56c62266b1dfa5b/USER	11896	7.806e-04	0.2	1.0
/BulkG_WW_inclusive_c0p2_M1100_GENSIM/shuai-BulkG_WW_inclusive_c0p2_M1100_AODSIM-2c74483358b1f8805e5601fc325d256c/USER	11933	4.038e-04	0.2	1.1
/BulkG_WW_inclusive_c0p2_M1200_GENSIM/shuai-BulkG_WW_inclusive_c0p2_M1200_AODSIM-2c74483358b1f8805e5601fc325d256c/USER	12020	2.167e-04	0.2	1.2
/BulkG_WW_inclusive_c0p2_M1300_GENSIM/shuai-BulkG_WW_inclusive_c0p2_M1300_AODSIM-2c74483358b1f8805e5601fc325d256c/USER	12099	1.206e-04	0.2	1.3
/BulkG_WW_inclusive_c0p2_M1400_GENSIM/shuai-BulkG_WW_inclusive_c0p2_M1400_AODSIM-2c74483358b1f8805e5601fc325d256c/USER	12048	6.907e-05	0.2	1.4
/BulkG_WW_jjjj_c0p2_M1500_JHU_qili-BulkG_WW_jjjj_c0p2_M1500_JHU-AODSIM-c8f8ed334db8a7d6f56c62266b1dfa5b/USER	11071	4.051e-05	0.2	1.5
/BulkG_WW_inclusive_c0p2_M1600_GENSIM/shuai-BulkG_WW_inclusive_c0p2_M1600_AODSIM-2c74483358b1f8805e5601fc325d256c/USER	11902	2.407e-05	0.2	1.6
/BulkG_WW_inclusive_c0p2_M1700_GENSIM/shuai-BulkG_WW_inclusive_c0p2_M1700_AODSIM-2c74483358b1f8805e5601fc325d256c/USER	12129	1.461e-05	0.2	1.7
/BulkG_WW_jjjj_c0p2_M1800_JHU_qili-BulkG_WW_jjjj_c0p2_M1800_JHU-AODSIM-c8f8ed334db8a7d6f56c62266b1dfa5b/USER	8776	8.961e-06	0.2	1.8
/BulkG_WW_jjjj_c0p2_M1900_JHU_qili-BulkG_WW_jjjj_c0p2_M1900_JHU-AODSIM-c8f8ed334db8a7d6f56c62266b1dfa5b/USER	11380	5.598e-06	0.2	1.9
/BulkG_WW_jjjj_c0p2_M2000_JHU_qili-BulkG_WW_jjjj_c0p2_M2000_JHU-AODSIM-c8f8ed334db8a7d6f56c62266b1dfa5b/USER	11805	3.522e-06	0.2	2.0
/BulkG_WW_inclusive_c0p2_M1500_GENSIM/dyang-BulkG_WW_inclusive_c0p2_M2100_AODSIM-2c74483358b1f8805e5601fc325d256c/USER	12081	2.225e-06	0.2	2.1
/BulkG_WW_jjjj_c0p2_M2200_JHU_qili-BulkG_WW_jjjj_c0p2_M2200_JHU-AODSIM-c8f8ed334db8a7d6f56c62266b1dfa5b/USER	11688	1.435e-06	0.2	2.2
/BulkG_WW_inclusive_c0p2_M2300_GENSIM/shuai-BulkG_WW_inclusive_c0p2_M2300_AODSIM-2c74483358b1f8805e5601fc325d256c/USER	11947	9.213e-07	0.2	2.3
/BulkG_WW_inclusive_c0p2_M2400_GENSIM/shuai-BulkG_WW_inclusive_c0p2_M2400_AODSIM-2c74483358b1f8805e5601fc325d256c/USER	12055	5.969e-07	0.2	2.4
/BulkG_WW_jjjj_c0p2_M2500_JHU_qili-BulkG_WW_jjjj_c0p2_M2500_JHU-AODSIM-c8f8ed334db8a7d6f56c62266b1dfa5b/USER	11059	3.895e-07	0.2	2.5

Table 2: Wide Bulk Graviton to WW signal MC samples. The W decays are inclusive but relative branching ratios of hadronic and leptonic decays are wrong as described in the text. In the analysis we select at gen level only the semi-leptonic final states. The number of events are reported for the semi-leptonic decay chain  $pp \rightarrow X \rightarrow WW \rightarrow \ell\nu q\bar{q}'$ , with  $\ell = e, \mu, \tau$ . We report also the mass and the intrinsic width ( $\Gamma$ ) of the resonance. The samples can be found at `cms_db/ph_analysis_01` as well as in global DBS (in the latter case the dataset name is slightly different, i.e. for example need to change “shuai” with “StoreResults” since these datasets were promoted from local DBS to global DBS).

Sample	$N$	$\Gamma$ [GeV] ( $\Gamma/M_G$ [%])	$M_G$ [GeV]
<b>Bulk graviton (wide resonance)</b>			
/BulkG_WW_inclusive_M1000_W50.GENSIM/shuai-BulkG_WW_inclusive_M1000_W50_AODSIM- 2c74483358b1f8805e5601fc325d256c/USER	11704	50 (5)	1000
/BulkG_WW_inclusive_M1000_W150.GENSIM/shuai-BulkG_WW_inclusive_M1000_W150_AODSIM- 2c74483358b1f8805e5601fc325d256c/USER	>10697	150 (15)	1000
/BulkG_WW_inclusive_M1000_W300.GENSIM/shuai-BulkG_WW_inclusive_M1000_W300_AODSIM- 2c74483358b1f8805e5601fc325d256c/USER	11722	300 (30)	1000
/BulkG_WW_inclusive_M1500_W75.GENSIM/shuai-BulkG_WW_inclusive_M1500_W75_AODSIM- 2c74483358b1f8805e5601fc325d256c/USER	11979	75 (5)	1500
/BulkG_WW_inclusive_M1500_W225.GENSIM/shuai-BulkG_WW_inclusive_M1500_W225_AODSIM- 2c74483358b1f8805e5601fc325d256c/USER	11728	225 (15)	1500
/BulkG_WW_inclusive_M1500_W450.GENSIM/shuai-BulkG_WW_inclusive_M1500_W450_AODSIM- 2c74483358b1f8805e5601fc325d256c/USER	11776	450 (30)	1500
/BulkG_WW_inclusive_M2100_W105.GENSIM/shuai-BulkG_WW_inclusive_M2100_W105_AODSIM- 2c74483358b1f8805e5601fc325d256c/USER	11993	105 (5)	2100
/BulkG_WW_inclusive_M2100_W315.GENSIM/shuai-BulkG_WW_inclusive_M2100_W315_AODSIM- 2c74483358b1f8805e5601fc325d256c/USER	11979	315 (15)	2100
/BulkG_WW_inclusive_M2100_W630.GENSIM/shuai-BulkG_WW_inclusive_M2100_W630_AODSIM- 2c74483358b1f8805e5601fc325d256c/USER	>11082	630 (30)	2100

Table 3: RS1 Graviton to WW signal MC samples. Only semi-leptonic decays are considered. The number of events quoted are reported for the semi-leptonic decay chain  $pp \rightarrow X \rightarrow WW \rightarrow \ell\nu q\bar{q}'$ , with  $\ell = e, \mu, \tau$ . The privately produced samples were generated as  $pp \rightarrow X \rightarrow WW \rightarrow \ell\nu q\bar{q}'$ , with  $\ell = e, \mu$  (no taus). The  $\tilde{k}$  parameter is shorthand for  $k/M_{Pl}$ . The samples can be found at `cms dbs ph analysis 01` or `02` (private samples) and in global DBS (official ones).

Sample	$N$	$\tilde{k}$	$M_G$ [TeV]
<b>RS1 graviton Pythia (official production)</b>			
/RSGravitonToWWToLNuJJ_kMpl005_M-750_TuneZ2star_8TeV-pythia6-tauola/ Summer12_DR53X-PU_S10_START53_V7A-v1/AODSIM	60192	0.05	0.75
/RSGravitonToWWToLNuJJ_kMpl005_M-1000_TuneZ2star_8TeV-pythia6-tauola/ Summer12_DR53X-PU_S10_START53_V7A-v1/AODSIM	60192	0.05	1.0
/RSGravitonToWWToLNuJJ_kMpl005_M-1250_TuneZ2star_8TeV-pythia6-tauola/ Summer12_DR53X-PU_S10_START53_V7A-v1/AODSIM	60192	0.05	1.25
/RSGravitonToWWToLNuJJ_kMpl005_M-1500_TuneZ2star_8TeV-pythia6-tauola/ Summer12_DR53X-PU_S10_START53_V7A-v1/AODSIM	60192	0.05	1.5
/RSGravitonToWWToLNuJJ_kMpl005_M-1750_TuneZ2star_8TeV-pythia6-tauola/ Summer12_DR53X-PU_S10_START53_V7A-v1/AODSIM	60192	0.05	1.75
/RSGravitonToWWToLNuJJ_kMpl005_M-2000_TuneZ2star_8TeV-pythia6-tauola/ Summer12_DR53X-PU_S10_START53_V7A-v1/AODSIM	60192	0.05	2.0
<b>RS1 graviton Madgraph (private production)</b>			
/RSGraviton_WWlvjj_kMpl02_M-600_TuneZ2star_8TeV-MG_qili-RSWW_600_02_AODSIM- c8f8ed334db8a7d6f56c62266b1dfa5b/USER	31875 (processed 27456)	0.2	0.6
/RSGraviton_WWlvjj_kMpl-005_M-1000_TuneZ2star_8TeV-MG_qili-RSWW_1000_005_AODSIM- c8f8ed334db8a7d6f56c62266b1dfa5b/USER	35421 (processed 27705)	0.05	1.0
/RSGraviton_WWlvjj_kMpl005_M-1000_TuneZ2star_8TeV-MG_qili-RSWW_1000_02_AODSIM- c8f8ed334db8a7d6f56c62266b1dfa5b/USER	33857 (processed 33186)	0.2	1.0
/RSGraviton_WWlvjj_kMpl02_M-1500_TuneZ2star_8TeV-MG_qili-RSWW_1500_02_AODSIM- c8f8ed334db8a7d6f56c62266b1dfa5b/USER	23879 (processed 23879)	0.2	1.5

Table 4:  $W'$  to  $WZ$  signal MC samples. Inclusive decays are considered.

Sample	$N$
/WprimeToWZ_M-1000_TuneZ2star_8TeV-pythia6/ Summer12_DR53X-PU_S10_START53_V7A-v1/AODSIM	30000
/WprimeToWZ_M-1500_TuneZ2star_8TeV-pythia6/ Summer12_DR53X-PU_S10_START53_V7A-v1/AODSIM	30000
/WprimeToWZ_M-2000_TuneZ2star_8TeV-pythia6/ Summer12_DR53X-PU_S10_START53_V7A-v1/AODSIM	30000
/WprimeToWZ_M_2500_TuneZ2star_8TeV_pythia6/ Summer12_DR53X-PU_S10_START53_V19-v1/AODSIM	30000

## 76    2.2 Background MC and cross-sections

77    The full list of the MC background samples is found in Table 5. These are the same backgrounds  
 78    used for the existing approved analysis. For this update we just increased the statistics of some  
 79    samples by processing the entire datasets.

Table 5: Background samples used in the analysis.

Sample	Number of events	$\sigma$ [pb]
<b>MadGraph samples</b>		
/WJetsToLNu_PtW-100_TuneZ2star_8TeV-madgraph/ Summer12_DR53X-PU_S10_START53_V7A-v1/AODSIM	12.74M	282.5
/WJetsToLNu_PtW-180.TuneZ2star_8TeV-madgraph-tarball/ Summer12_DR53X-PU_S10_START53_V7C-v1/AODSIM	9.73M	29.00
<b>DYJetsToLL_PtZ-70To100.TuneZ2star_8TeV_ext-madgraph-tarball/</b>		
Summer12_DR53X-PU_S10_START53_V7C-v1/AODSIM	11.76M	62.9
<b>DYJetsToLL_PtZ-100.TuneZ2star_8TeV_ext-madgraph-tarball/</b>		
Summer12_DR53X-PU_S10_START53_V7C-v1/AODSIM	12.51M	39.1
<b>Powheg samples</b>		
/TT_CT10_TuneZ2star_8TeV-powheg-tauola/ Summer12_DR53X-PU_S10_START53_V7A-v2/AODSIM	21.7M	225.2
/T_s-channel_TuneZ2star_8TeV-powheg-tauola/ Summer12_DR53X-PU_S10_START53_V7A-v1/AODSIM	0.26M	3.79
/T_t-channel_TuneZ2star_8TeV-powheg-tauola/ Summer12_DR53X-PU_S10_START53_V7A-v1/AODSIM	3.75M	56.4
/T_tW-channel-DR_TuneZ2star_8TeV-powheg-tauola/ Summer12_DR53X-PU_S10_START53_V7A-v1/AODSIM	0.498M	11.1
/Tbar_s-channel_TuneZ2star_8TeV-powheg-tauola/ Summer12_DR53X-PU_S10_START53_V7A-v1/AODSIM	0.140M	1.76
/Tbar_t-channel_TuneZ2star_8TeV-powheg-tauola/ Summer12_DR53X-PU_S10_START53_V7A-v1/AODSIM	1.93M	30.7
/Tbar_tW-channel-DR_TuneZ2star_8TeV-powheg-tauola/ Summer12_DR53X-PU_S10_START53_V7A-v1/AODSIM	0.493M	11.1
<b>Pythia samples</b>		
/WW_TuneZ2star_8TeV_pythia6_tauola/ Summer12_DR53X-PU_S10_START53_V7A-v1/AODSIM	10M	57.1
/WZ_TuneZ2star_8TeV_pythia6_tauola/ Summer12_DR53X-PU_S10_START53_V7A-v1/AODSIM	9.95M	33.2
/ZZ_TuneZ2star_8TeV_pythia6_tauola/ Summer12_DR53X-PU_S10_START53_V7A-v1/AODSIM	9.80M	8.06

---

### 2.3 Data samples

In the previous version of the analysis we used a combination of prompt reco and re-reco datasets produced in 2012. In this analysis, we use the  $19.7 \text{ fb}^{-1}$  of data collected in 2012 and re-reco'ed in CMSSW\_5\_3\_X (22Jan2013 rereco). The data samples are listed in Table 6. We use only lumi sections that have been declared good for analysis by the central certification team, listed in the following official JSON file:

- Cert\_190456-208686\_8TeV\_22Jan2013ReReco\_Collisions12\_JSON.txt – for Run2012A,B,C and D re-reconstruction.

Table 6: Data samples used in the analysis.

Sample	Run Range	$\mathcal{L} [\text{pb}]^{-1}$
/SingleMu/Run2012A-22Jan2013-v1/AOD	190456–193621	876
/SingleMu/Run2012B-22Jan2013-v1/AOD	193834–196531	4412
/SingleMu/Run2012C-22Jan2013-v1/AOD	198022–203742	7050
/SingleMu/Run2012D-22Jan2013-v1/AOD	203777–208686	7368
TOTAL SingleMu	190456–208686	19706
<hr/>		
/SingleElectron/Run2012A-22Jan2013-v1/AOD	190456–193621	876
/SingleElectron/Run2012B-22Jan2013-v1/AOD	193834–196531	4405
/SingleElectron/Run2012C-22Jan2013-v1/AOD	198022–203742	7040
/SingleElectron/Run2012D-22Jan2013-v1/AOD	203777–208686	7362
TOTAL SingleElectron	190456–208686	19683

---

### 88    3 Event Reconstruction and Selection

89    The reconstruction of physics objects and the selection criteria is almost unchanged with respect  
90    to the approved analysis with the few exceptions reported below:

- 91    • We now use the new High-pT Muon ID and new TuneP momentum assignment  
92    (after CMSSW\_5\_3\_6\_patch1) which is recommended for high  $p_T$  muons in the Exot-  
93    ica group. The main effects on the analysis is small increase of 5% in the muon ID  
94    efficiency.
- 95    • The latest jet energy scale corrections for 22Jan2013 rereco are applied. The global  
96    tag is START53\_V23 (FT\_53\_V21\_AN4) for MC (data), as recommended at  
97    <https://hypernews.cern.ch/HyperNews/CMS/get/JetMET/1461.html>.
- 98    • If a CA8 jet is within  $\Delta R < 0.8$  of any well identified and isolated electron or muon,  
99    the jet is not used in the analysis. The previous cut was at 1.0. We changed the cut  
100   in order to synchronize with the EXO-12-022 search.

101   A summary of the final kinematic and jet substructure selection criteria is presented in Table 7.



Table 7: Summary of final selection.

Selection	Value	Comments
<b>Tight Lepton selection</b>		
Electron $p_T$	$p_T > 90 \text{ GeV}$	
Muon $p_T$	$p_T > 50 \text{ GeV}$	
Electron $\eta$	$ \eta _{\text{SC}} < 2.5$ except [1.4442, 1.566] range	Avoid the ECAL gap.
Muon $\eta$	$ \eta  < 2.1$	
<b>Loose Lepton selection</b>		
Electron $p_T$	$p_T > 35 \text{ GeV}$	
Muon $p_T$	$p_T > 20 \text{ GeV}$	
Electron $\eta$	$ \eta _{\text{SC}} < 2.5$ except [1.4442, 1.566] range	Avoid the ECAL gap.
Muon $\eta$	$ \eta  < 2.4$	
<b>CA8 jet selections</b>		
Jet $p_T$	$p_T > 80 \text{ GeV}$	Used for hadronic W reconstruction
Jet $\eta$	$ \eta  < 2.4$	
<b>AK5 jet selections</b>		
Jet $p_T$	$p_T > 30 \text{ GeV}$	Used for b-tag jet selection
Jet $\eta$	$ \eta  < 2.4$	
<b><math>E_T^{\text{miss}}</math> selections</b>		
$E_T^{\text{miss}}$ (electron ch.)	$E_T^{\text{miss}} > 80 \text{ GeV}$	
$E_T^{\text{miss}}$ (muon ch.)	$E_T^{\text{miss}} > 40 \text{ GeV}$	
<b>Boson selections</b>		
Pruned jet mass (signal)	$65 < m_{\text{jet}}^{\text{pruned}} < 105 \text{ GeV}$	
Pruned jet mass (low-mass sideband)	$40 < m_{\text{jet}}^{\text{pruned}} < 65 \text{ GeV}$	
Pruned jet mass (high-mass sideband)	$105 < m_{\text{jet}}^{\text{pruned}} < 130 \text{ GeV}$	
Leptonic W $p_T$	$p_T > 200 \text{ GeV}$	
Hadronic W $p_T$	$p_T > 200 \text{ GeV}$	
Back-to-back topology	$\Delta R(\ell, W_{\text{had}}) > \pi/2$ , $\Delta\phi(W_{\text{had}}, E_T^{\text{miss}}) > 2$ $\Delta\phi(W_{\text{had}}, W_{\text{lep}}) > 2$	
<b>Veto</b>		
Number of loose electrons	0	in addition to tight lepton
Number of loose muons	0	in addition to tight lepton
Number of b-tag jets	0	CSV medium working point
<b>Diboson selections</b>		
2- to 1-subjettiness ratio (high purity)	$\tau_{21} < 0.50$	
2- to 1-subjettiness ratio (low purity)	$0.50 \leq \tau_{21} < 0.75$	

### 3.1 Control plots in the hadronic W mass sideband

We use the low and high sideband regions (events with  $40 < m_{jet}^{pruned} < 65$  GeV or  $105 < m_{jet}^{pruned} < 130$  GeV, and no cut on  $\tau_{21}$ ) to form a sample of data events with small signal contamination from a potential new  $X \rightarrow WW$  resonance. In this control sample we compare data and MC simulation. All the backgrounds (except W+jets) are normalized to the cross sections described in Section 2.2. Instead, the W+jets cross section described in Section 2.2 is multiplied by a factor around 1.5, such that the total integral of the MC matches the number of events in data in the low+high sideband region.

Various distributions are shown for both electron and muon channels.

The agreement between data and simulation is not perfect, although the main kinematic features of these events in data are correctly described by the MC. The discrepancies are related to the fact that we select a sample dominated by W+jets events in the tails of the pruned jet mass distribution events which is a quantity particularly sensitive to the parton shower algorithm and in general not well described by the simulation; in these events, the hadronic W candidate is in fact a massive jet originated from a light quark and not a real W decaying to pair of quarks. In this analysis we rely on data-driven methods for the W+jets background estimation which allow to reduce this dependence on the final background prediction.

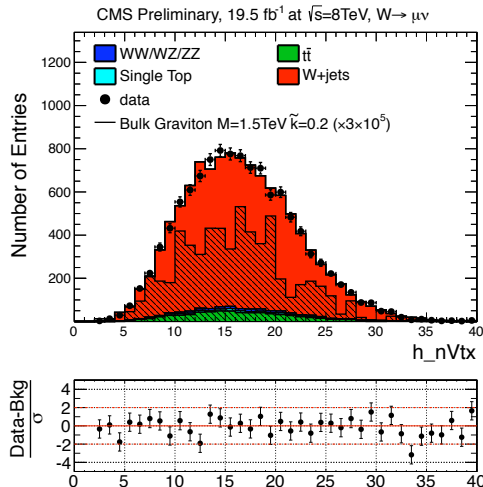


Figure 1: Number of reconstructed vertexes after the reweighting of the MC sample by the pile-up corrections. Points with error bars show data, histograms show contribution of dominant background channels, both after the selection. **The bulk graviton signal cross section should be multiplied by a factor 1/4, due to a bug recently found in the theoretical calculation. More details can be found in Section 3 of [9]. We don't plan to update this AN. The values in the EXO-13-009 will be correct.**

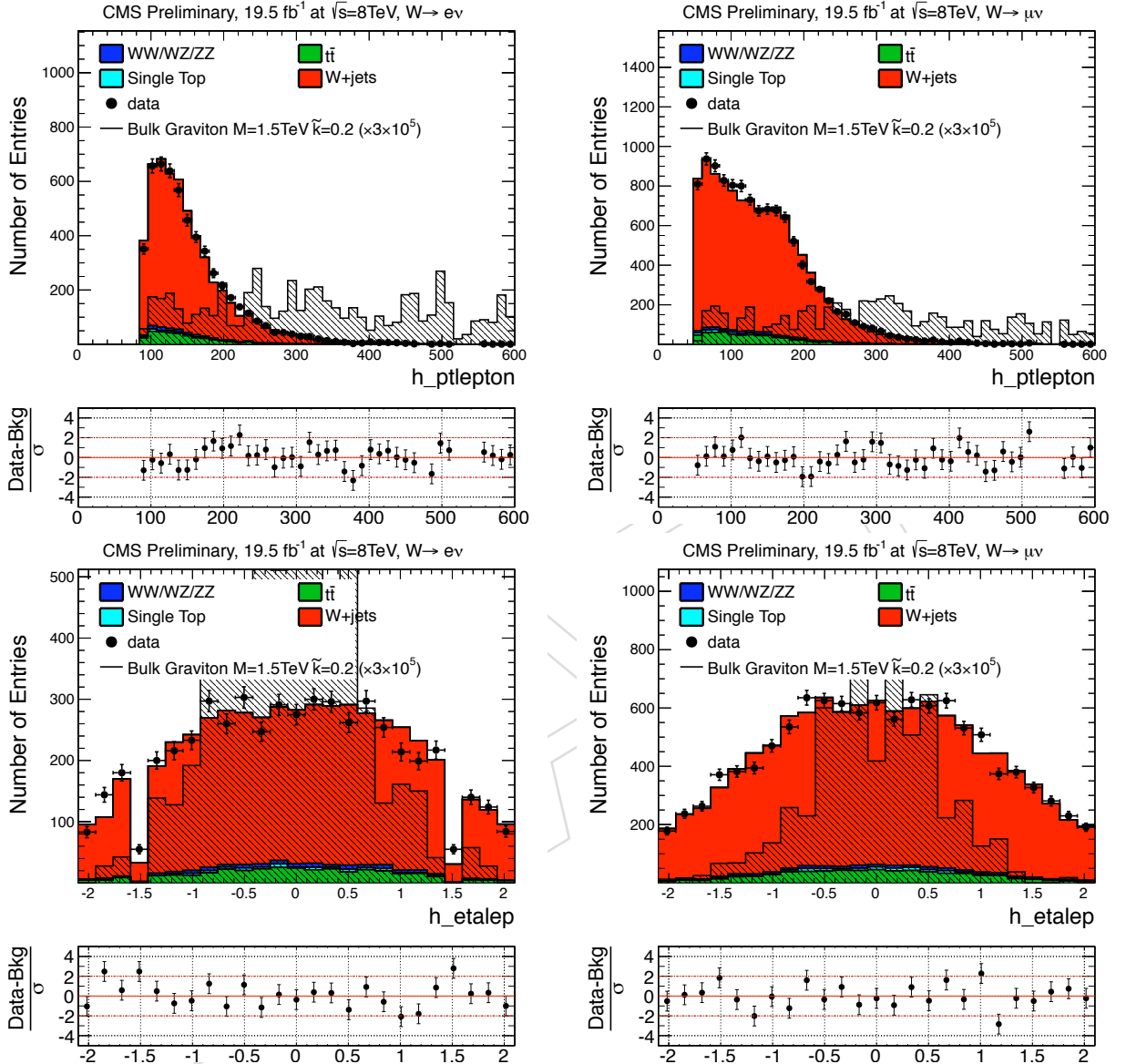


Figure 2: Lepton  $p_T$  and  $\eta$  for electron channel (left) and muon channel (right) for events with  $40 < m_{jet}^{pruned} < 65$  GeV or  $105 < m_{jet}^{pruned} < 130$  GeV. The signal is normalized to  $3 \cdot 10^5$  times than the expected cross section for the model considered (bulk graviton,  $M = 1.5$  TeV,  $\tilde{k} = 0.2$ ). The bulk graviton signal cross section should be multiplied by a factor 1/4, due to a bug recently found in the theoretical calculation. More details can be found in Section 3 of [9]. We don't plan to update this AN. The values in the EXO-13-009 will be correct.

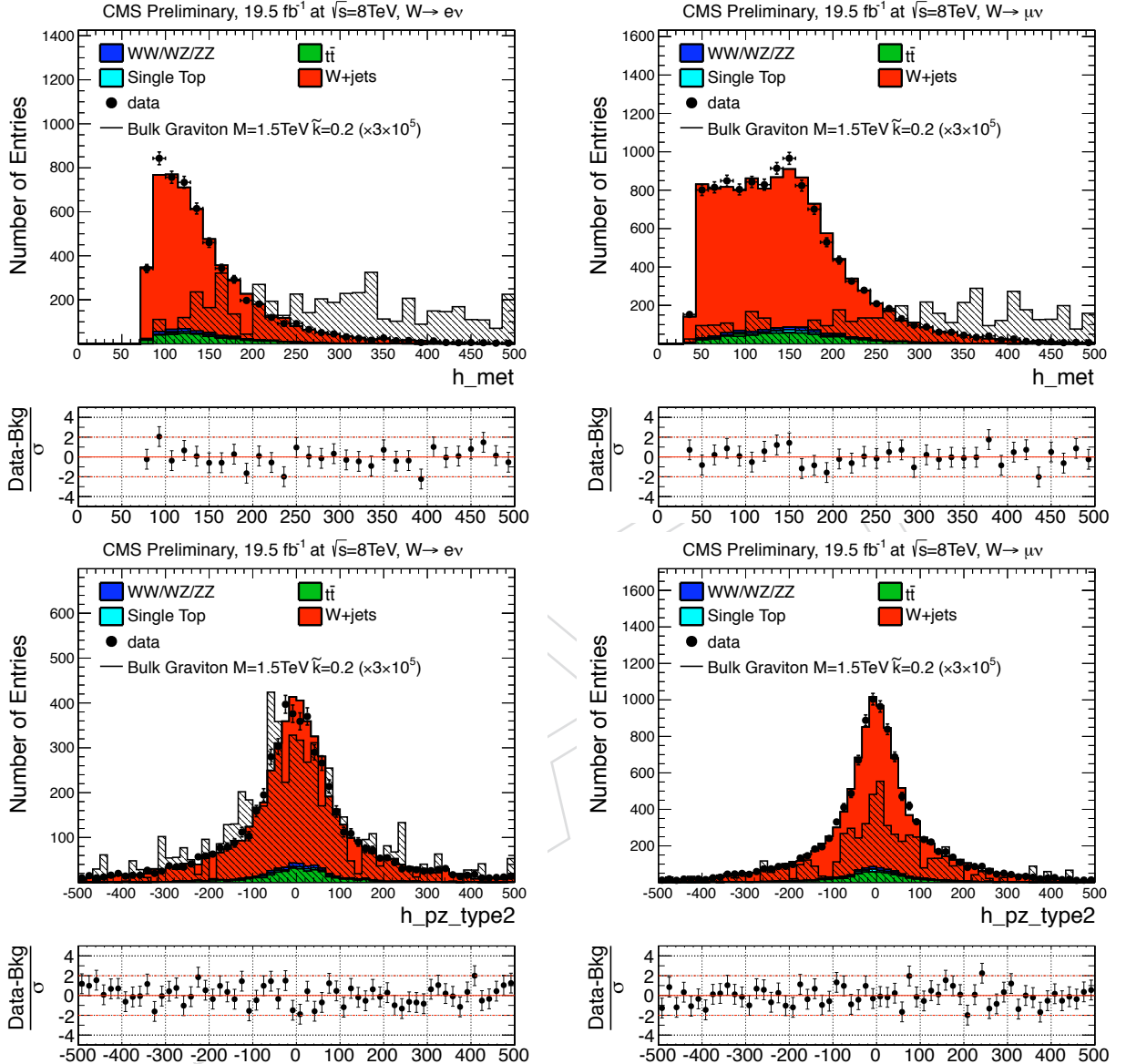


Figure 3:  $E_T^{\text{miss}}$  and  $p_{z\nu}$  for electron channel (left) and muon channel (right) for events with  $40 < m_{\text{jet}}^{\text{pruned}} < 65 \text{ GeV}$  or  $105 < m_{\text{jet}}^{\text{pruned}} < 130 \text{ GeV}$ . The signal is normalized to  $3 \cdot 10^5$  times than the expected cross section for the model considered (bulk graviton,  $M = 1.5 \text{ TeV}$ ,  $\tilde{k} = 0.2$ ). The bulk graviton signal cross section should be multiplied by a factor 1/4, due to a bug recently found in the theoretical calculation. More details can be found in Section 3 of [9]. We don't plan to update this AN. The values in the EXO-13-009 will be correct.

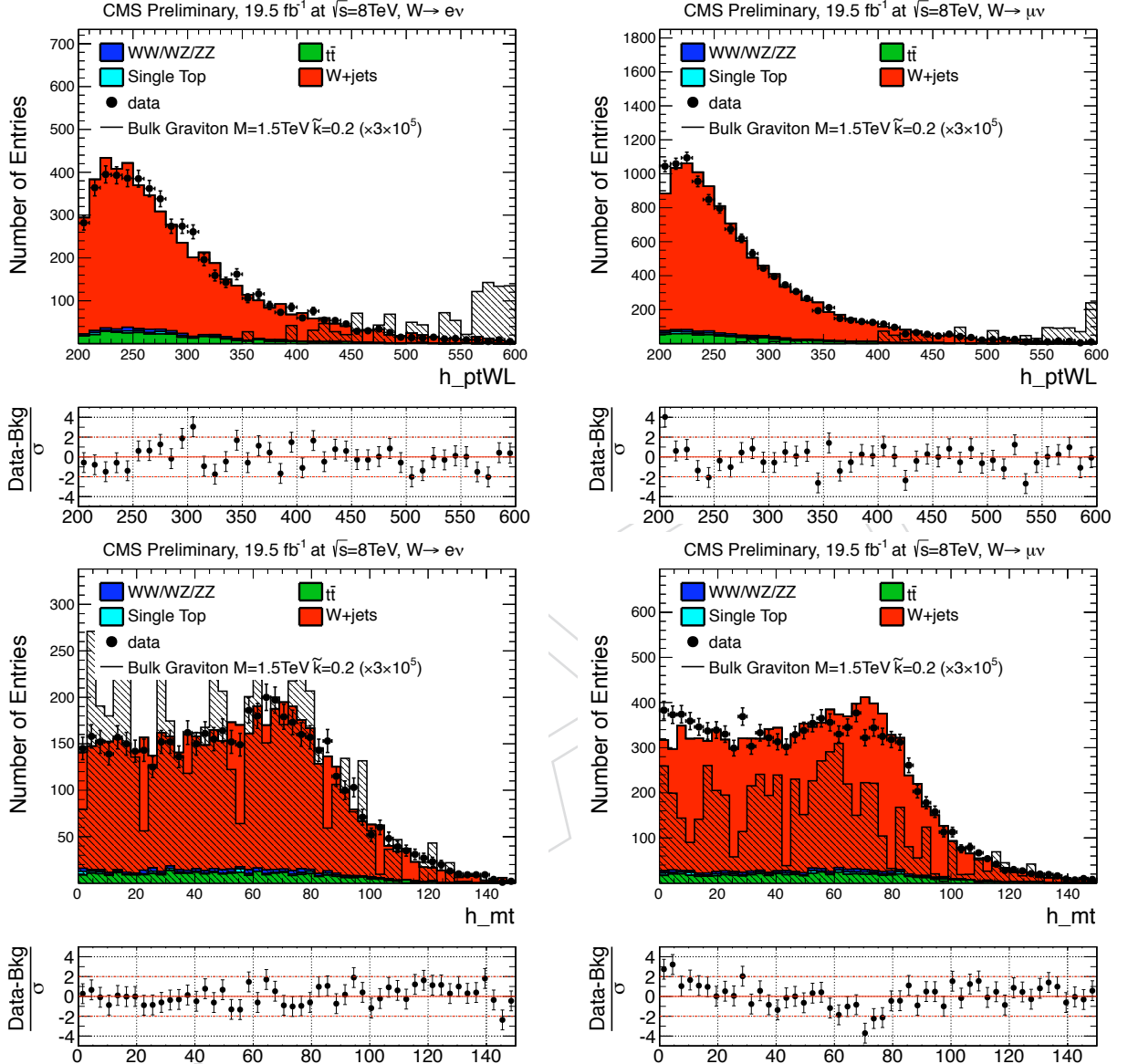


Figure 4: Leptonic  $W$   $p_T$  and  $m_T(\ell\nu)$  for electron channel (left) and muon channel (right) for events with  $40 < m_{jet}^{pruned} < 65$  GeV or  $105 < m_{jet}^{pruned} < 130$  GeV. The signal is normalized to  $3 \cdot 10^5$  times than the expected cross section for the model considered (bulk graviton,  $M = 1.5$  TeV,  $\tilde{k} = 0.2$ ). The bulk graviton signal cross section should be multiplied by a factor 1/4, due to a bug recently found in the theoretical calculation. More details can be found in Section 3 of [9]. We don't plan to update this AN. The values in the EXO-13-009 will be correct.

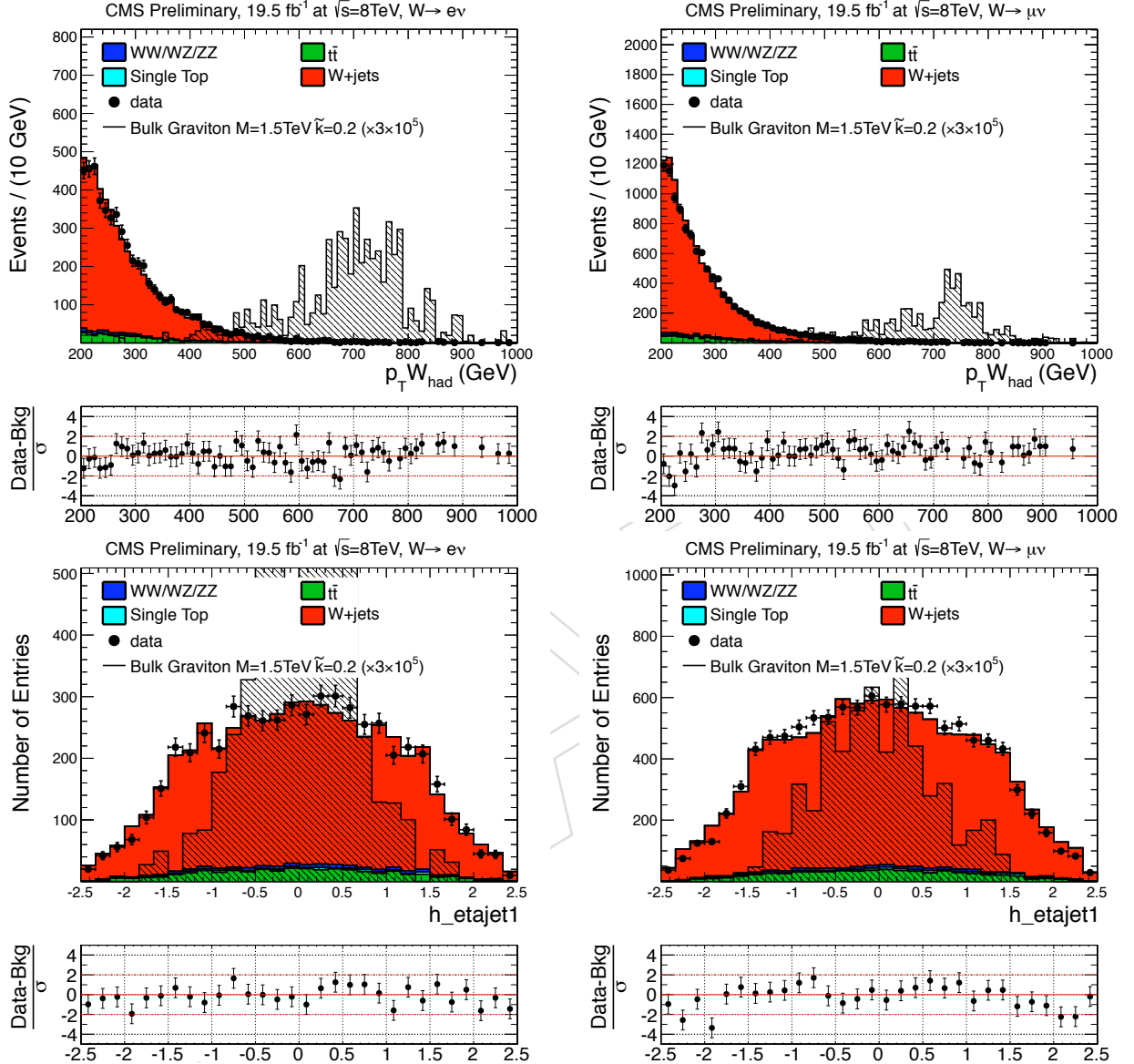


Figure 5: Hadronic  $W$   $p_T$  and  $\eta$  for electron channel (left) and muon channel (right) for events with  $40 < m_{\text{jet}}^{\text{pruned}} < 65$  GeV or  $105 < m_{\text{jet}}^{\text{pruned}} < 130$  GeV. The signal is normalized to  $3 \cdot 10^5$  times than the expected cross section for the model considered (bulk graviton,  $M = 1.5$  TeV,  $\tilde{k} = 0.2$ ). The bulk graviton signal cross section should be multiplied by a factor 1/4, due to a bug recently found in the theoretical calculation. More details can be found in Section 3 of [9]. We don't plan to update this AN. The values in the EXO-13-009 will be correct.

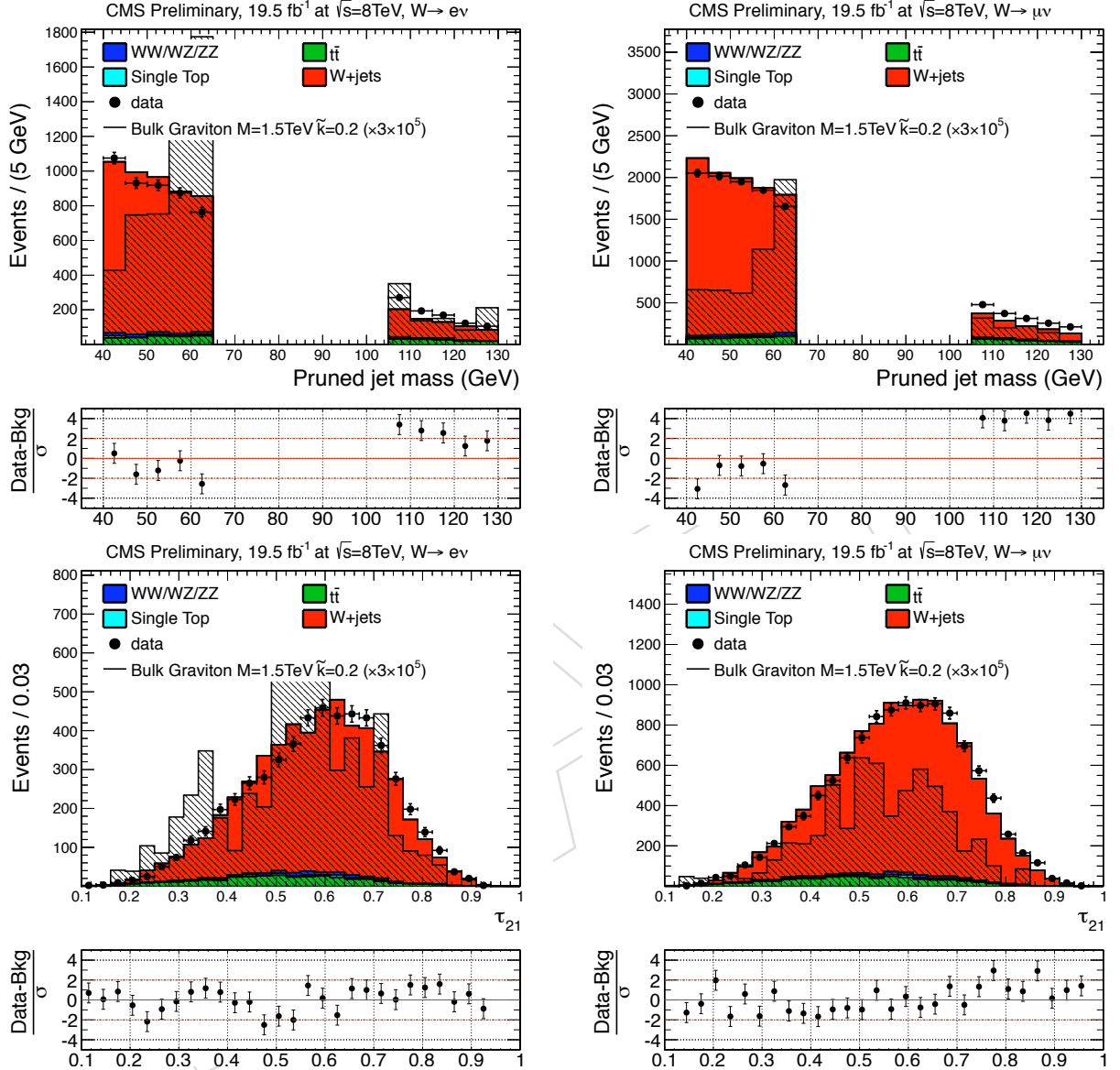


Figure 6:  $m_{jet}^{pruned}$  and  $\tau_{21}$  for electron channel (left) and muon channel (right) for events with  $40 < m_{jet}^{pruned} < 65\text{ GeV}$  or  $105 < m_{jet}^{pruned} < 130\text{ GeV}$ . The signal is normalized to  $3 \cdot 10^5$  times than the expected cross section for the model considered (bulk graviton,  $M = 1.5\text{ TeV}$ ,  $\tilde{k} = 0.2$ ). The bulk graviton signal cross section should be multiplied by a factor 1/4, due to a bug recently found in the theoretical calculation. More details can be found in Section 3 of [9]. We don't plan to update this AN. The values in the EXO-13-009 will be correct.

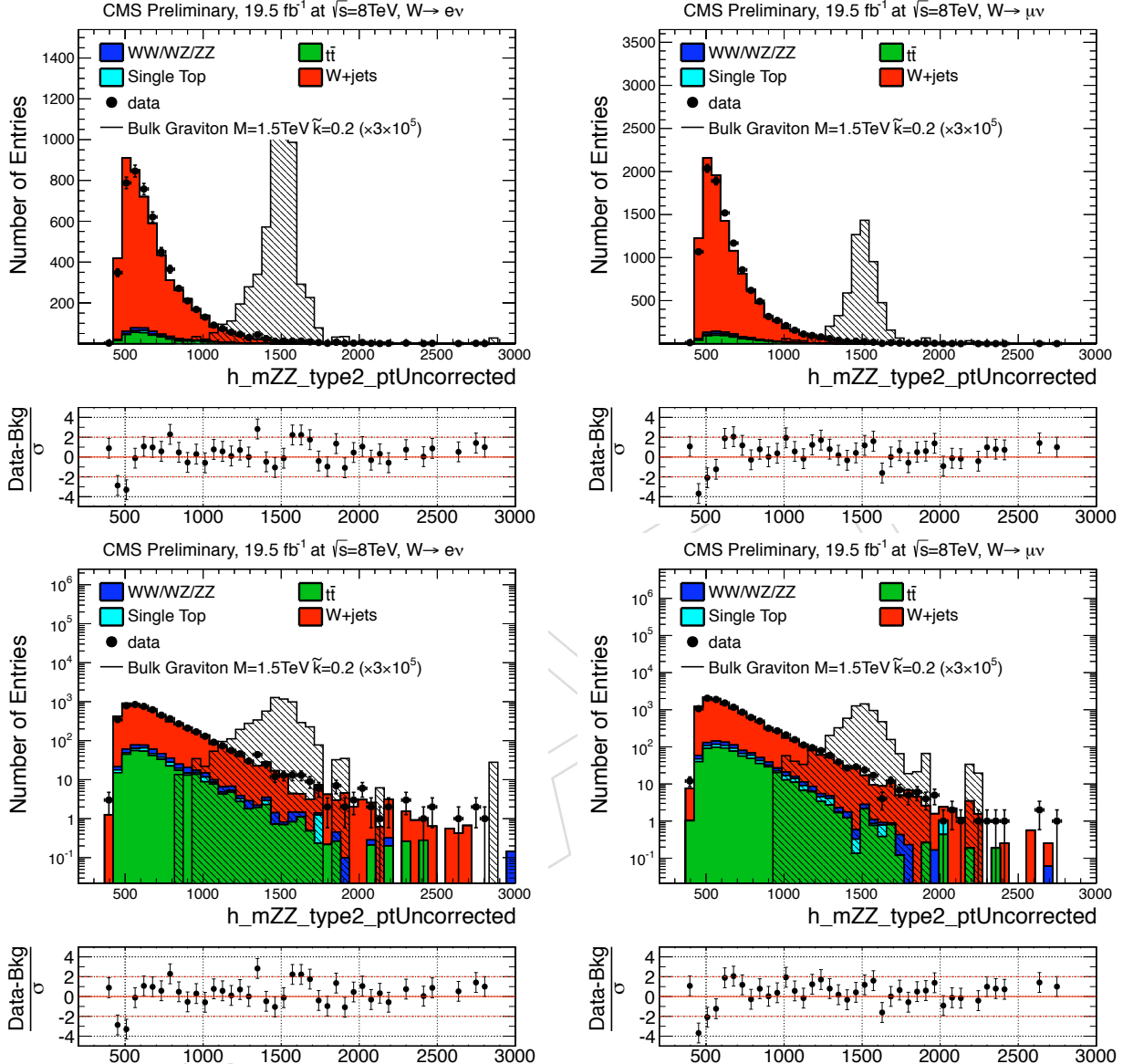


Figure 7:  $m_{WW}$  (using the  $p_{T\nu}$  in linear and log scale for electron channel (left) and muon channel (right) for events with  $40 < m_{jet}^{pruned} < 65 \text{ GeV}$  or  $105 < m_{jet}^{pruned} < 130 \text{ GeV}$ ). The signal is normalized to  $3 \cdot 10^5$  times than the expected cross section for the model considered (bulk graviton,  $M = 1.5 \text{ TeV}$ ,  $\tilde{k} = 0.2$ ). The bulk graviton signal cross section should be multiplied by a factor 1/4, due to a bug recently found in the theoretical calculation. More details can be found in Section 3 of [9]. We don't plan to update this AN. The values in the EXO-13-009 will be correct.

119 **3.2 Data vs MC comparison in signal region**

120 Figure 8 show the  $m_{WW}$  distribution in data after full selection compared with the MC prediction.  
 121 The 4 analysis categories are shown separately. In this specific set of plots, the W+jets  
 122 background have been scaled in order that the total background would match the number of  
 123 events in data. All the other backgrounds are fixed to the cross section values specified in  
 124 Section 2.2

125 No significant excess of data above this MC background prediction is visible across the entire  
 126 WW mass spectra. It should be noted that the final results of this analysis are not derived  
 127 from these MC background predictions. The final background estimate is obtained using data-  
 128 driven methods.

129 We have noticed small differences in the events in the tails of the distributions. We performed  
 130 a detailed study in the HP category which is summarized below:

131 For muon HP, SR,  $m_{WW} > 1800$ ,  
 132 Old events (9)  $\rightarrow$  1 event go to LP (8)  $\rightarrow$  1 event go to SB (7)  
 133  $\rightarrow$  2 events jump from 17XX to 18XX (9)  $\rightarrow$  New events (9)  
 134  
 135 For electron HP, SR,  $m_{WW} > 1800$ ,  
 136 Old events (6)  $\rightarrow$  2 events to go LP (4)  $\rightarrow$  2 events jump from 17XX to 18XX (6)  
 137  $\rightarrow$  1 event jumps from SB to SR (7)  $\rightarrow$  New events (7)

138 The migrations are all threshold effects due to selection requirements (mainly jets) applied.  
 139 These small effects are rather common when the rereco conditions changes, as happened in  
 140 this update of the analysis.

141 Finally, we report in Figure 9 a few control plots for electron and muon channel (all purity  
 142 categories) in the signal region only. The combined ele+mu plots in Figure 10 will be included  
 143 in the paper.

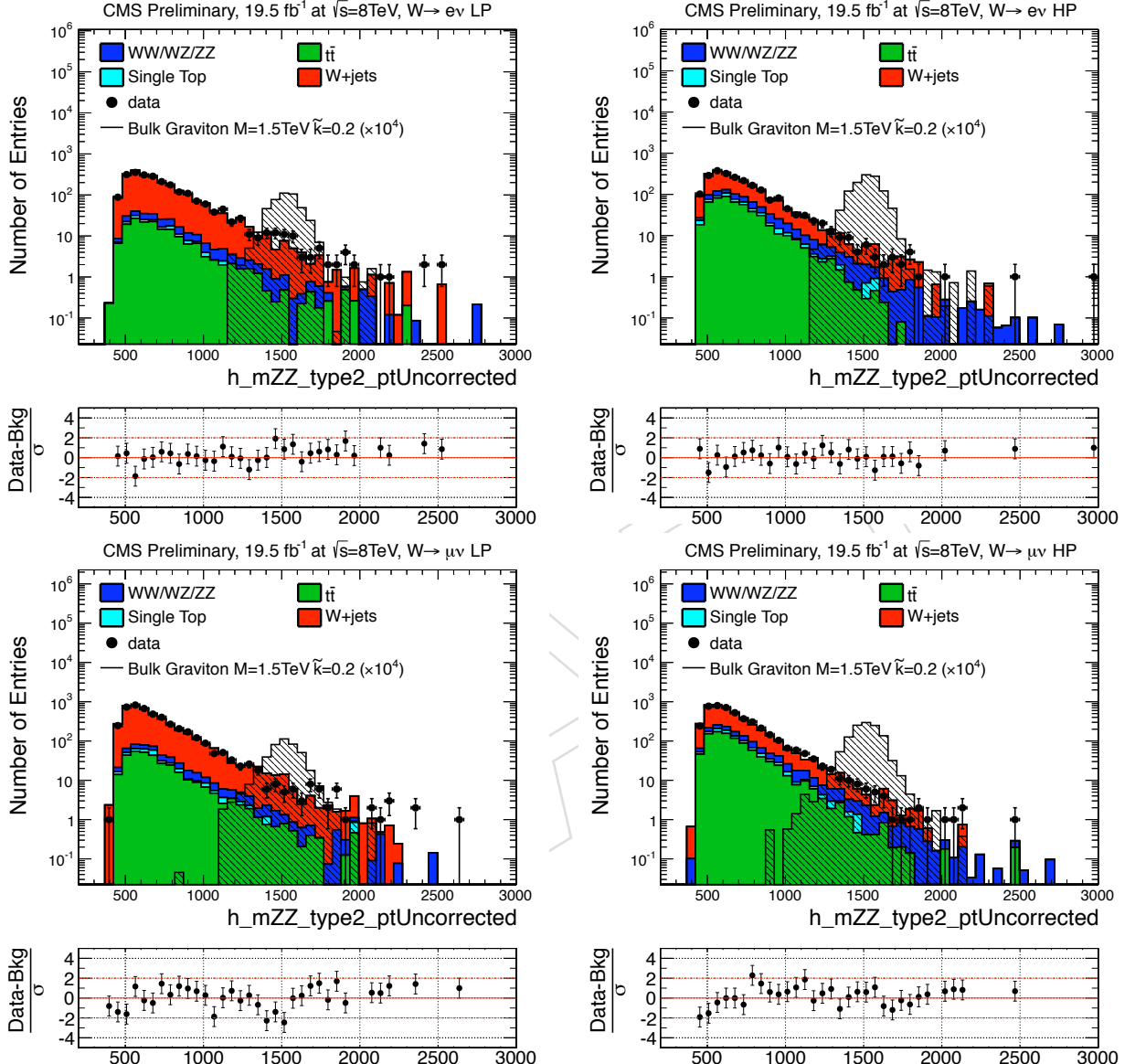


Figure 8:  $m_{WW}$  for electron LP (top-left), electron HP (top-right), muon LP (bottom-left), muon HP (bottom-right) for events passing the full selection with  $65 < m_{jet}^{pruned} < 105\text{ GeV}$ . The signal is scaled by 60000 (34800) for the muon (electron) channel. **The bulk graviton signal cross section should be multiplied by a factor 1/4, due to a bug recently found in the theoretical calculation.** More details can be found in Section 3 of [9]. We don't plan to update this AN. The values in the EXO-13-009 will be correct.

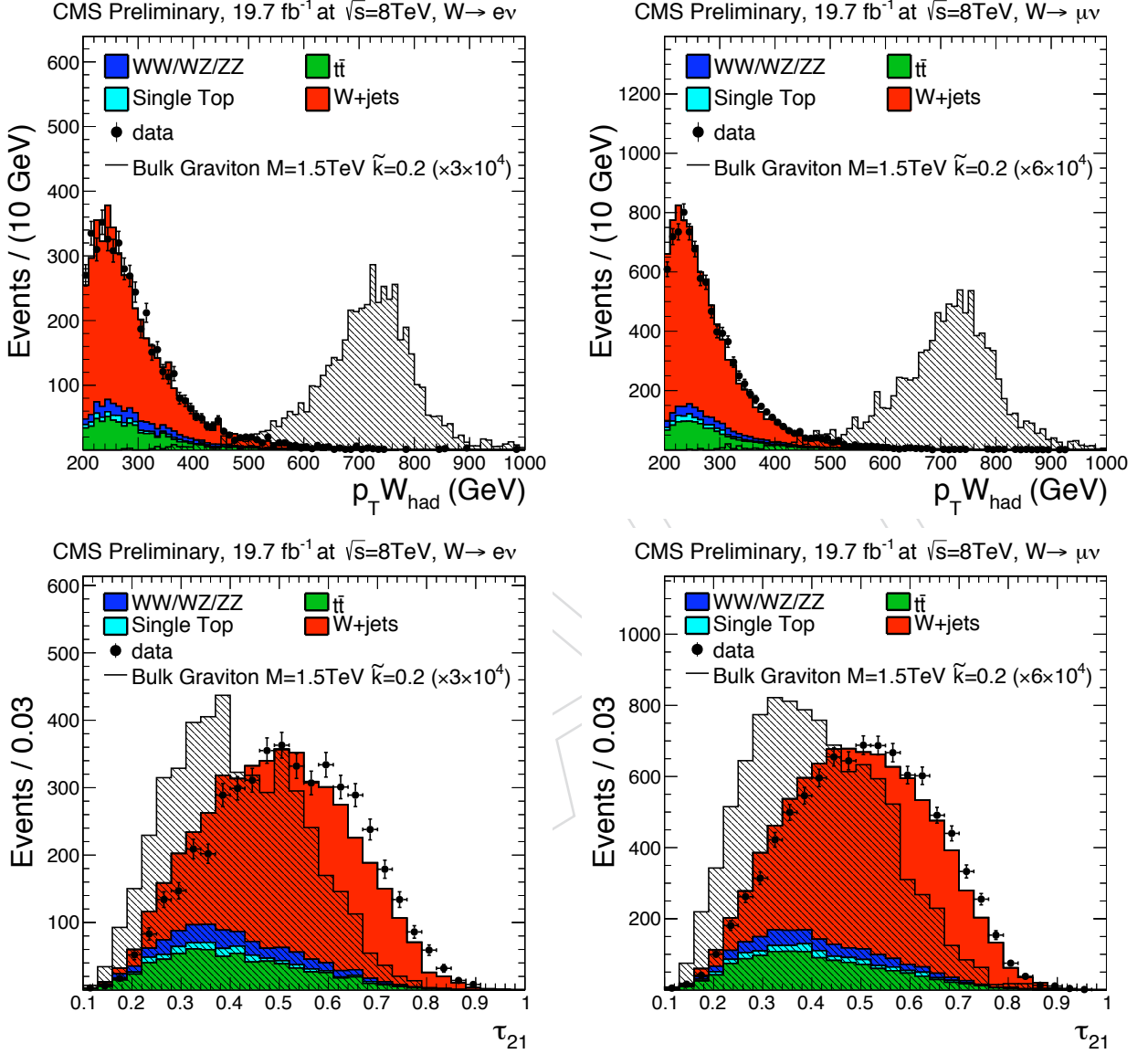


Figure 9: Hadronic  $W$   $p_T$  and  $\tau_{21}$  for electron channel (left) and muon channel (right) for events with  $65 < m_{\text{jet}}^{\text{pruned}} < 105 \text{ GeV}$ . The signal is scaled by 60000 (34800) for the muon (electron) channel. The bulk graviton signal cross section should be multiplied by a factor 1/4, due to a bug recently found in the theoretical calculation. More details can be found in Section 3 of [9]. We don't plan to update this AN. The values in the EXO-13-009 will be correct.

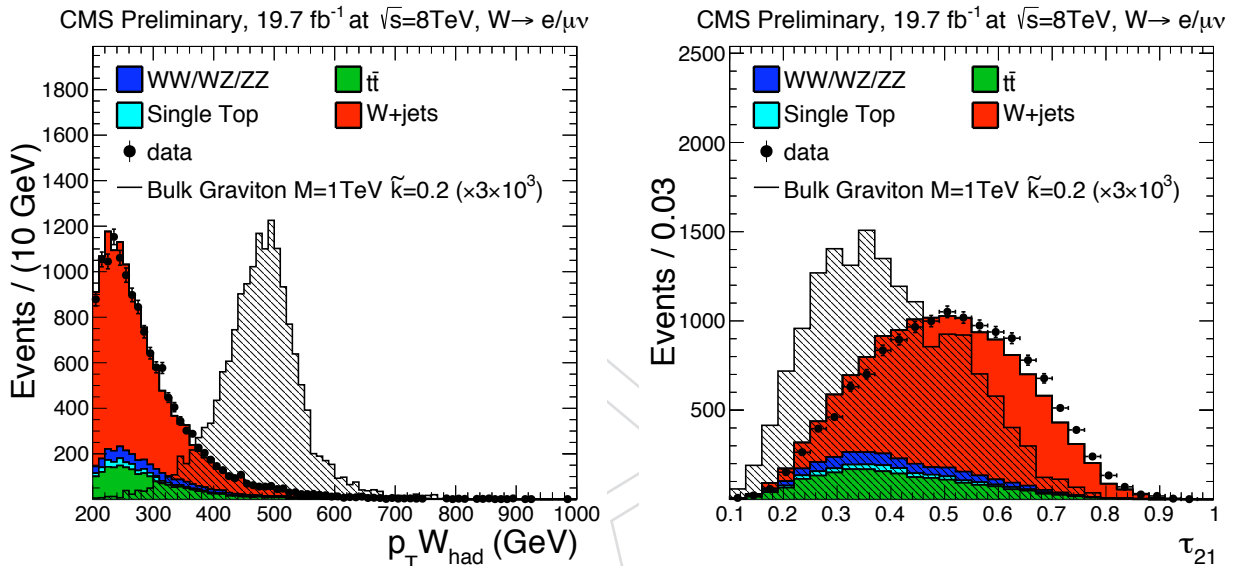


Figure 10: Hadronic  $W p_T$  and  $\tau_{21}$  for electron+muon channels combined for events with  $65 < m_{jet}^{pruned} < 105 \text{ GeV}$ . The signal is scaled by 3000. **The bulk graviton signal cross section should be multiplied by a factor 1/4, due to a bug recently found in the theoretical calculation.** More details can be found in Section 3 of [9]. We don't plan to update this AN. The values in the EXO-13-009 will be correct.

## 144 4 Signal modeling: $m_{WW}$ shapes and efficiency

### 145 4.1 Parametrization of the $m_{WW}$ signal shape (narrow resonances)

146 We used the bulk graviton samples with  $\tilde{k} = 0.2$  listed in Sect. 2.1 for modeling the shape of  
 147 the reconstructed  $m_{WW}$  distribution of the signal. Fig.11 shows the dependence of the width of  
 148 the graviton line shape at the parton level (taken from [6]). The natural width of the resonance  
 149 obtained using the chosen value of  $\tilde{k}$  is sufficiently small to be neglected when compared to  
 150 the detector resolution. This makes our modeling of the detector effects on the signal shape  
 151 independent of the actual model used for generating the events and allows us to apply it to a  
 152 model-independent search for narrow-resonances.

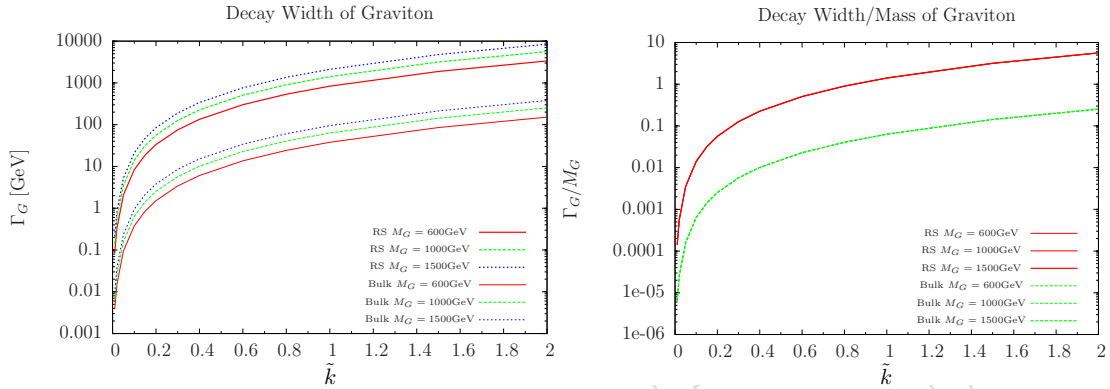


Figure 11: Dependence of the natural width of the graviton (GeV) as a function of the coupling constant  $\tilde{k}$  in the RS1 and Bulk graviton models (left). The relative width (width divided by the mass) is shown on the right.

153 The  $m_{WW}$  spectrum of the signal is modeled with a Double Crystal-Ball function (i.e. a Gaussian  
 154 core with powerlaw tails on both sides, `RooDoubleCB` implemented in `RooFit`). In the previous  
 155 analysis group2 was using a one-sided Crystal-Ball function. We moved to the two-sided one  
 156 for consistency with group1. The  $m_{WW}$  signal distribution varies depending on the resonance  
 157 mass hypothesis. Several examples are shown in Fig. 12 for electron and muon channels.

158 A summary of the natural width and the standard deviation of the Gaussian core of the matched  
 159 part of the signal is presented for several mass points in Table 8 for the electron and muon  
 160 channels. The electron and muon shapes are very similar, even at high  $m_{WW}$ , since the mass  
 161 resolution is dominated anyway by the  $E_T^{\text{miss}}$  contribution. No significant dependence in the  
 162  $m_{WW}$  shape on the V-tag purity category has been found in our studies.

Resonance mass [GeV]	Total Natural Width, $\Gamma$ [GeV]	Mean of CB function [GeV]	$\sigma$ of CB function [GeV]
electron channel			
1000	2.5 (13.0)	$1021.2 \pm 2.2$	$61.5 \pm 1.9$
1500	3.75 (19.5)	$1524.1 \pm 2.7$	$78.8 \pm 2.5$
2000	5.0 (26.0)	$2012.4 \pm 3.1$	$93.7 \pm 3.6$
2500	6.25 (32.5)	$2524.5 \pm 2.5$	$102.4 \pm 7.1$
muon channel			
1000	2.5 (13.0)	$1023.1 \pm 2.0$	$55.7 \pm 2.5$
1500	3.75 (19.5)	$1515.2 \pm 2.5$	$81.6 \pm 2.4$
2000	5.0 (26.0)	$2012.8 \pm 2.9$	$100.1 \pm 3.0$
2500	6.25 (32.5)	$2513.8 \pm 4.4$	$115.7 \pm 4.9$

Table 8: The main parameters (mass/mean and width/ $\sigma$ ) of the signal shape for different mass points at the generator and reconstructed level for the electron and muon channels. The total natural width,  $\Gamma$ , refers to bulk graviton samples with  $\tilde{k} = 0.2$  (or  $\tilde{k} = 0.5$  in parenthesis) and is taken from [6]. The MC samples used for fitting the signal shape parameters are the ones described in Sect. 2.1 (i.e. generated with  $\tilde{k} = 0.2$ ).

<sup>163</sup> **4.2 Parametrization of the  $m_{WW}$  signal shape (wide resonances)**

<sup>164</sup> Please refer to Section 8.2, since the wide resonances are considered in the model-independent analysis.

DRAFT

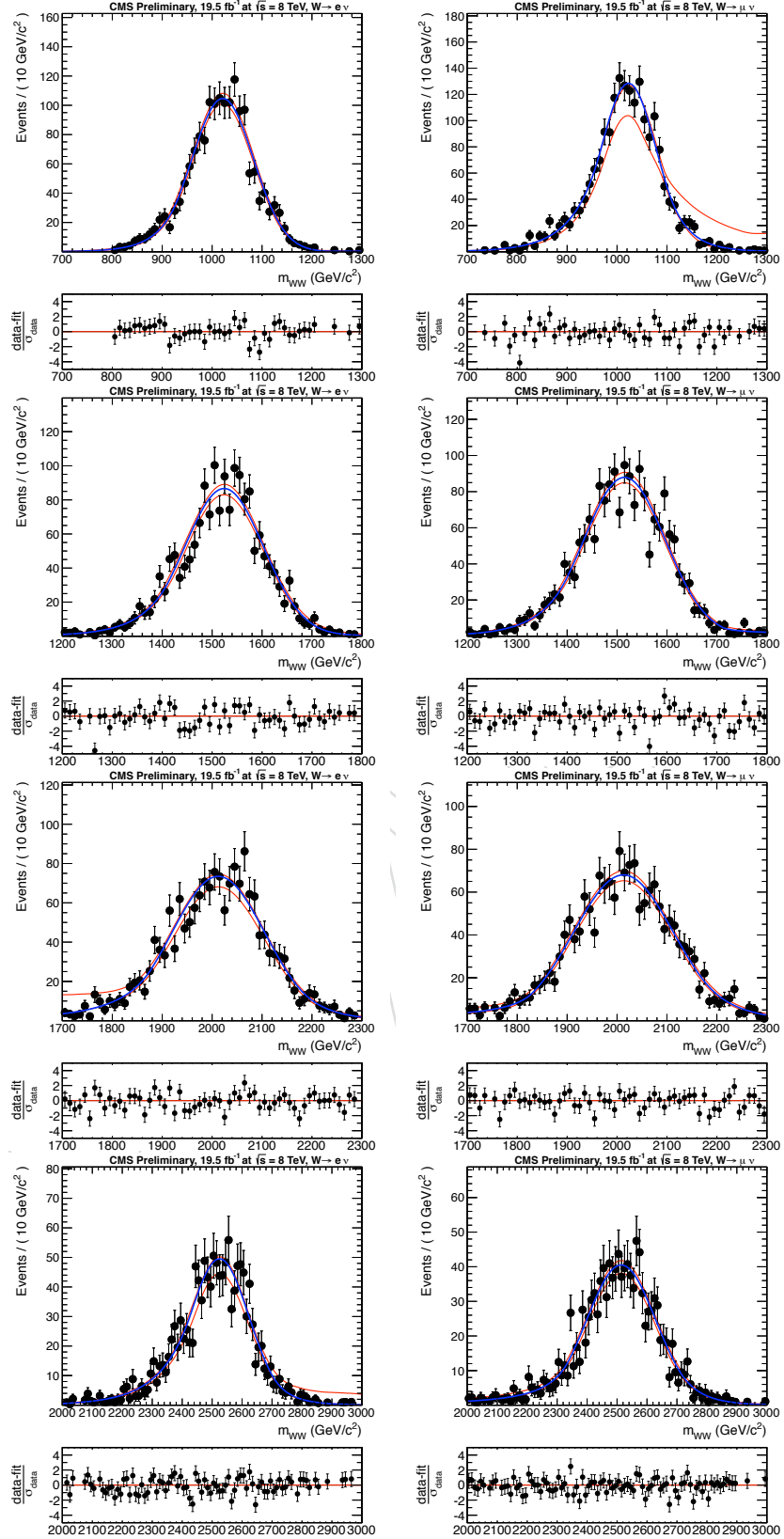


Figure 12: Distribution of the invariant mass,  $m_{WW}$ , and probability parameterization for MC bulk graviton with events with  $\tilde{k} = 0.2$  and resonance mass of 1, 1.5, 2, and 2.5 TeV. Events reconstructed in electron (muon) channel are shown in the left (right) column.

<sup>166</sup> **4.3 Signal efficiency**

<sup>167</sup> The signal reconstruction efficiency in each of the 4 channels (electron HP/LP, muon HP/LP)  
<sup>168</sup> is defined as the ratio:

$$\varepsilon_{SIG} = \frac{\text{Nr. of events passing the full selection in that category}}{\text{Total nr. of events generated}} \quad (1)$$

<sup>169</sup> where the total number of events generated includes all semi-leptonic WW decays  
<sup>170</sup> ( $X \rightarrow WW \rightarrow \ell\nu q\bar{q}'$  events with  $\ell = e, \mu$ , and  $\tau$  decays). Also the effect of  $W \rightarrow \tau\nu \rightarrow e$  or  $\mu + \nu\nu\nu$  decays is included.

<sup>172</sup> The signal efficiencies (as defined above) for the final selection criteria reported in Table 7 (sig-  
<sup>173</sup> nal region, i.e.  $65 < m_{jet}^{pruned} < 105$  GeV) are summarized in Table 9. Compared to the previous  
<sup>174</sup> version of the analysis we noticed two effects: i) relative increase of the signal rate in the HP  
<sup>175</sup> category of about 10% (at high mass) mainly due to the inclusion of tau decays, ii) relative  
<sup>176</sup> increase of the signal rate in LP category of about 20-30% due to both the inclusion of tau de-  
<sup>177</sup> cays and a moderate shift in the  $\tau_{21}$  distribution of signal towards higher values with the new  
<sup>178</sup> rereco conditions.

<sup>179</sup> The efficiency is parameterized as a function of the nominal graviton mass and it is interpolated  
<sup>180</sup> to all the mass points considered in this search. The efficiency parameterization is shown in  
<sup>181</sup> Fig. 13.

<sup>182</sup> The HP efficiency drops at high values of the resonance mass mainly due to the inefficiency of  
<sup>183</sup> the  $\tau_{21} < 0.50$  cut. This inefficiency is partially recovered in the LP category ( $0.50 \leq \tau_{21} < 0.75$ ).  
<sup>184</sup> At high mass also the  $m_{jet}^{pruned}$  reduces the efficiency due to a degradation of the pruned jet mass  
<sup>185</sup> distribution (wider and with more low-mass tails). The rest of the overall inefficiency is due to  
<sup>186</sup> the kinematic requirements on leptons,  $E_T^{\text{miss}}$ , jets, and bosons, as well as on the lepton ID and  
<sup>187</sup> ISO requirements.

$M_G$ [GeV]	Signal Efficiency			
	ELE HP	MU HP	ELE LP	MU LP
600	0.060	0.096	0.014	0.021
700	0.089	0.125	0.022	0.031
800	0.110	0.140	0.029	0.038
900	0.114	0.146	0.034	0.040
1000	0.124	0.149	0.039	0.045
1100	0.134	0.154	0.042	0.048
1200	0.135	0.159	0.044	0.051
1300	0.140	0.153	0.047	0.056
1400	0.140	0.153	0.051	0.057
1500	0.143	0.151	0.056	0.055
1600	0.145	0.152	0.050	0.062
1700	0.141	0.151	0.059	0.065
1800	0.136	0.146	0.060	0.066
1900	0.139	0.145	0.060	0.065
2000	0.138	0.135	0.062	0.067
2100	0.129	0.131	0.066	0.068
2200	0.124	0.124	0.063	0.073
2300	0.115	0.118	0.070	0.073
2400	0.114	0.117	0.071	0.070
2500	0.110	0.101	0.076	0.071

Table 9: Bulk graviton signal efficiency for high-purity (HP), and low-purity (LP) categories, in electron and muon channel separately, for several resonance mass hypotheses.

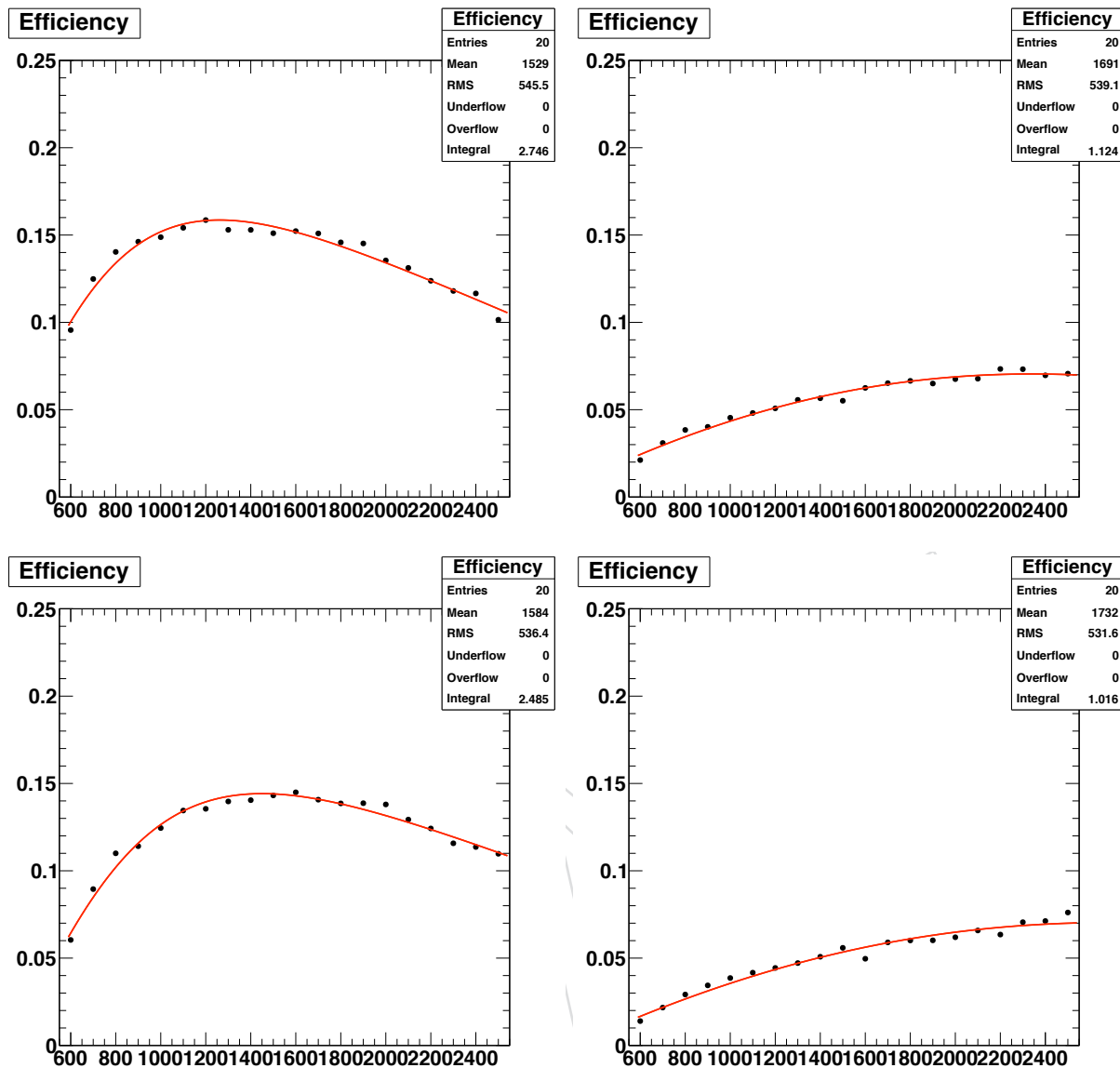


Figure 13: Parameterization of signal efficiency as a function of Graviton mass hypothesis in MU\_HP (top-left), MU\_LP (top-right), ELE\_HP (bottom-left), ELE\_LP (bottom-right)

## 188 5 Background estimate

189 We search for bumps in the  $m_{WW}$  spectrum due to new, heavy  $X \rightarrow WW$  resonances. This sec-  
 190 tion describes the methods used to derive both the normalization and the shape of the  $m_{WW}$  dis-  
 191 tribution for SM background events.

192 The background in the signal region is estimated from data (with the aid of MC for cross-checks  
 193 and corrections) using two different methods:

- 194 • **Main Method** - In the first method ( $\alpha$  method), the dominant  $W+jets$  background  
 195 prediction in the signal region is obtained from the data in the low-mass sideband  
 196 region ( $40 < m_{jet}^{pruned} < 65$  GeV), rescaled for an appropriate transfer function from  
 197 the sideband to the signal region derived from simulation. We use the group2 imple-  
 198 mentation for this method, which is the same choice we made for the approved PAS.  
 199 More details on the method can be found in Section 5.4 of [5]. The sub-dominant  
 200  $t\bar{t}$  and SM VV backgrounds are taken from simulation after correction for data/MC  
 201 scale factors. The procedure to get the scale factors is described in Section 5.3 of [5].
- 202 • **Cross-Check Method** - In the second method, we perform directly a “smoothness  
 203 test” to the  $m_{WW}$  distribution of data in the signal region ( $65 < m_{jet}^{pruned} < 105$  GeV),  
 204 and we search for bumps on top of an exponentially falling background spectrum,  
 205 which is described by an empirical parameterization. This is the cross-check method  
 206 of the analysis. More details on the method can be found in Section 8.2 of [4].

207 We do not describe again the analysis methods, but just report below the updated results for  
 208 each method.

### 209 5.1 Main Method - $\alpha$ Method

#### 210 5.1.1 $t\bar{t}$ control region

211 The  $t\bar{t}$  selection is described in Section 8.1.1 of [4]. We report some control plots in the following  
 212 Figures 14, 15, 16.

- 213 • The data/MC scale factors for  $t\bar{t}$  and single top background are reported in Table 10  
 214 for each category.
- 215 • We fit the  $W$ -jet mass distribution, for events that pass and fail the  $\tau_{21} < 0.5$  cut,  
 216 in data and MC to extract informations on the  $W$ -tag efficiency and the  $W$ -jet mass  
 217 peak (mean and  $\sigma$ ). The method is described in Section 5.3 of [5]; more plots and fits  
 218 can be found at [10] and in Figure 17. The data/MC scale factors for tagging a real  
 219 hadronic  $W$  are reported in Table 11 for the separate categories and combining also  
 220 electron and muon channels. The fitted mean and  $\sigma$  of the  $W$  mass peak in data and  
 221 MC is reported in Table 12 combining electron and muon channels.

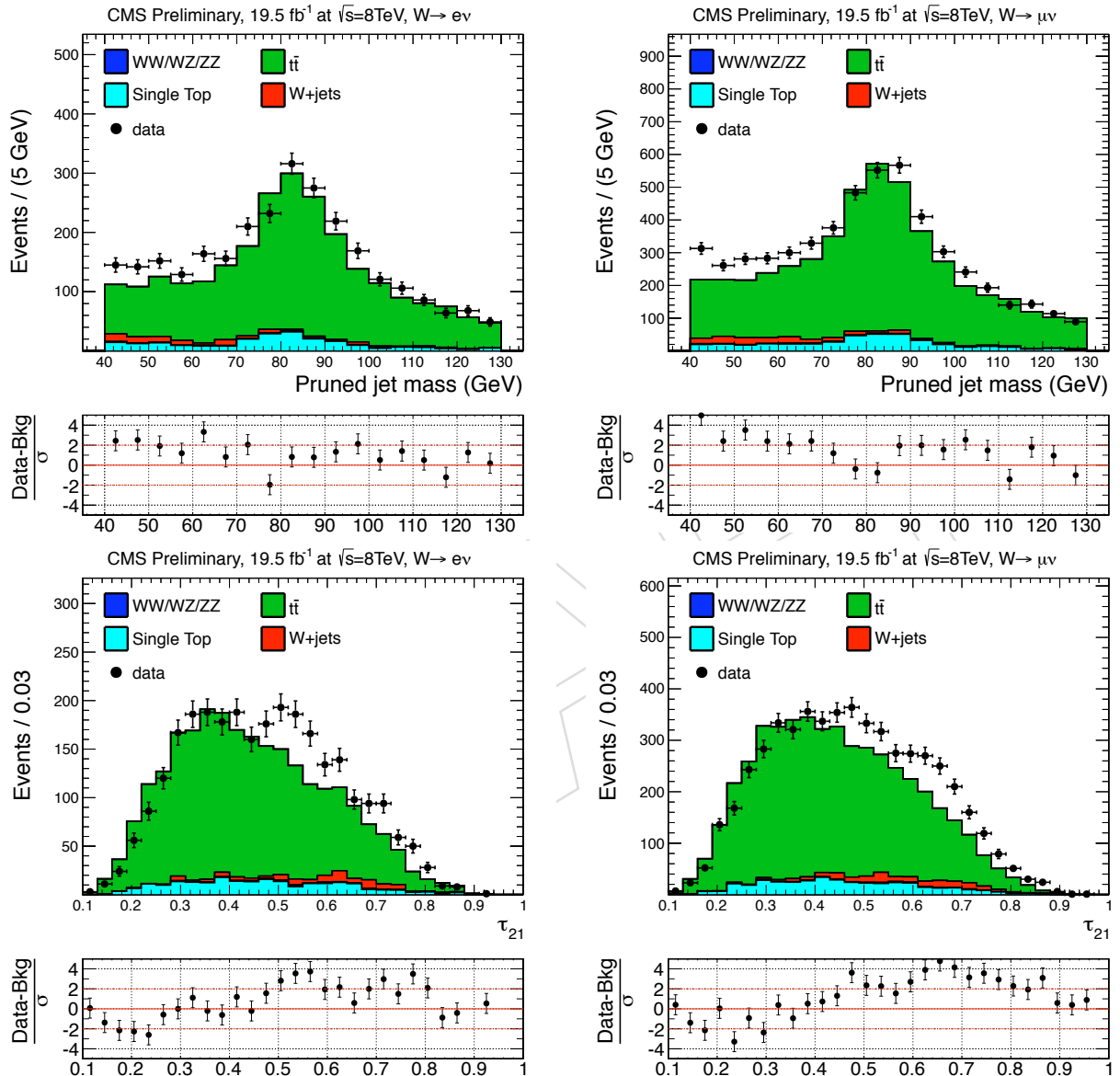


Figure 14:  $m_{jet}^{pruned}$  and  $\tau_{21}$  for electron channel (left) and muon channel (right) for events with  $40 < m_{jet}^{pruned} < 130$  GeV in the top control sample.

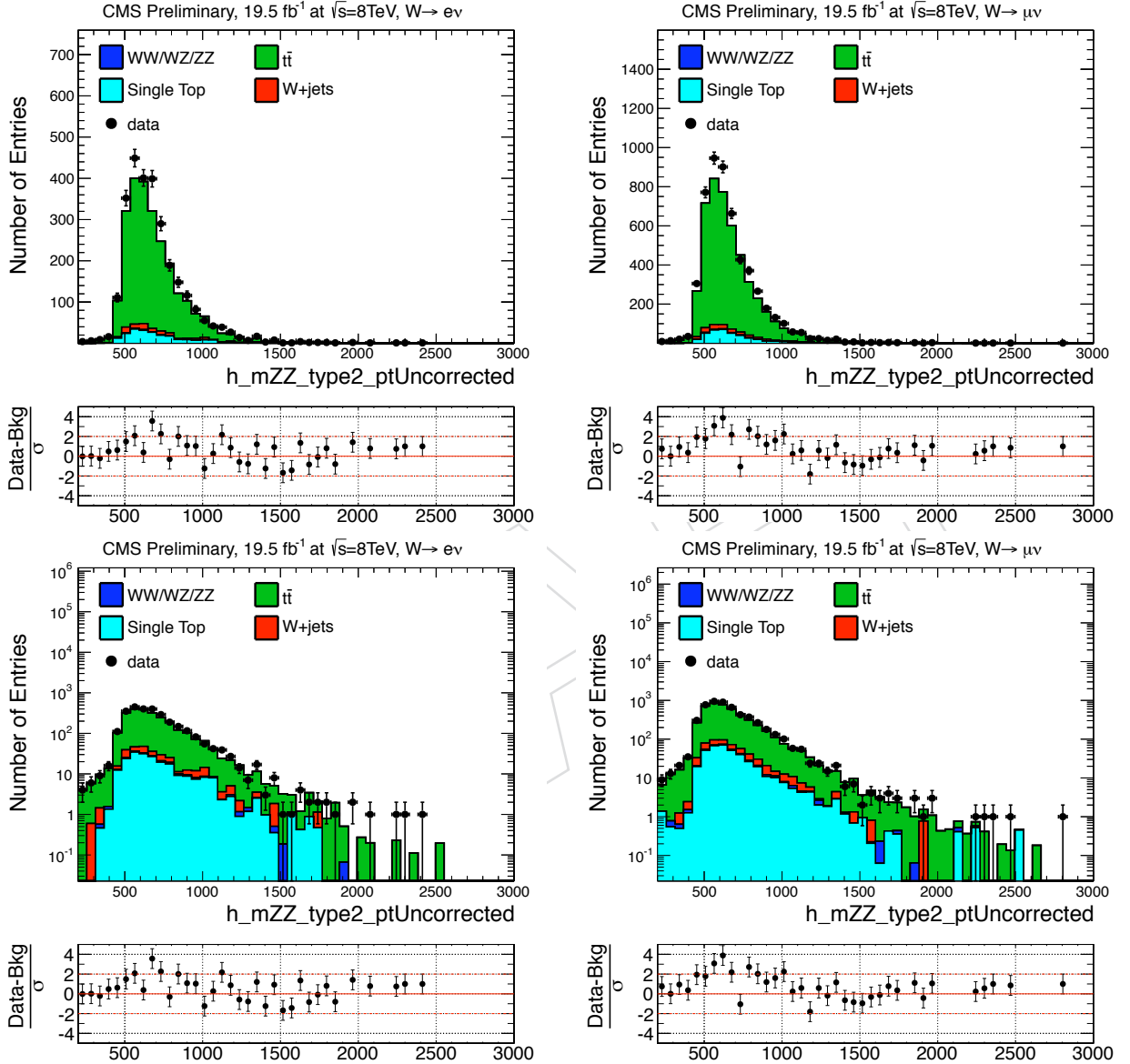


Figure 15:  $m_{WW}$  in linear and log scale for electron channel (left) and muon channel (right) for events with  $40 < m_{jet}^{pruned} < 130$  GeV in the top control sample.

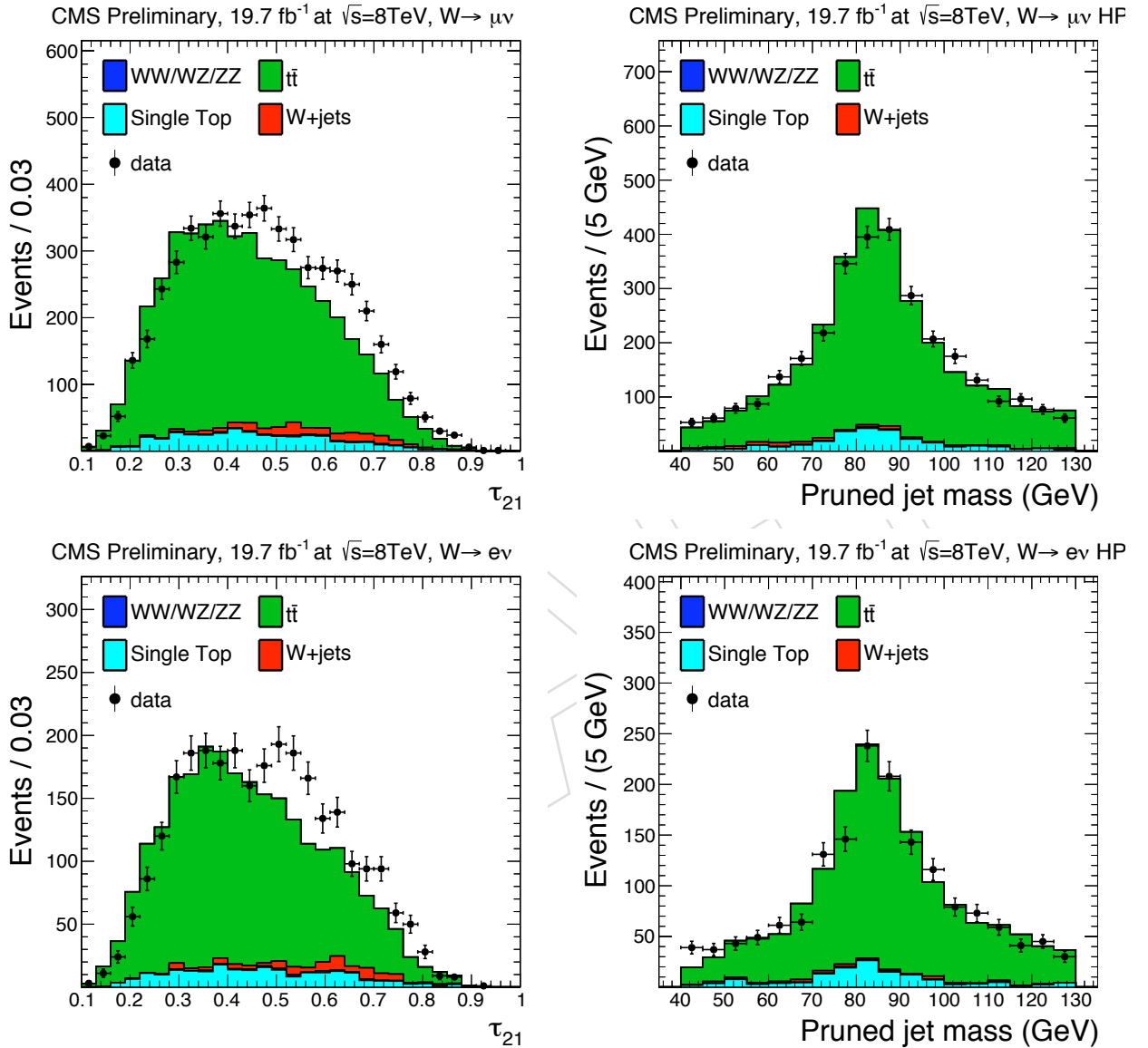


Figure 16: The  $\tau_2/\tau_1$  distribution in the top-enriched control sample is shown on the top left for the muon channel and bottom left for the electron channel. The pruned jet mass distribution in the top-enriched control sample is shown on the right after applying the  $\tau_2/\tau_1 < 0.5$  requirement, for muon (top) and electron channel (bottom).

Table 10: Scale factors for  $t\bar{t}$  and single top background MC derived from the top control sample.

Electron LP	Electron HP	Muon LP	Muon HP
$1.39 \pm 0.08$	$0.96 \pm 0.03$	$1.31 \pm 0.05$	$0.97 \pm 0.02$

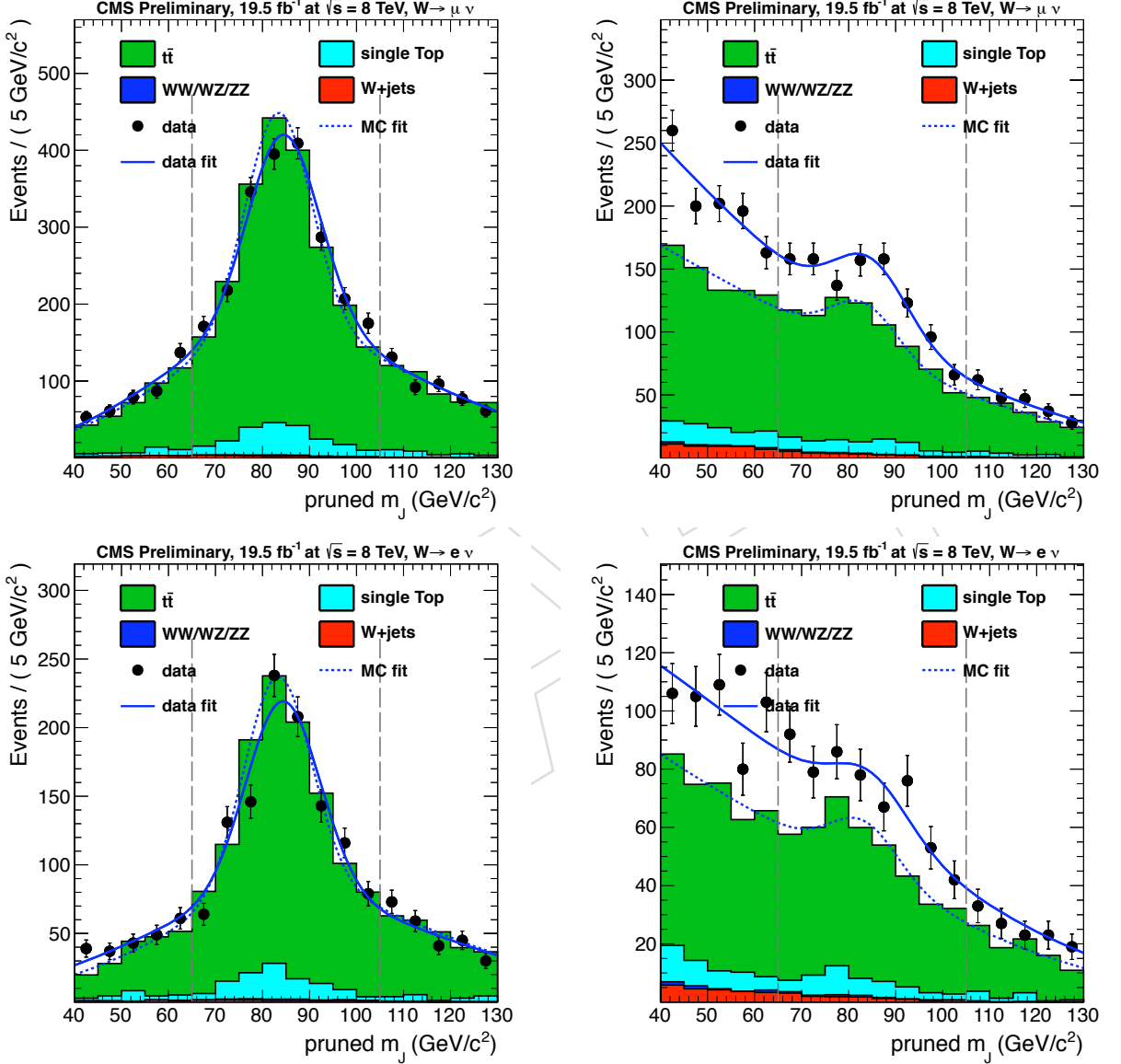


Figure 17: Fits to the W-jet mass distribution to extract scale factors of W-tagging and info on the W-jet mass peak. More details on the method are described in Section 5.3 of [5]. Events that PASS ( $\tau_{21} < 0.5$ ) or FAIL ( $\tau_{21} > 0.5$ ) the  $\tau_{21}$  requirement are shown. MU\_PASS (top-left), MU\_FAIL (top-right), ELE\_PASS (bottom-left), ELE\_FAIL (bottom-right).

Table 11: W-tag scale factors derived from the top control sample.

High Purity Category (HP)	Muon	Electron
$\varepsilon$ Data	$0.621 \pm 0.047$	$0.758 \pm 0.080$
$\varepsilon$ MC	$0.725 \pm 0.046$	$0.772 \pm 0.067$
Data/MC $\varepsilon$ SF	$0.855 \pm 0.085$	$0.981 \pm 0.134$
Data/MC $\varepsilon$ SF ( $e+\mu$ )		$0.89 \pm 0.08$

Low Purity Category (LP)	Muon	Electron
$\varepsilon$ Data	$0.376 \pm 0.067$	$0.242 \pm 0.095$
$\varepsilon$ MC	$0.274 \pm 0.055$	$0.227 \pm 0.074$
Data/MC $\varepsilon$ SF	$1.373 \pm 0.366$	$1.067 \pm 0.544$
Data/MC $\varepsilon$ SF ( $e+\mu$ )		$1.28 \pm 0.30$

Table 12: Fitted mean and  $\sigma$  of the W-jet mass peak in data and MC.

W-jet Mass Peak	Mean [GeV]	$\sigma$ [GeV]
Data	$84.7 \pm 0.4$	$7.9 \pm 0.6$
MC	$83.4 \pm 0.3$	$7.2 \pm 0.4$

222 **5.1.2 W+jets background estimation**

223 We report the updated results with the new rereco datasets.

- 224 • The fits to extract the normalization of the W+jets background are reported in Figure 18.
- 225 • The  $\alpha$  extrapolation functions are reported in Figure 19.
- 226 • The fits to the data in the sideband are shown in Figure 20.
- 227 • The final background prediction compared to the data is shown in Figure 21. In these plots we overlay also the background prediction from the cross-check method, described in the next section, to show the good agreement between the two.

In this analysis update, we use the leveled exponential function, Eq. 2, to fit the W+jets background in order to synchronize with the EXO-12-022 analysis (ZZ) and with the cross-check method. In the previous version a different modified exponential function was used, Eq. 3. The latter function is still used an alternative function for cross checks.

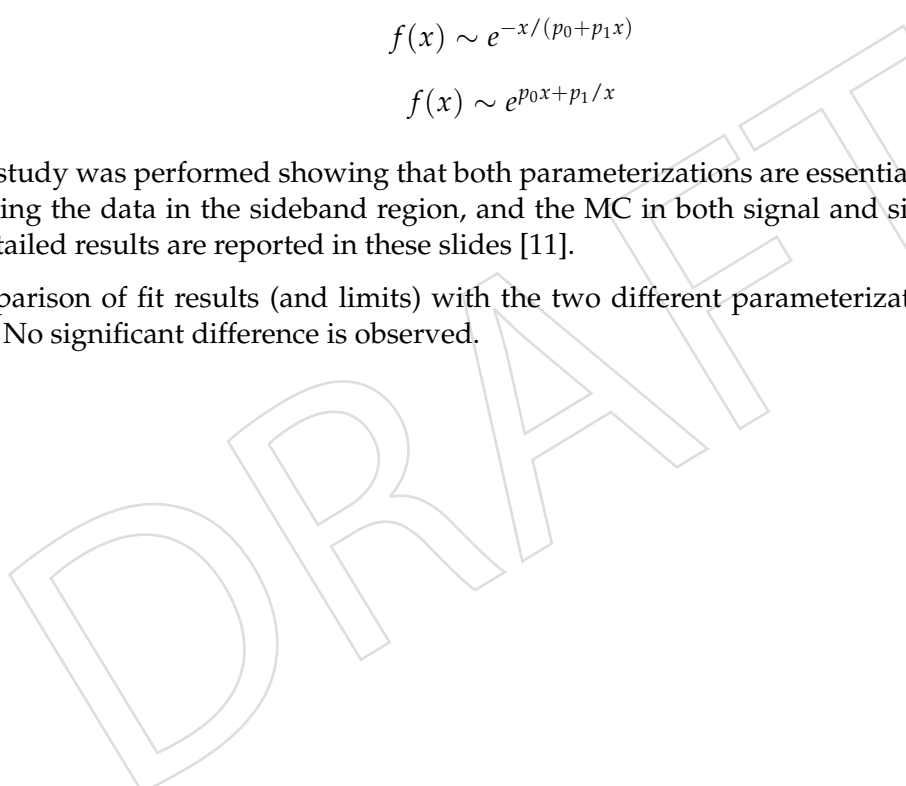
$$f(x) \sim e^{-x/(p_0+p_1x)} \quad (2)$$

$$f(x) \sim e^{p_0x+p_1/x} \quad (3)$$

231 A bias study was performed showing that both parameterizations are essentially equivalent in describing the data in the sideband region, and the MC in both signal and sideband regions.

232 The detailed results are reported in these slides [11].

233 A comparison of fit results (and limits) with the two different parameterizations is reported at [12]. No significant difference is observed.



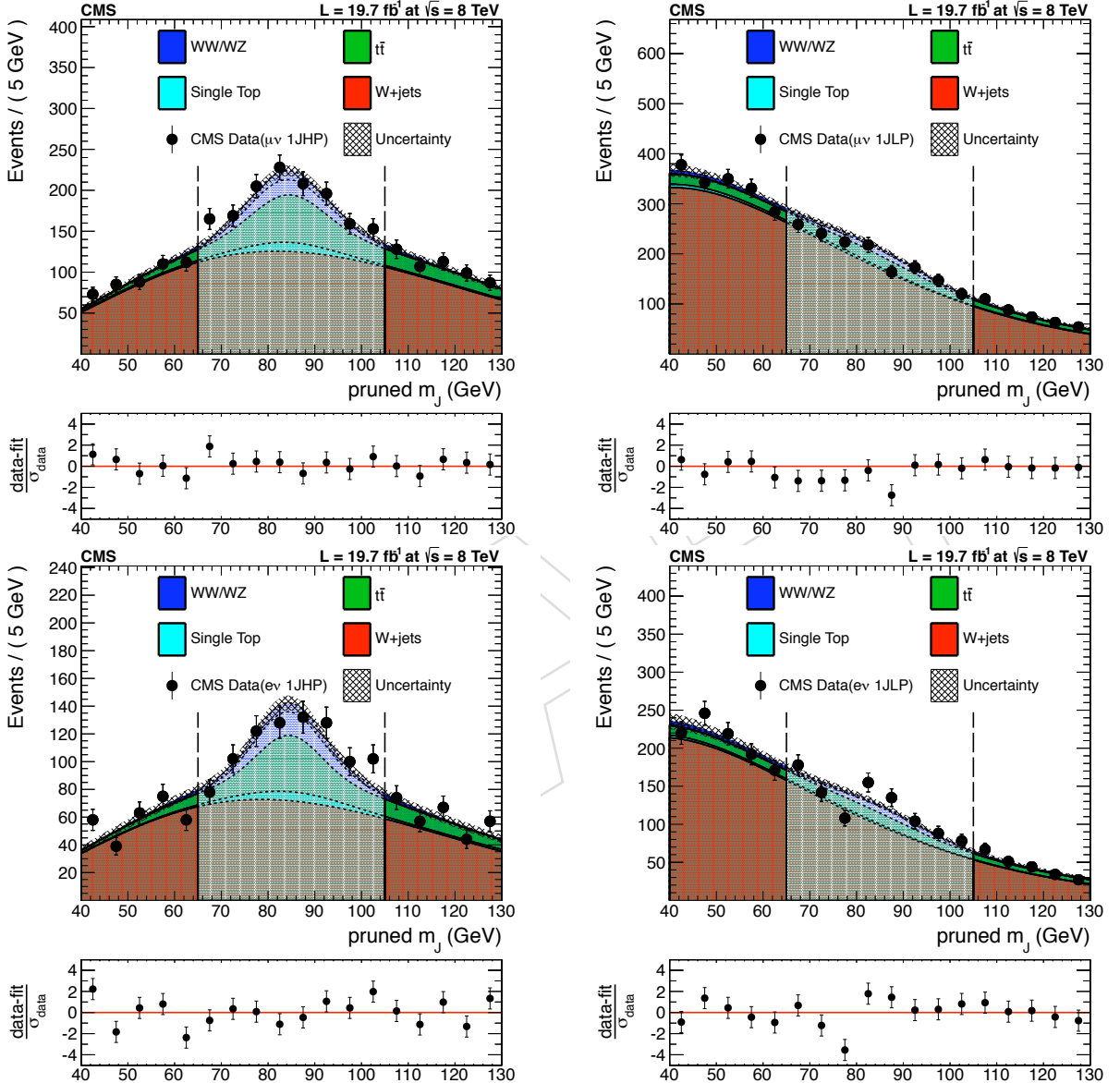


Figure 18: Fits to extract the normalization of the W+jets background. MU\_HP (top-left), MU\_LP (top-right), ELE\_HP (bottom-left), ELE\_LP (bottom-right).

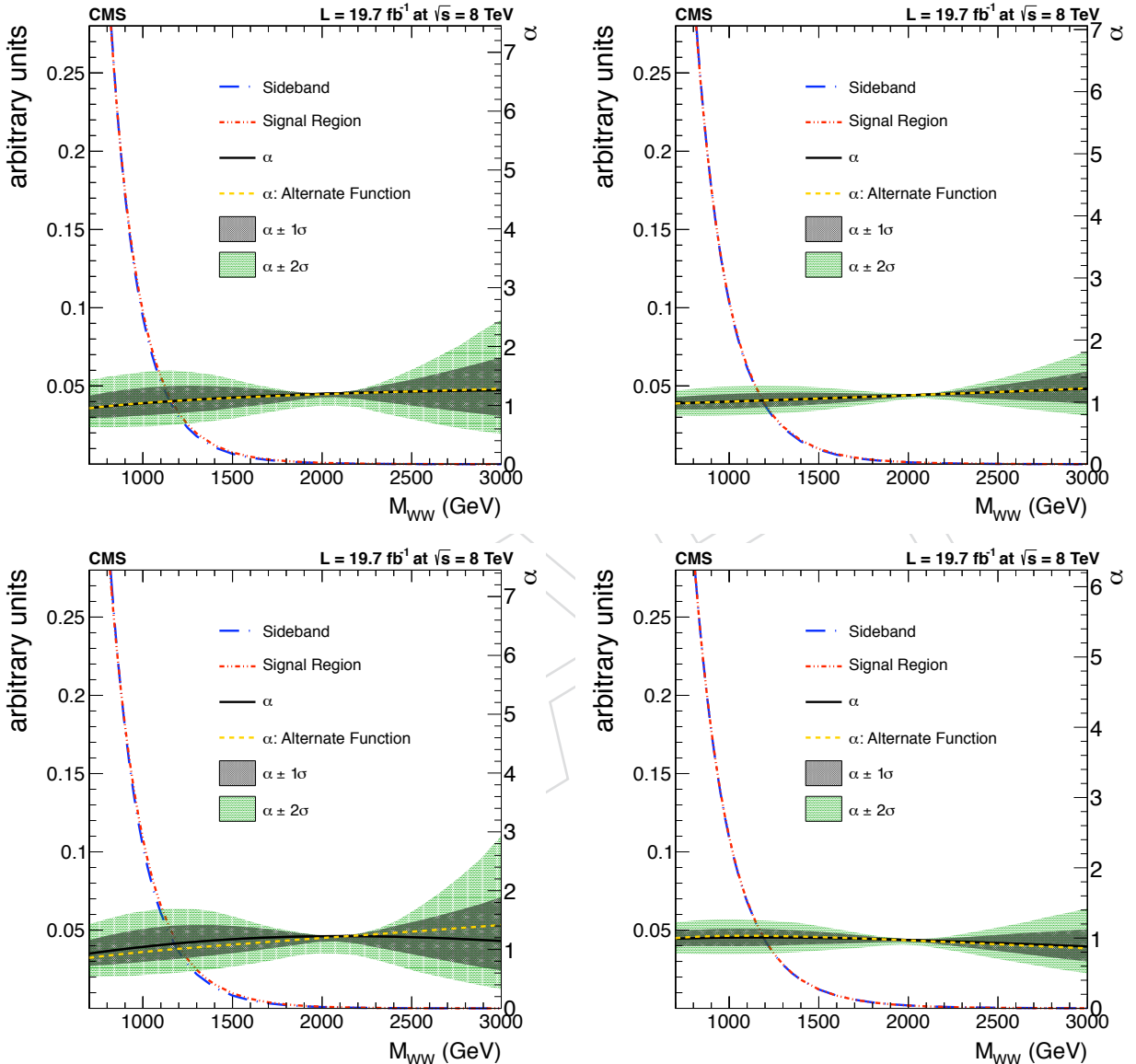


Figure 19:  $\alpha$  extrapolation functions. MU\_HP (top-left), MU\_LP (top-right), ELE\_HP (bottom-left), ELE\_LP (bottom-right).

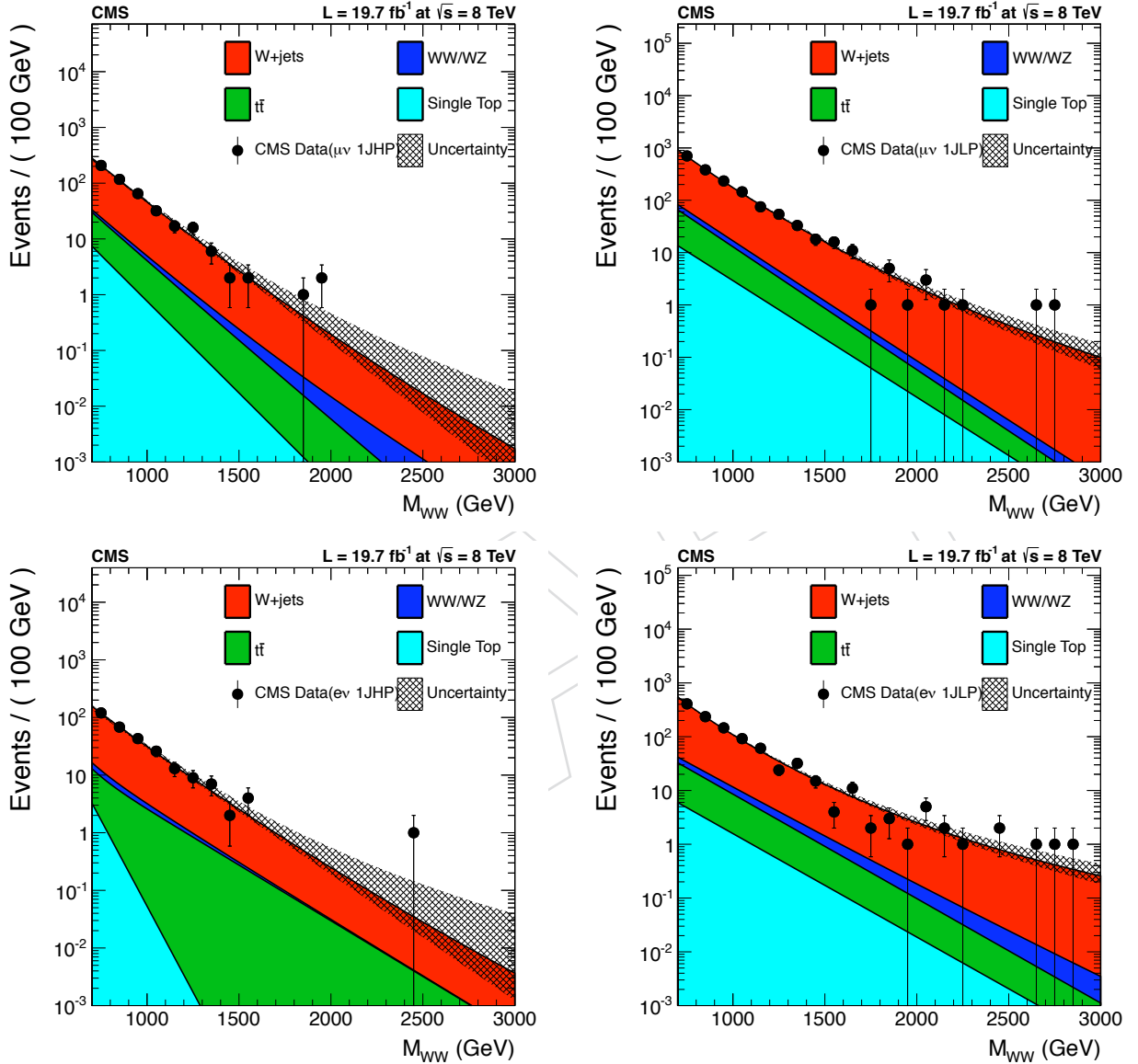


Figure 20: Fits to data in sideband region. MU\\_HP (top-left), MU\\_LP (top-right), ELE\\_HP (bottom-left), ELE\\_LP (bottom-right).

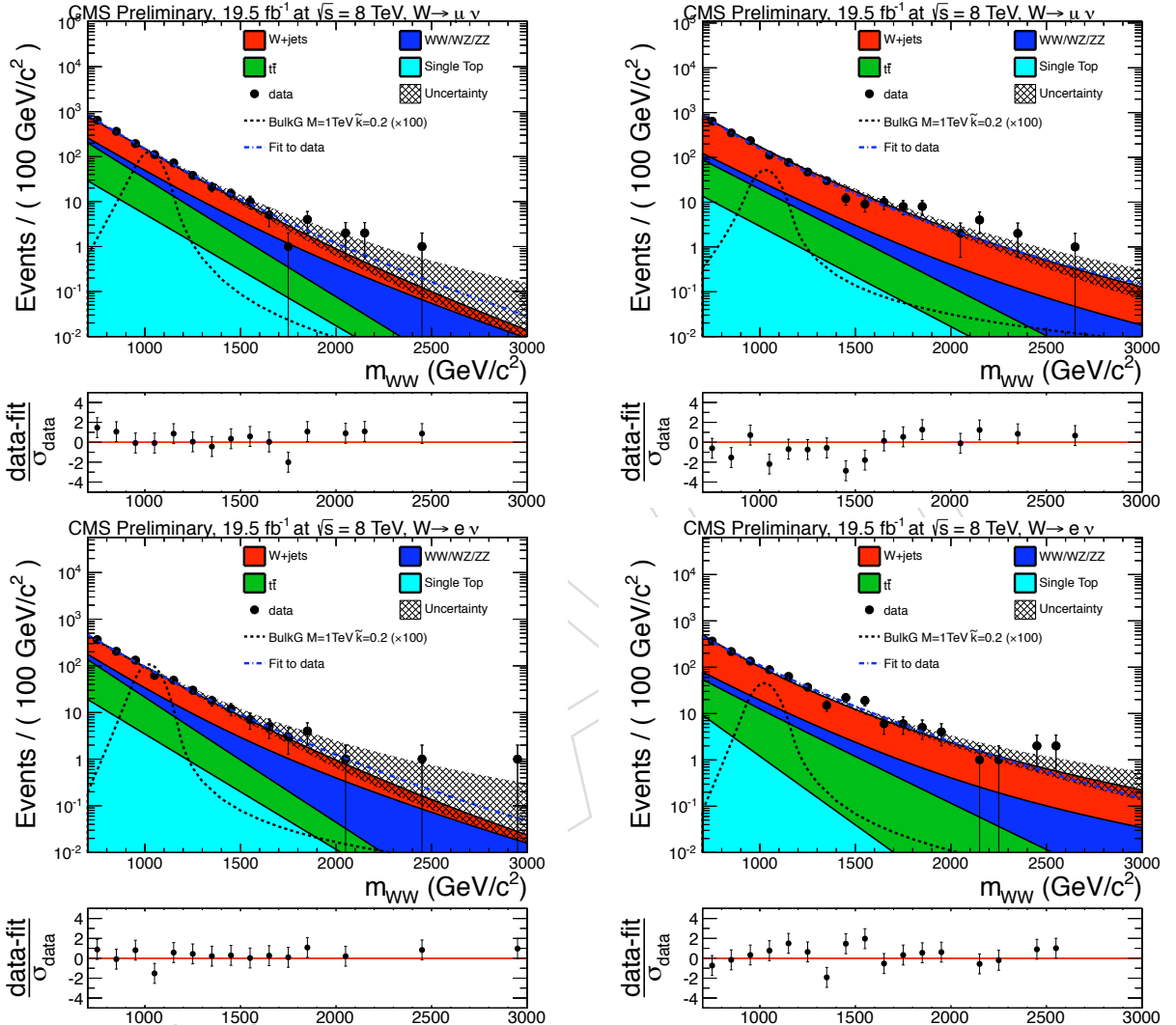


Figure 21: Fits to data in signal region. MU\_HP (top-left), MU\_LP (top-right), ELE\_HP (bottom-left), ELE\_LP (bottom-right). The bulk graviton signal cross section should be multiplied by a factor 1/4, due to a bug recently found in the theoretical calculation. More details can be found in Section 3 of [9]. We don't plan to update this AN. The values in the EXO-13-009 will be correct.

236 **5.2 Cross-Check Method -  $m_{WW}$  Smoothness Test**

237 The background-only fits using the leveled exponential function of Eq. 2 for the smoothness  
 238 test method are reported in Figure 22. Details on the fit parameters and the fit quality are  
 239 reported. The best fit line is also reported in Figure 21 where it's compared to the  $\alpha$  method in  
 240 each category.

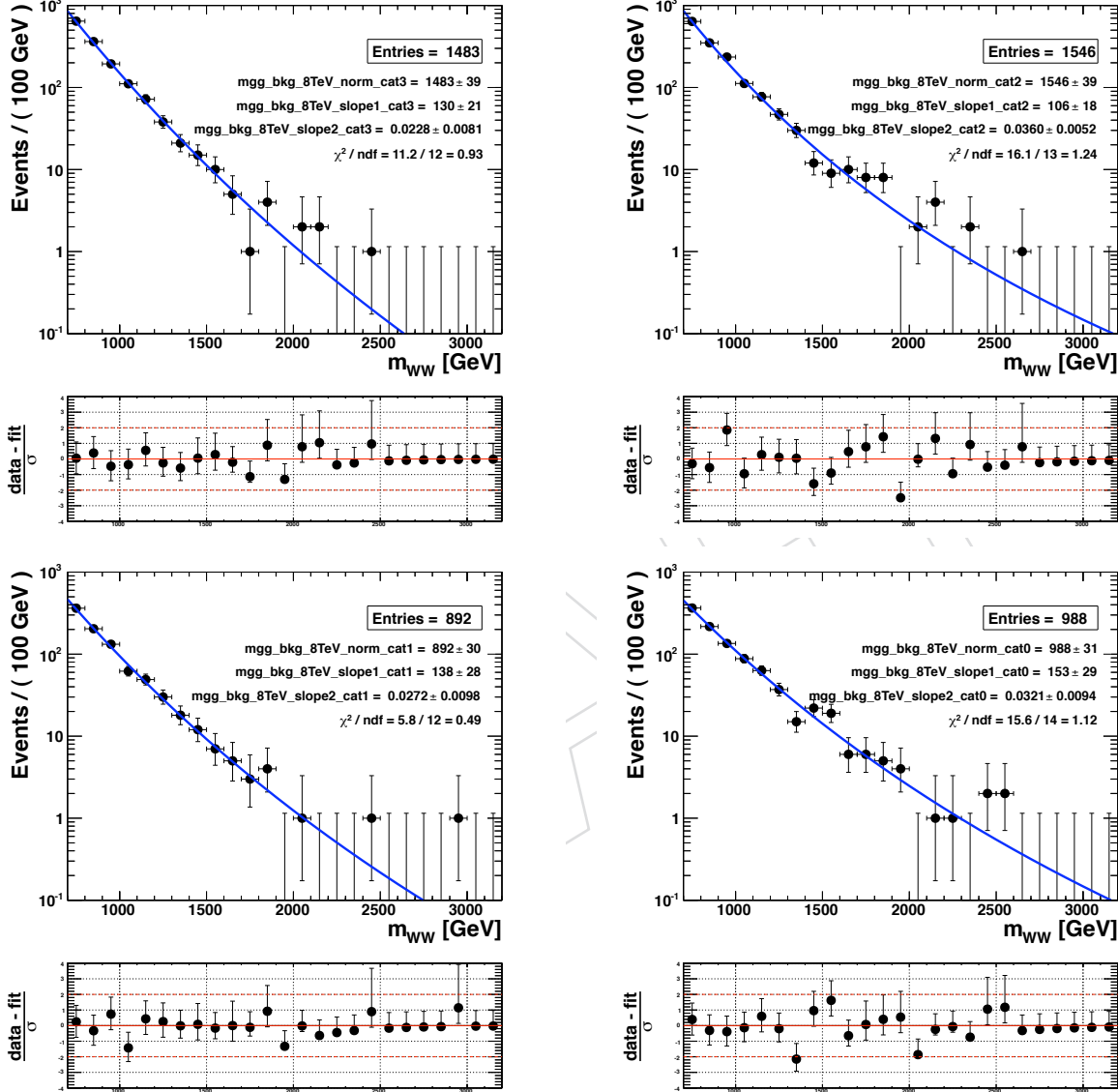


Figure 22: Background-only fits to data in signal region using the smoothness test. MU\_HP (top-left), MU\_LP (top-right), ELE\_HP (bottom-left), ELE\_LP (bottom-right).

## 241 6 Systematic Uncertainties

242 The methods to derive systematic uncertainties did not change compared to the approved re-  
243 sult of this analysis.

- 244 • **Background uncertainties for main method**,  $\alpha \rightarrow$  the method is described in Section  
245 6.1, 6.2, and 6.3 of [5] and the results updated using the new data and MC samples.
- 246 • **Background uncertainties for cross-check method ( $m_{WW}$  smoothness test)** → the  
247 method is described in Section 9.1.2 of [4] and the results updated using the new  
248 data samples.
- 249 • **Uncertainties on signal normalization and signal shape** → the method is described  
250 in Sections 9.2 and 9.3 of [4]. The results are reported in Table 13. These are the same  
251 numbers used for the approved PAS. We did not update to new jet energy scale  
252 uncertainties. This is a conservative approach since the jet energy scale uncertainties  
253 are slightly reduced in the last global tag compared to the approved results. We  
254 updated however the W-tag efficiency uncertainties with the new numbers reported  
255 in Table 11.
- 256 • **Luminosity uncertainty** is updated (now 2.6%).

Table 13: Summary of sources of systematic uncertainties and their impact on the number of signal events expected after full selection and on the reconstructed  $m_{WW}$  signal shape (peak position and width). The total uncertainty is reported as the sum in quadrature of the different terms. See text for more details.

Source of Syst. Uncert.	Number of Signal Events [%]	$m_{WW}$ Signal Shape	
		Mean [%]	Width [%]
Electron energy (Muon momentum) scale	0.2 (0.7)	< 0.1	0.1 (0.5)
Electron energy (Muon momentum) resolution	< 0.1	< 0.1	0.1
Jet energy scale	1–3	1.3	2–3
Jet energy resolution	0.3	< 0.1	3
Unclustered energy scale	0.1	< 0.1	3–1
$E_T^{\text{miss}}$ scale and resolution	Included in lepton/jet/unclust.en. uncert.		
Trigger	1	-	-
Electron (Muon) identification/isolation efficiency	3 (1)	-	-
W-tagging efficiency HP (LP)	9.5 (24)	-	-
b-tag identification efficiency	< 0.2	-	-
Pileup modeling	0.5	-	-
Integrated luminosity	2.6	-	-
Total Syst. Uncert. HP (LP)	10–11 (24–25)	1.3	4.5

## 257 7 Results

258 In this section we present the limits for the narrow resonance case using the bulk graviton  
 259 as model benchmark. For the limits we followed the modified frequentist prescription de-  
 260 scribed in [13, 14] ( $CL_S$ ). Here we use Asymptotic  $CL_S$  [15]. Systematic uncertainties are  
 261 treated as nuisance parameters and profiled in the statistical interpretation. For the implemen-  
 262 tation of the statistical analysis of the WW results stand-alone, we use the Higgs combination  
 263 tool [16] in CMSSW\_5\_3\_9. The statistical combination with other analyses is performed with  
 264 CMSSW\_6\_1\_1. We plan to move to CMSSW\_6\_1\_1 consistently.

### 265 7.1 Limits - Main Method $\alpha$

266 Figure 23 shows the 95% CL upper limits on the cross section of the process  $pp \rightarrow X \rightarrow WW$   
 267 combining the four event categories as a function of the resonance mass. Figure 24 shows the  
 268 limits separately for the 4 categories considered in this analysis.

269 By comparing the combination of the LP and HP categories for a given lepton flavour and  
 270 the limits for the LP and HP separately, it can be appreciated how the sensitivity of the HP  
 271 category is the dominant one. The LP one contributes only marginally to the final sensitivity of  
 272 the analysis and only at high values of the resonance mass hypothesis (above 2 TeV).

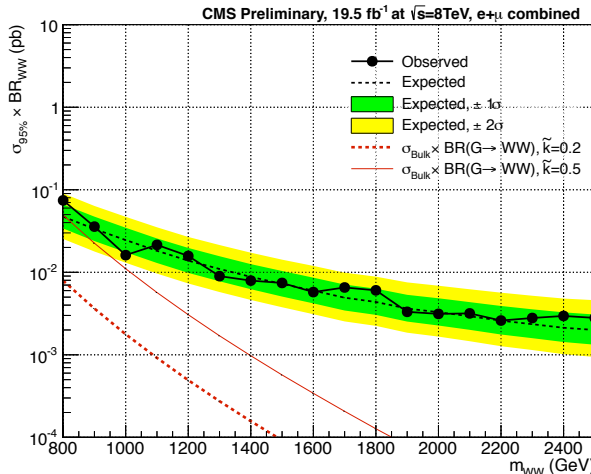


Figure 23: Main Method  $\alpha$  - All analysis categories combined - Observed (solid) and expected (dashed) 95% CL upper limit on the product of the graviton production cross section and the branching fraction of  $G^* \rightarrow WW$  using  $19.7 \text{ fb}^{-1}$  of data. The 68% and 95% ranges of expectation are also shown with green and yellow bands. The theoretical cross section times BR for  $G^* \rightarrow WW$  is shown as a red dashed (solid) curve for  $\tilde{k} = 0.2$  ( $\tilde{k} = 0.5$ ). **The bulk graviton signal cross section should be multiplied by a factor 1/4, due to a bug recently found in the theoretical calculation. More details can be found in Section 3 of [9]. We don't plan to update this AN. The values in the EXO-13-009 will be correct.**

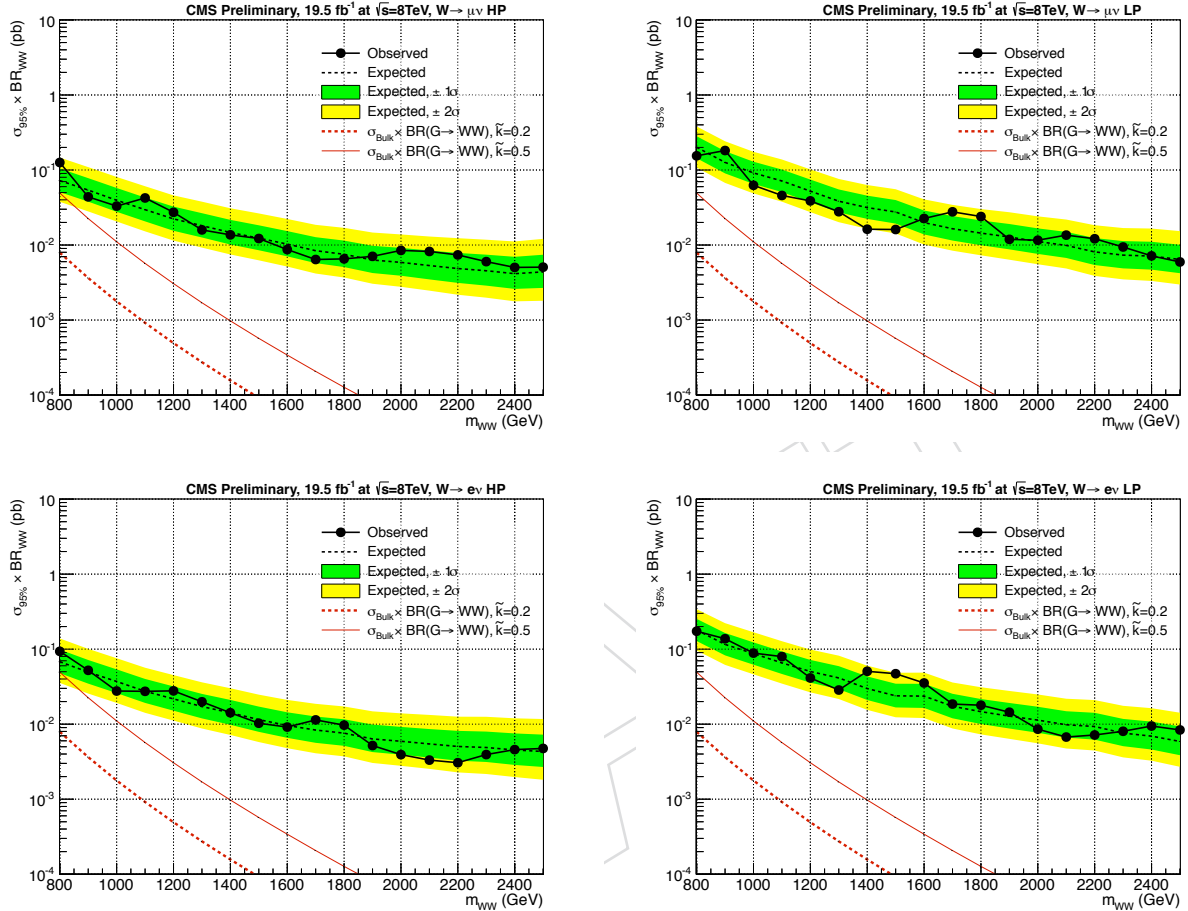


Figure 24: Main Method  $\alpha$  - MU\_HP (top-left), MU\_LP (top-right), ELE\_HP (bottom-left), ELE\_LP (bottom-right) - Observed (solid) and expected (dashed) 95% CL upper limit on the product of the graviton production cross section and the branching fraction of  $G^* \rightarrow WW$  using  $19.7 \text{ fb}^{-1}$  of data. The 68% and 95% ranges of expectation are also shown with green and yellow bands. The theoretical cross section times BR for  $G^* \rightarrow WW$  is shown as a red dashed (solid) curve for  $\tilde{k} = 0.2$  ( $\tilde{k} = 0.5$ ). The bulk graviton signal cross section should be multiplied by a factor 1/4, due to a bug recently found in the theoretical calculation. More details can be found in Section 3 of [9]. We don't plan to update this AN. The values in the EXO-13-009 will be correct.

<sup>273</sup> **7.2 Limits - Cross-Check Method ( $m_{WW}$ smoothness test)**

<sup>274</sup> Figure 25 shows the 95% CL upper limits on the cross section of the process  $pp \rightarrow X \rightarrow WW$   
<sup>275</sup> combining the four event categories as a function of the resonance mass. Figure 26 shows the  
<sup>276</sup> limits separately for the 4 categories considered in this analysis.

<sup>277</sup> By comparing the combination of the LP and HP categories for a given lepton flavour and  
<sup>278</sup> the limits for the LP and HP separately, it can be appreciated how the sensitivity of the HP  
<sup>279</sup> category is the dominant one. The LP one contributes only marginally to the final sensitivity of  
<sup>280</sup> the analysis and only at high values of the resonance mass hypothesis (above 2 TeV).

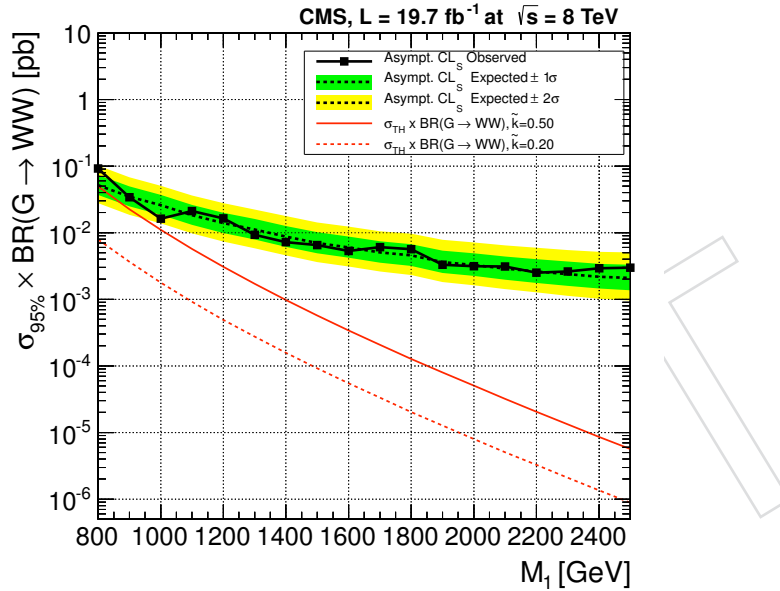


Figure 25: Cross-Check Method ( $m_{WW}$ smoothness test) - All analysis categories combined - Observed (solid) and expected (dashed) 95% CL upper limit on the product of the graviton production cross section and the branching fraction of  $G^* \rightarrow WW$  using  $19.7 \text{ fb}^{-1}$  of data. The 68% and 95% ranges of expectation are also shown with green and yellow bands. The theoretical cross section times BR for  $G^* \rightarrow WW$  is shown as a red dashed (solid) curve for  $\tilde{k} = 0.2$  ( $\tilde{k} = 0.5$ ). The bulk graviton signal cross section should be multiplied by a factor 1/4, due to a bug recently found in the theoretical calculation. More details can be found in Section 3 of [9]. We don't plan to update this AN. The values in the EXO-13-009 will be correct.

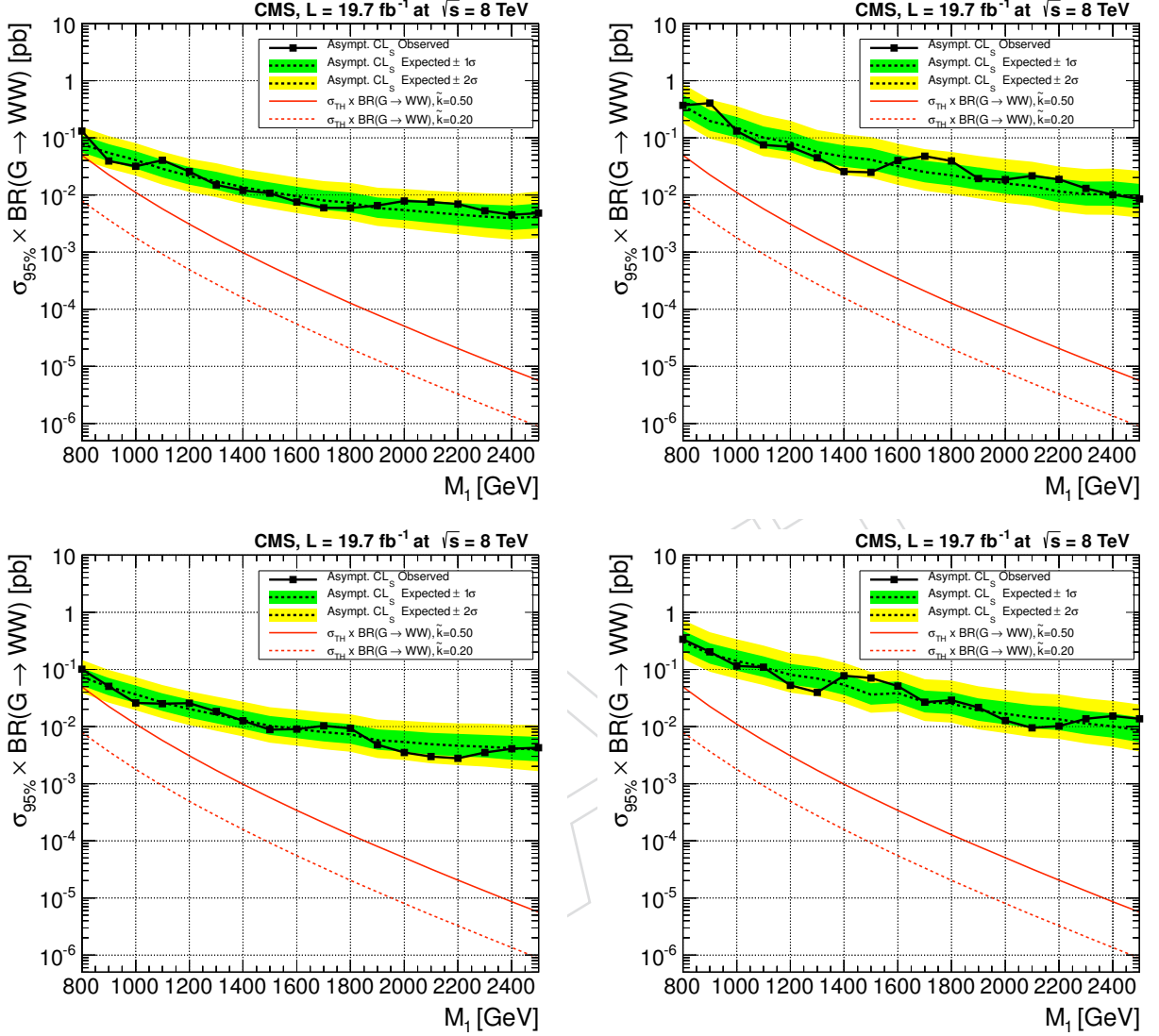


Figure 26: Cross-Check Method ( $m_{WW}$  smoothness test) - MU\_HP (top-left), MU\_LP (top-right), ELE\_HP (bottom-left), ELE\_LP (bottom-right) - Observed (solid) and expected (dashed) 95% CL upper limit on the product of the graviton production cross section and the branching fraction of  $G^* \rightarrow WW$  using  $19.7 \text{ fb}^{-1}$  of data. The 68% and 95% ranges of expectation are also shown with green and yellow bands. The theoretical cross section times BR for  $G^* \rightarrow WW$  is shown as a red dashed (solid) curve for  $\tilde{k} = 0.2$  ( $\tilde{k} = 0.5$ ). **The bulk graviton signal cross section should be multiplied by a factor 1/4, due to a bug recently found in the theoretical calculation. More details can be found in Section 3 of [9]. We don't plan to update this AN. The values in the EXO-13-009 will be correct.**

### 281 7.3 Limits - Comparison between two methods

282 Figure 27 shows the direct comparison between the limits obtained with the main method  $\alpha$   
 283 and the cross-check method ( $m_{WW}$ smoothness test). The results are in very good agreement  
 284 within less than 10%. It should be noted that the two background predictions are completely  
 285 independent in the two cases, thus giving very good confidence on the final results of this search.

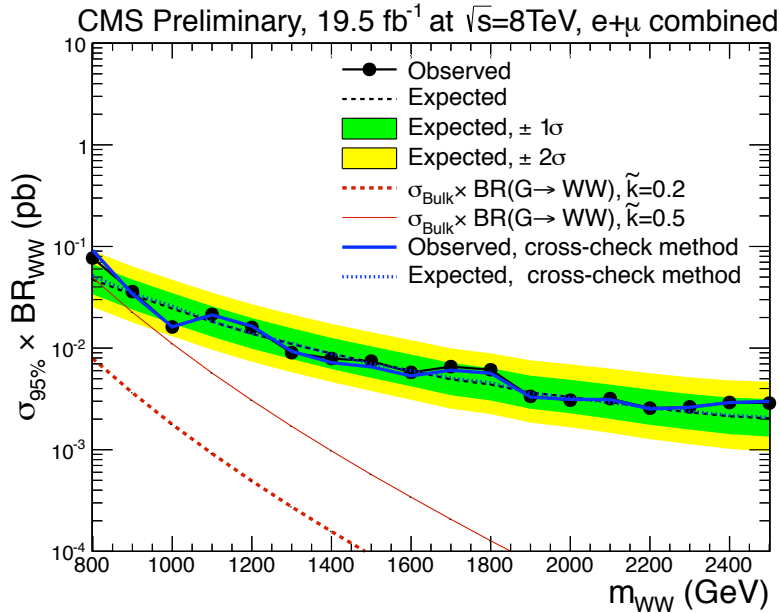


Figure 27: Main Method  $\alpha$  vs Cross-Check Method ( $m_{WW}$ smoothness test) - All analysis categories combined - Observed (solid) and expected (dashed) 95% CL upper limit on the product of the graviton production cross section and the branching fraction of  $G^* \rightarrow WW$  using  $19.7 \text{ fb}^{-1}$  of data. The 68% and 95% ranges of expectation are also shown with green and yellow bands. The theoretical cross section times BR for  $G^* \rightarrow WW$  is shown as a red dashed (solid) curve for  $\tilde{k} = 0.2$  ( $\tilde{k} = 0.5$ ). The bulk graviton signal cross section should be multiplied by a factor 1/4, due to a bug recently found in the theoretical calculation. More details can be found in Section 3 of [9]. We don't plan to update this AN. The values in the EXO-13-009 will be correct.

### 286 7.4 Statistical combination with other analyses

287 More analyses at CMS investigated the final state with two SM gauge bosons in the final state.  
 288 In particular, other two analyses exploit jet substructure techniques and set limits on narrow  
 289 bulk gravitons too:

- 290 • EXO-12-022 (“Search for a BSM resonance decaying to Z vector bosons in the semilep-  
 291 tonic final state”) [2, 9]
- 292 • EXO-12-024 (“Search for heavy resonances in the W/Z-tagged dijet mass spectrum  
 293 in pp collisions at 8 TeV”) [3]

294 In particular, the connections with the analysis EXO-12-022 are evident under many aspects,  
 295 from the treatment of physics objects (both leptons and jets) to the estimation of background.  
 296 Not only these analyses are similar from the experimental point of view, but they all set limits  
 297 on the same narrow bulk graviton model. The bulk graviton model represents a good bench-

mark for this type of searches because it is a well-defined model, with a small number of free parameters, still able to accommodate new physics without strong tensions with the electro-weak precision tests. Therefore, it is natural to try to maximize our sensitivity to this model by performing a statistical combination of the three results, along the lines of what is done for Higgs searches [16–18]. Not only this strategy allows us to set the most stringent limits on bulk gravitons, it also shows neatly the capabilities of CMS and the coordination in its physics program.

The three analyses considered in the combination use the same techniques for reconstructing leptons (high-PT electrons and muons), jets (CA8 jets) and V-jets (jet pruning and N-subjettiness ratio). The standard tools provided by the Higgs Combination group are used for the combination. In this procedure it is important to assess the sources of systematic uncertainty that are fully correlated between the analyses. The list of systematics fully correlated between all the three analyses is summarized in Table 14. Some systematic uncertainties involving the leptons are shared only between the semi-leptonic analyses (EXO-12-021 and EXO-12-022) and are listed in Table 15.

Table 14: List of systematics uncertainties correlated at 100% between the three analyses entering the combination. The entries marked with a star are systematics of very small size ( $< 1\%$ ) in all the analyses, and are considered only for completeness.

Systematic Uncertainty	Type
Jet Energy Scale	Normalization
Jet Energy Resolution	Normalization
V-tagging scale factors	Normalization
Luminosity	Normalization
Jet Energy Scale	Signal shape (mean)
Jet Energy Resolution [*]	Signal shape (mean)
Jet Energy Scale	Signal shape (sigma)
Jet Energy Resolution	Signal shape (sigma)

The limits are set on the production cross section for narrow bulk graviton, without any further branching ratio applied. The decay rates of the graviton to WW and ZZ are calculated with a dedicated CalcHep routine <sup>1</sup>, and kept fixed to the model prediction during the statistical analysis. The 95% C.L. exclusions for the three individual analyses are presented in Figure 28. One can notice how the semi-leptonic WW analysis is the most sensitive one. At low values of the graviton mass,  $M_{G^*}$ , the search in the semi-leptonic ZZ final state is equally competitive. The semi-leptonic ZZ search loses power with increasing mass because of the lower branching ratio to this final state. With increasing  $M_{G^*}$ , the fully-hadronic, double V-jet analysis becomes more and more relevant thanks to the larger BR.

The analyses cover different  $M_{G^*}$  ranges: semi-leptonic ZZ starts to set limits at  $M_{G^*} = 600$  GeV, the semi-leptonic WW starts at  $M_{G^*} = 800$  GeV, while the fully-hadronic starts at  $M_{G^*} = 1000$  GeV (the higher starting point of the fully-hadronic is due to the trigger thresholds). This means that in the final combination the analyses will be included progressively as a function of  $M_{G^*}$ . The resulting limits are shown in Figure 29. Despite the dominance of the general semi-leptonic channel, the statistical combination improves the results and allows to exclude larger graviton masses compared to what could have been achieved by the single anal-

<sup>1</sup>The routine is available at <http://cp3-origins.dk/research/units/ed-tools>.

Table 15: List of systematics uncertainties correlated at 100% between the two semi-leptonic analyses [1] and [2]. The entries marked with a star are systematics of very small size ( $< 1\%$ ) in all the analyses, and are considered only for completeness.

Systematic Uncertainty	Type
Electron reco and ID eff.	Normalization
Electron Scale [*]	Normalization
Electron Resolution [*]	Normalization
Muon reco and ID eff.	Normalization
Muon Scale [*]	Normalization
Muon Resolution [*]	Normalization
Electron Scale	Signal shape (mean)
Electron Resolution	Signal shape (mean)
Muon Scale [*]	Signal shape (mean)
Muon Resolution [*]	Signal shape (mean)
Electron Scale [*]	Signal shape (sigma)
Electron Resolution [*]	Signal shape (sigma)
Muon Scale	Signal shape (sigma)
Muon Resolution [*]	Signal shape (sigma)

329   yses alone. The range of graviton masses excluded at 95% C.L. goes from 600 GeV to 1200 GeV  
 330   for a value of the model parameter  $k/M_{Pl} = 0.5$ .

331   The behavior of the limits and of the combination can be studied in more detail looking at Fig-  
 332   ure 30. The expected sensitivity of WW is improved by about a relative 10% after the inclusion  
 333   of the other semi-leptonic analysis. Beginning at  $M_{G^*} = 1500$  GeV, the fully-hadronic analysis  
 334   plays a significant role, improving the total limit by approximately 40%, relative to the semi-  
 335   leptonic only upper limit. The scan of the p-value as a function of the mass is presented in  
 336   Figure 31 and shows only very mild excess, none of them statistically significant.

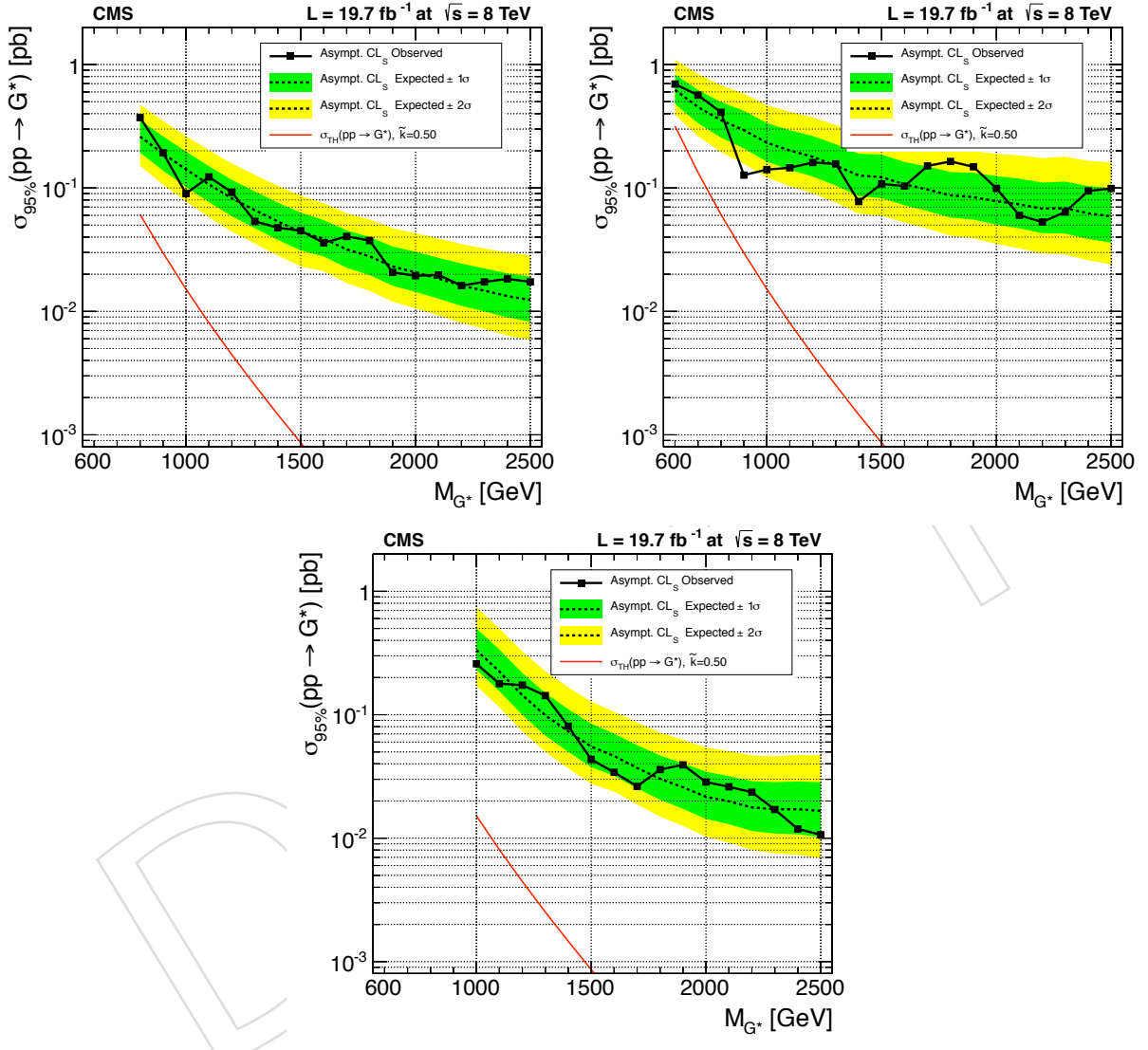


Figure 28: Exclusion limits on the production cross section for narrow bulk gravitons for the individual channels: WW semi-leptonic (this analysis, top left), ZZ semi-leptonic ([2], top right), and VV fully hadronic ([3], bottom center). Exclusion limits at 95% C.L. were calculated with the asymptotic  $CL_s$  method.

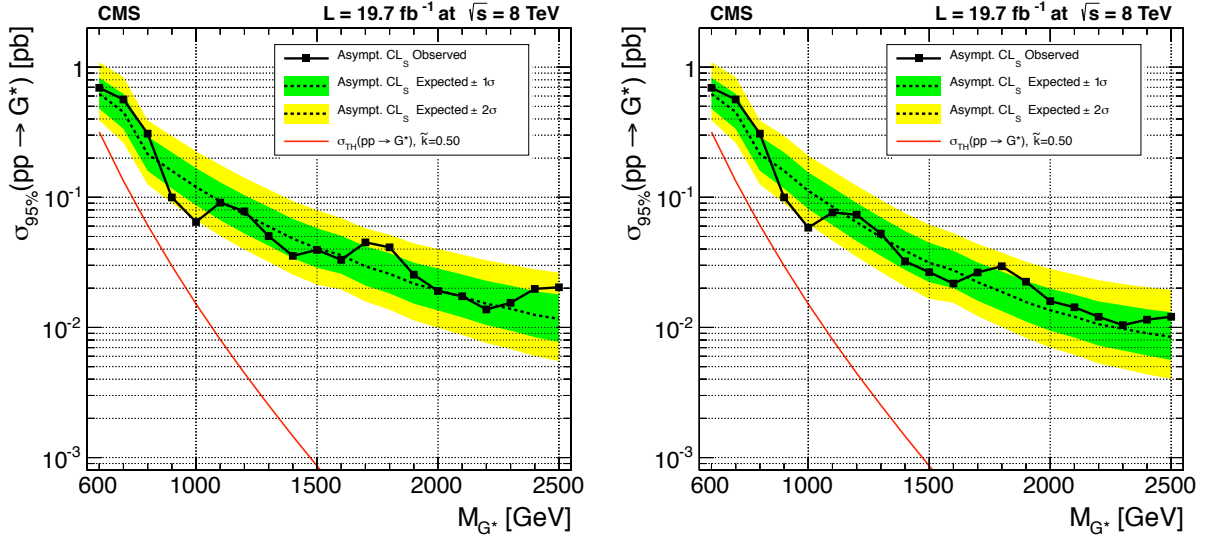


Figure 29: Exclusion limits on the production cross section for narrow bulk gravitons for the combination of different analysis. Left: combination of semi-leptonic channels, WW semi-leptonic (this analysis) and ZZ semi-leptonic ([2]). Right: full combination, including the semi-leptonic channels and the VV fully hadronic search ([3]). Exclusion limits at 95% C.L. were calculated with the asymptotic  $CL_s$  method.

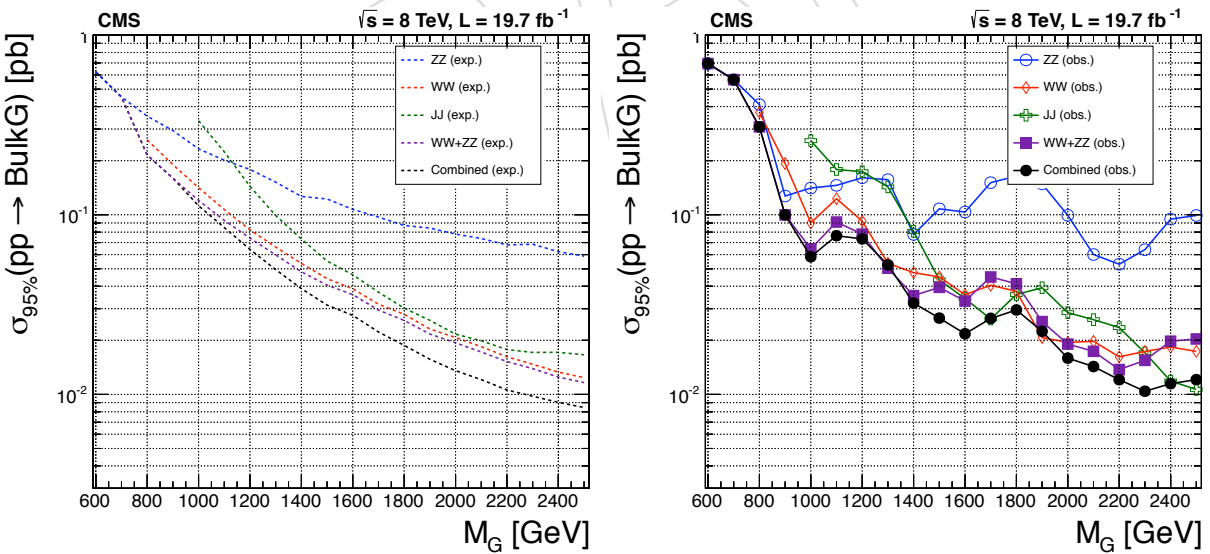


Figure 30: Exclusion limits on the production cross section for narrow bulk gravitons for the combination of different analysis. Left: expected limits, broken down by category. Right: observed limits, broken down by category. Exclusion limits at 95% C.L. were calculated with the asymptotic  $CL_s$  method.

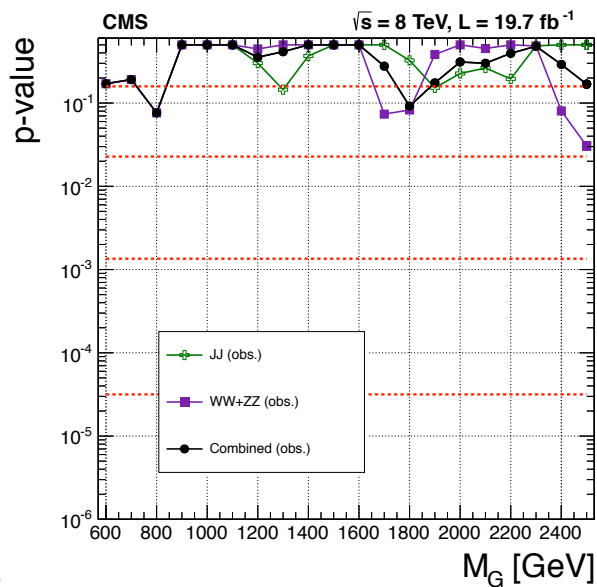


Figure 31: Scan of the p-value as function of the mass of the bulk graviton,  $M_{G^*}$ , using the combination of the three analyses as described in the text. The contributions from the individual categories are also presented.

## 337 8 Model-independent Analysis

338 The analysis as presented above is specific to the case of a narrow Bulk Graviton model. This is  
 339 an appealing scenario but not the only extension of the SM predicting resonances decaying to  
 340 vector bosons. From the point of view of theorists and model-builders, it would be extremely  
 341 interesting to have the opportunity to test their models on the results of this analysis. In order  
 342 to allow the interpretation of the results in terms of models not explicitly studied here, several  
 343 additional ingredients are necessary.

344 **Simplified Limits** The nominal limit combines four categories (two lepton flavors, two purity  
 345 categories). The relative expectations in these categories are fixed to the expectations from  
 346 the Bulk Graviton model. These expectations cannot be disentangled from the final limit  
 347 and depend on the specific model via both the angular dependence of efficiencies and the  
 348 dependence of the jet-tagging efficiency on the boson polarization. We solve this issue by  
 349 using a single category, the so called *simplified limit*, which is slightly less powerful than  
 350 the full analysis, but free of model dependence.

351 **Wide Resonances** The nominal limit is presented in the narrow-width approximation, while  
 352 alternative models can potentially predict wide resonances. We solve this problem by  
 353 constructing signal shapes with variable width and presenting the limit in two dimen-  
 354 sions, as function of the mass and width of the resonance.

355 **Parametrized Selection Efficiencies** As the efficiencies of the reconstructed objects depends  
 356 on their kinematics, there exists a dependence of the efficiency on the decay kinematics  
 357 of a specific model. This includes effects of the boson polarization on the efficiency of the  
 358 jet-sub-structure studies.

### 359 8.1 Simplified Limits

360 To avoid the dependence on assumptions in the construction of the separate categories, we  
 361 reduce the whole limit to one single category. We do this by adding the electron and muon  
 362 channels and dropping the low-purity categories ( $LP: 0.5 < \tau_{21} < 0.75$ ), which have little  
 363 exclusion power.

364 The signal shapes do not differ significantly between electron and muon channel as shown in  
 365 Table 8. The electron and muon samples are merged and fitted together to extract the new  
 366 signal shapes to be used in the simplified limit.

367 The systematic uncertainty on the total signal yield receives different contributions from elec-  
 368 trons and muons. These individual contributions must be now rescaled because the relative  
 369 variation allowed by the uncertainty refers to the total sum of electron and muon channels.  
 370 When combining the two lepton flavors, the individual systematic uncertainties are divided  
 371 by two, assuming equal amounts of events in electron and muon channels. This approxima-  
 372 tion simplifies the implementation and is accurate enough, given that the efficiencies for the  
 373 two lepton flavours are very similar and that anyway the dominant systematics come from the  
 374 hadronic part of the event. Systematics on the Vtag scale factors reported in Table 11 are al-  
 375 ready the weighted average of electron and muon channels.  $t\bar{t}$  and single-top scale factors are  
 376 obtained averaging the electron and muon values for HP reported in Table 10.

377 We report the W-jet mass normalization plot, the  $\alpha$  plot, the sideband region  $m_{WW}\text{spectrum}$ ,  
 378 and the signal region  $m_{WW}\text{spectrum}$  for the simplified case in Figure 32. The resulting limit  
 379 calculated with the Asymptotic  $CL_s$  formula is shown in Fig 33 and is compared to the nominal

limit. The figure shows that the reduction in complexity and model dependence leads only to a small loss of exclusion power (see expected limits), more pronounced at high  $m_{WW}$  where the LP category starts to have an influence on the combined result.

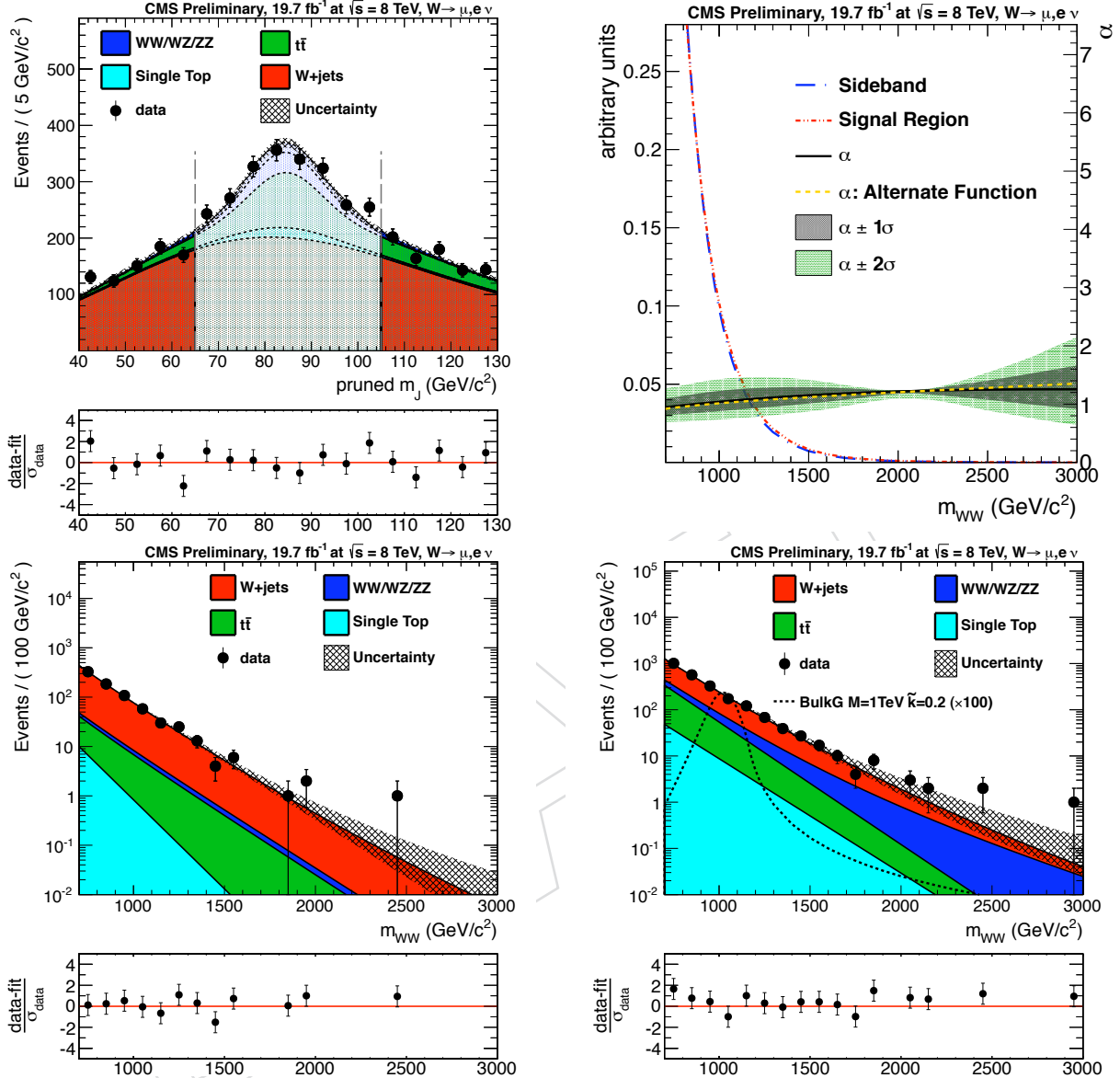


Figure 32: Simplified category (ele+mu HP only). Top-left: Fits to extract the normalization of the  $W+jets$  background. Top-right:  $\alpha$  extrapolation function. Bottom-left:  $m_{WW}$  distribution in sideband region. Bottom-right:  $m_{WW}$  distribution in signal region. **The bulk graviton signal cross section should be multiplied by a factor 1/4, due to a bug recently found in the theoretical calculation. More details can be found in Section 3 of [9]. We don't plan to update this AN. The values in the EXO-13-009 will be correct.**

## 383 8.2 Wide Resonances

384 As described in the Section 4.1, the nominal analysis (search for narrow resonances) models the  
 385  $m_{WW}$  profile of the signal with a two-sided Crystal-Ball (CB) function (i.e., a Gaussian core with  
 386 power-law tails on each side). The parameters of the double CB are extracted with a fit to the  
 387 bulk Graviton simulation samples. The resulting shape represents effectively a resolution func-

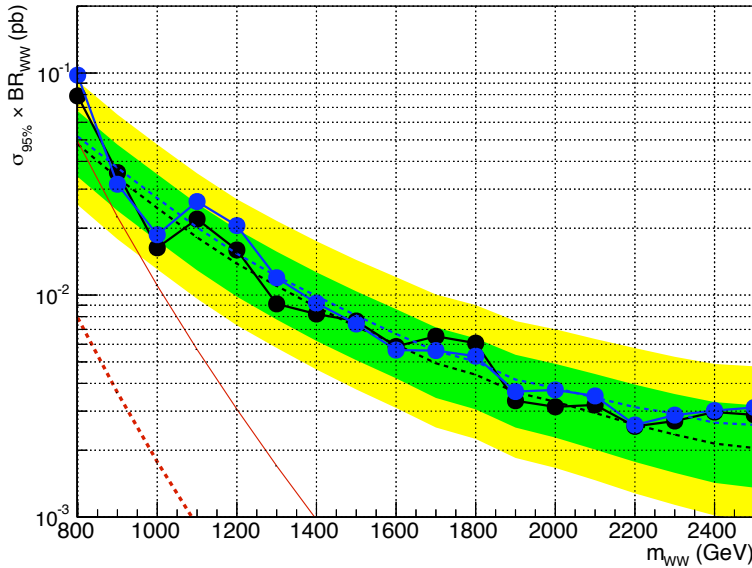


Figure 33: Simplified limit with a single category ele+mu HP (blue) compared to the full limit with standard 4 categories eleHP, eleLP, muHP, muLP (black). **The bulk graviton signal cross section should be multiplied by a factor 1/4, due to a bug recently found in the theoretical calculation. More details can be found in Section 3 of [9]. We don't plan to update this AN. The values in the EXO-13-009 will be correct.**

388 tion, as the generated width of these samples is much narrower than the detector resolution.  
 389 For  $\tilde{k} = 0.2$ , the width of the Breit-Wigner line shape is about  $\Gamma \approx 0.002 \cdot M_{G^*}$ .  
 390 To access also wide resonances we use the two-sided Crystal-Ball resolution function convo-  
 391 luted with a Breit-Wigner line shape. The parameters of the two-sided Crystal-Ball function  
 392 are taken from the nominal analysis. We validated this strategy with special signal samples  
 393 generated with natural width significantly larger than zero reported in Table 2. Three different  
 394 nominal mass points have been considered ( $M_{G^*} = 1000, 1500, 2100$  GeV), and for each of  
 395 them a sample with enlarged natural width has been generated and passed to the FullSim. The  
 396 natural widths ( $\Gamma / M$ ) considered are: 5%, 15% and 30% of the resonance mass.  
 397 Fig 34 shows the comparison of the resulting signal shapes (Breit-Wigner convoluted with two-  
 398 sided Crystal-Ball) with the histograms obtained from MC samples of wide resonances. Note  
 399 the good agreement even though the signal shapes have no free parameters (since the two-  
 400 sided Crystal-Ball function is fully constrained by the fit to the narrow samples and the Breit-  
 401 Wigner parameter are set by the mass and width of the resonance under investigation).

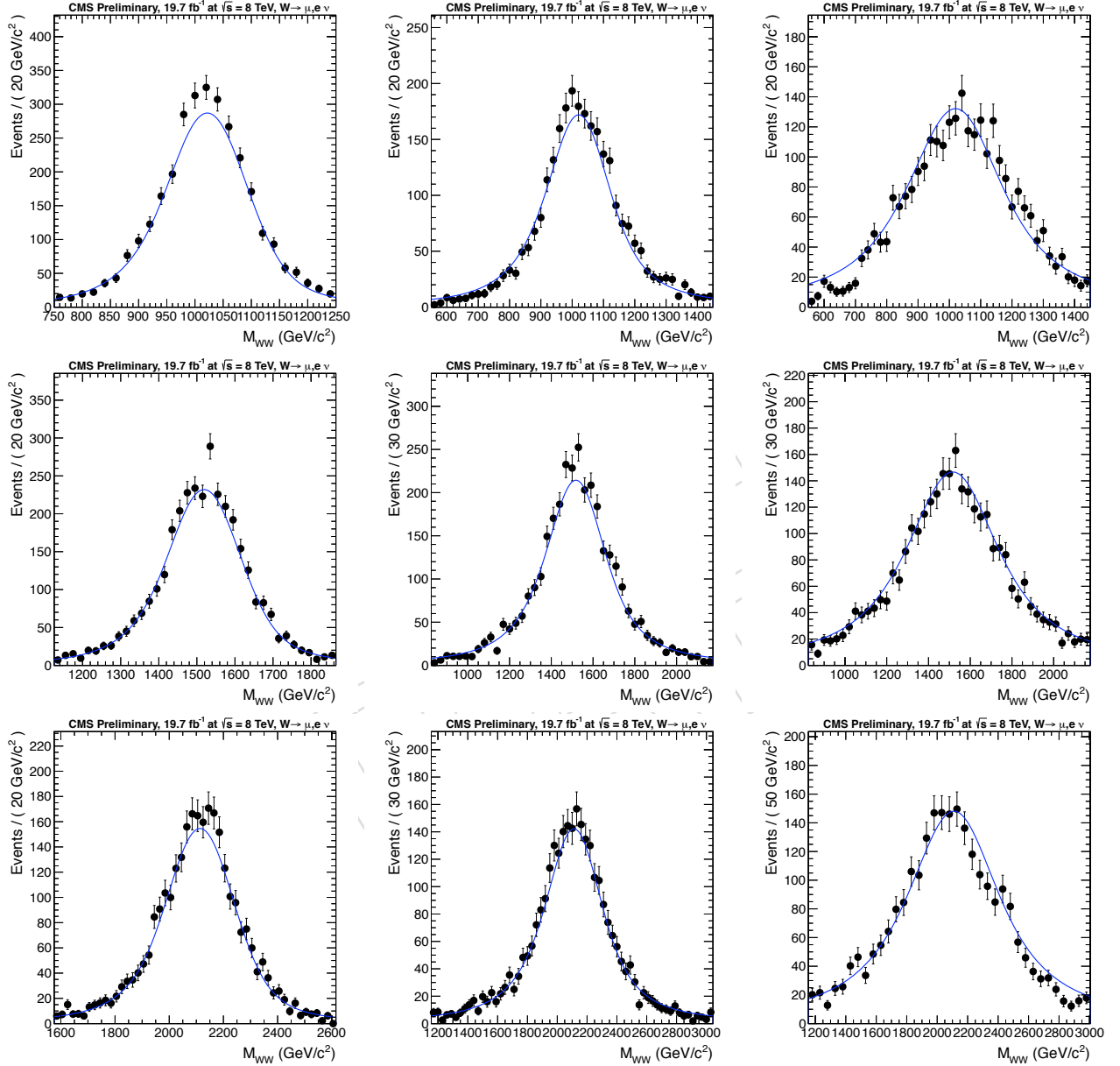


Figure 34: Comparison of the wide signal shapes to MC simulation. From left to right: relative width is 5%, 15%, 30%. From top to bottom: mass is 1 TeV, 1.5 TeV, 2.1 TeV. The line is not a fit to the simulation, but is obtained as convolution of the resolution function (extracted from narrow resonance samples) with a Breit-Wigner function of the nominal width.

402 It has been checked that the increase of width does not affect significantly the signal efficiency  
 403 times acceptance (tot efficiency). The result of the study is shown in Table ?? and in Figure 35.  
 404 We can notice a moderate decrease of the total efficiency for increasing relative widths. The  
 405 most pronounced trend is visible in muon 2.1 TeV case. If we fit the points with a linear function  
 406 ( $ax+b$ ) we get  $b = 0.132 \pm 0.002$  and  $a = -0.00048 \pm 0.00014$ . This corresponds to a relative  
 407 change in the total efficiency of 10% for the 30% width case compared to the narrow resonance  
 408 case. This should be considered an upper limit, since the effect is not visible at the same level  
 409 also for the other mass points. This effect is not corrected in the analysis, but it is covered by  
 410 the systematic uncertainty on the W boson efficiency which are discussed in the next section.  
 411 Within systematics, the total selection efficiency and the modeling of the signal shape can then  
 be treated separately in the analysis .

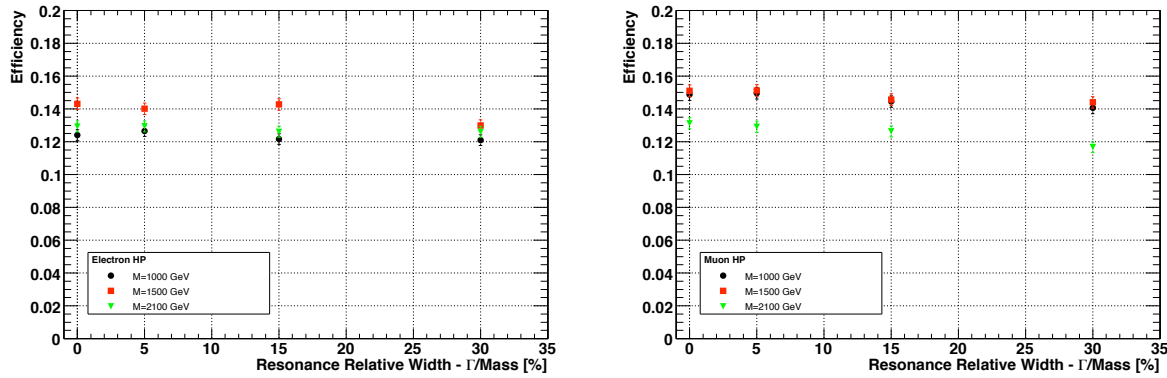


Figure 35: Comparison of signal efficiencies for MC samples of Bulk Graviton as a function of the intrinsic width of the resonance. Left: EleHP, Right: MuHP.

413 **8.3 Parametrized Selection Efficiencies**

414 **8.3.1 W Boson Reconstruction Efficiencies**

415 We provide the reconstruction  $\times$  identification efficiencies for hadronic and leptonic Ws as func-  
 416 tion of the kinematic properties of the W bosons.

417 The efficiencies listed below are obtained by first pre-selecting signal simulation events ac-  
 418 cording to the generator-level acceptance cuts of Table 16, corresponding to the kinematical  
 419 selections of the analysis. We apply the acceptance cuts also to the electrons and muons com-  
 420 ing from both  $W \rightarrow \ell\nu$  decay and  $W \rightarrow \tau\nu \rightarrow \ell\nu\nu$  decays with  $\ell = e, \mu$ . The  $E_T^{\text{miss}}$  cut is applied  
 421 on the vectorial sum ( $\vec{\sum}$  in Table 16) of the generator-level neutrinos from  $W \rightarrow \ell\nu$  and  $\tau \rightarrow \ell\nu\nu$   
 422 decays with  $\ell = e, \mu$ . The number of leptonic or hadronic W candidates at this stage represents  
 423 the denominator for the efficiency calculation.

Object	Requirement
$W_{\ell\nu} (\ell = e, \mu, \tau \rightarrow e/\mu \nu\nu)$	$p_T > 200 \text{ GeV}$
Electrons	$ \eta  < 2.5$
Electrons	$p_T > 90 \text{ GeV}$
Muons	$ \eta  < 2.1$
Muons	$p_T > 50 \text{ GeV}$
$\vec{\sum}$ Neutrinos $\sim E_T^{\text{miss}}$ (Electron Ch.)	$p_T > 80 \text{ GeV}$
$\vec{\sum}$ Neutrinos $\sim E_T^{\text{miss}}$ (Muon Ch.)	$p_T > 40 \text{ GeV}$
$W_{qq}$	$p_T > 200 \text{ GeV}$
$W_{qq}$	$ \eta  < 2.4$
$W_{qq}$	$65 < \text{mass} < 105 \text{ GeV}$
WW System	$\text{mass} > 700 \text{ GeV}$
WW System	$\Delta R(W_{qq}, \text{Charged Lepton}) > \pi/2$
WW System	$\Delta\Phi(W_{qq}, \vec{\sum}\text{Neutrinos}) > 2$
WW System	$\Delta\Phi(W_{qq}, W_{\ell\nu}) > 2$

Table 16: Generator-level acceptance requirements of the analysis.

424 For preselected events, the reconstructed W candidates are then matched with the generator  
 425 level W candidates and required to pass the full analysis selection (leptonic and hadronic can-  
 426 didates are checked separately). The number of leptonic or hadronic W candidates after this  
 427 selection represent the numerator for the efficiency calculation. Efficiencies are calculated as  
 428 function of  $p_T$  and  $\eta$  of the W bosons from the resonance decay, separately for the leptonic and  
 429 hadronic W candidates. The efficiencies are all reported in Figure 36 and Tables 17, 18, and 19;  
 430 they are obtained merging all the Bulk Graviton MC signal samples reported in Table 1 and  
 431 Table 2 (Ws are longitudinally polarized in this model).

432 We verified that reconstruction efficiencies for  $W \rightarrow \ell\nu$  and  $W \rightarrow \tau\nu \rightarrow \ell\nu\nu$  candidates are in  
 433 good agreement. Therefore we combine them, for each lepton type separately ( $\ell = e$  or  $\mu$ ), as  
 434 shown in Figure 36 (top). The efficiencies of the single-lepton triggers and the scale factors for  
 435 lepton ID are included in the leptonic W efficiency.

436 The efficiency for  $W \rightarrow q\bar{q}'$  are reported in Figure 36 (bottom). The hadronic W efficiency is  
 437 already corrected for the data/MC scale factor for W-tagging HP category, equal to 0.89 (see  
 438 Table 11). At very high- $p_T$  we notice a drop of the W hadronic efficiency, which is due to the  
 439 known fact that the pruning algorithm does not work optimally in this regime. This is going

440 to be studied in the next iteration of the analysis (at 14 TeV) to further optimize this search for  
 441 very energetic W bosons.

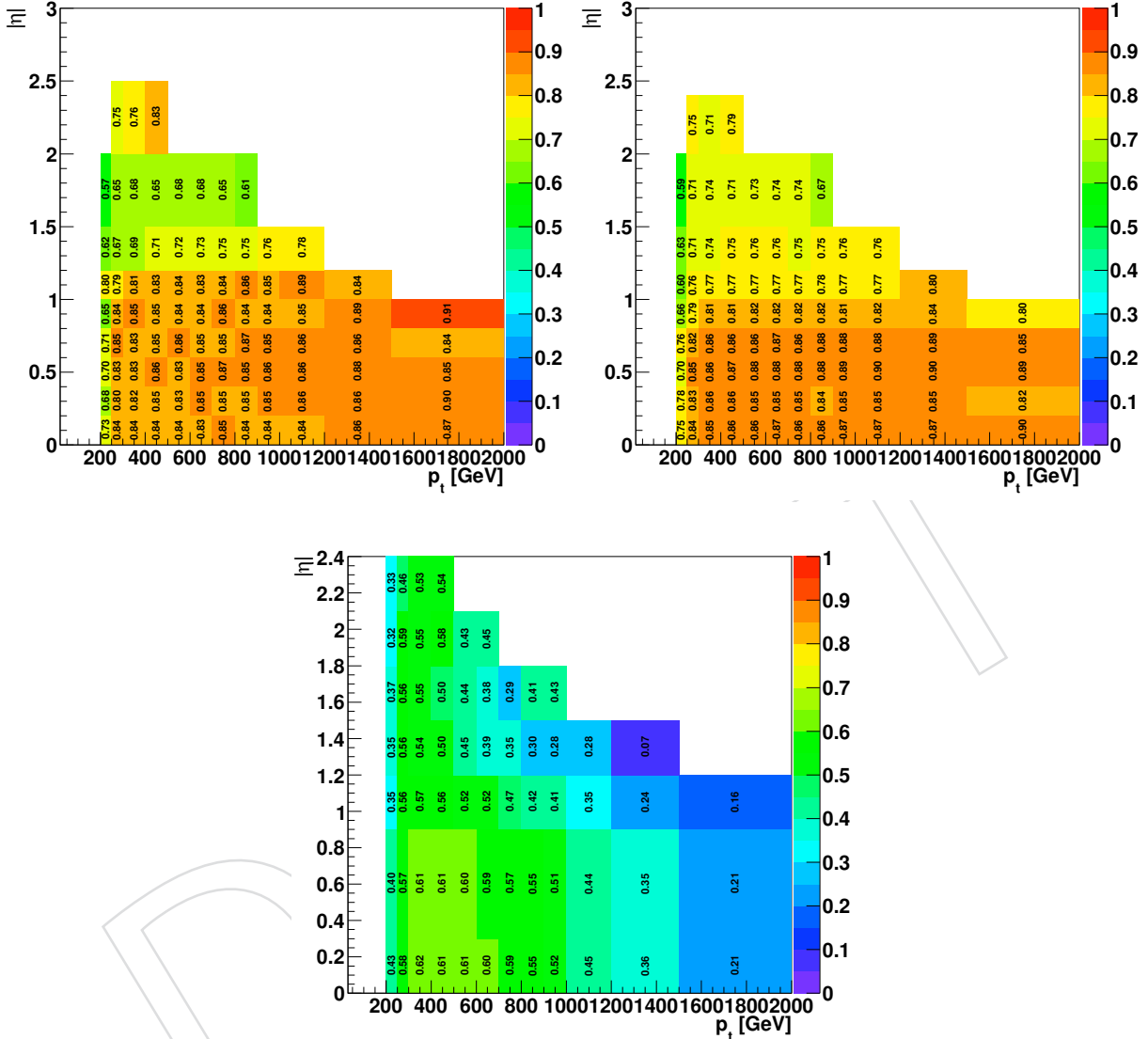


Figure 36: Reconstruction and identification efficiencies for longitudinally polarized W bosons with leptonic and hadronic decays using all available Bulk Graviton MC samples (top-left:  $W \rightarrow e\nu$  plus  $W \rightarrow \tau\nu \rightarrow e\nu\nu$ , top-right:  $W \rightarrow \mu\nu$  plus  $W \rightarrow \tau\nu \rightarrow \mu\nu\nu$ , and bottom:  $W \rightarrow q\bar{q}'$ ) as function of  $p_{T,W}$  and  $\eta_W$ .

$p_T$ range in GeV	$\eta$ range									
	0.0 – 0.2	0.2 – 0.4	0.4 – 0.6	0.6 – 0.8	0.8 – 1.0	1.0 – 1.2	1.2 – 1.5	1.5 – 2.0	2.0 – 2.5	2.5 – 3.0
200 – 250	0.73	0.68	0.70	0.71	0.65	0.80	0.62	0.57	-	-
250 – 300	0.84	0.80	0.83	0.85	0.84	0.79	0.67	0.65	0.75	-
300 – 400	0.84	0.82	0.83	0.83	0.85	0.81	0.69	0.68	0.76	-
400 – 500	0.84	0.85	0.86	0.85	0.85	0.83	0.71	0.65	0.83	-
500 – 600	0.84	0.83	0.83	0.86	0.84	0.84	0.72	0.68	-	-
600 – 700	0.83	0.85	0.85	0.85	0.84	0.83	0.73	0.68	-	-
700 – 800	0.85	0.85	0.87	0.85	0.86	0.84	0.75	0.65	-	-
800 – 900	0.84	0.85	0.85	0.87	0.84	0.86	0.75	0.61	-	-
900 – 1000	0.84	0.85	0.86	0.85	0.84	0.85	0.76	-	-	-
1000 – 1200	0.84	0.86	0.86	0.86	0.85	0.89	0.78	-	-	-
1200 – 1500	0.86	0.86	0.88	0.86	0.89	0.84	-	-	-	-
1500 – 2000	0.87	0.90	0.85	0.84	0.91	-	-	-	-	-

Table 17:  $W \rightarrow e\nu$  and  $W \rightarrow \tau\nu \rightarrow e\nu\nu$  efficiencies for longitudinally polarized bosons (Bulk Graviton MC)

$p_T$ range in GeV	$\eta$ range									
	0.0 – 0.2	0.2 – 0.4	0.4 – 0.6	0.6 – 0.8	0.8 – 1.0	1.0 – 1.2	1.2 – 1.5	1.5 – 2.0	2.0 – 2.4	2.4 – 3.0
200 – 250	0.75	0.78	0.70	0.76	0.66	0.60	0.63	0.59	-	-
250 – 300	0.84	0.83	0.85	0.82	0.79	0.76	0.71	0.71	0.75	-
300 – 400	0.85	0.86	0.86	0.86	0.81	0.77	0.74	0.74	0.71	-
400 – 500	0.86	0.86	0.87	0.86	0.81	0.77	0.75	0.71	0.79	-
500 – 600	0.86	0.85	0.88	0.86	0.82	0.77	0.76	0.73	-	-
600 – 700	0.87	0.85	0.88	0.87	0.82	0.77	0.76	0.74	-	-
700 – 800	0.86	0.85	0.88	0.86	0.82	0.77	0.75	0.74	-	-
800 – 900	0.86	0.84	0.88	0.88	0.82	0.78	0.75	0.67	-	-
900 – 1000	0.87	0.85	0.89	0.88	0.81	0.77	0.76	-	-	-
1000 – 1200	0.87	0.85	0.90	0.88	0.82	0.77	0.76	-	-	-
1200 – 1500	0.87	0.85	0.90	0.89	0.84	0.80	-	-	-	-
1500 – 2000	0.90	0.82	0.89	0.85	0.80	-	-	-	-	-

Table 18:  $W \rightarrow \mu\nu$  and  $W \rightarrow \tau\nu \rightarrow \mu\nu\nu$  efficiencies for longitudinally polarized bosons (Bulk Graviton MC)

$p_T$ range in GeV	$\eta$ range						
	0.0 – 0.3	0.3 – 0.9	0.9 – 1.2	1.2 – 1.5	1.5 – 1.8	1.8 – 2.1	2.1 – 2.4
200 – 250	0.43	0.40	0.35	0.35	0.37	0.32	0.33
250 – 300	0.58	0.57	0.56	0.56	0.56	0.59	0.46
300 – 400	0.62	0.61	0.57	0.54	0.55	0.55	0.53
400 – 500	0.61	0.61	0.56	0.50	0.50	0.58	0.54
500 – 600	0.61	0.60	0.52	0.45	0.44	0.43	-
600 – 700	0.60	0.59	0.52	0.39	0.38	0.45	-
700 – 800	0.59	0.57	0.47	0.35	0.29	-	-
800 – 900	0.55	0.55	0.42	0.30	0.41	-	-
900 – 1000	0.52	0.51	0.41	0.28	0.43	-	-
1000 – 1200	0.45	0.44	0.35	0.28	-	-	-
1200 – 1500	0.36	0.35	0.24	0.07	-	-	-
1500 – 2000	0.21	0.21	0.16	-	-	-	-

Table 19:  $W \rightarrow q\bar{q}'$  efficiencies for longitudinally polarized bosons (Bulk Graviton MC)

### 442 8.3.2 Efficiencies for Veto Requirements

443 The analysis selection criteria includes also:

- 444 • a veto on the presence of b-tag jets far from the hadronic W candidate
- 445 • a veto on the presence of a second isolated lepton.

446 It is found that the efficiency for these vetoes is almost independent on the di-boson event kinematic in signal events, with few % level variations between different resonance mass points.  
 447 We use a constant efficiency of 91.5% for the b-tag veto and 98.3% for the second-lepton veto,  
 448 resulting in a total efficiency for the two combined vetoes of  $\varepsilon_{\text{vetoes}} = 90.0\%$ . The small variations  
 449 observed as a function of the resonance mass (i.e. event kinematic) are included in the  
 450 systematics uncertainties of the method, discussed later.

### 452 8.3.3 Calculation of the Signal Efficiency in a Generic Model

453 The efficiencies calculated in the previous sections can be applied to any model with a resonance decaying to a pair of W bosons by following this procedure:

- 455 1. Generate a sample of events, including the decay of the resonance down to leptons and  
 456 quarks (let also the  $\tau$  decay in all possible ways, including fully leptonic decays).
- 457 2. Filter the events according to the criteria listed in Table 16. In each event you should have  
 458 one W leptonic and one W hadronic candidate.
- 459 3. Calculate the efficiency for the leptonic W candidate (either  $W \rightarrow \ell\nu$  or  $W \rightarrow \tau\nu \rightarrow \ell\nu\nu$ ,  
 460 where  $\ell$  is either electron or muon) using the Tables 17 and 18 ( $\varepsilon_{W_{\text{lep}}}$ ), parametrized as  
 461 function of  $p_T$  and  $\eta$  of the W boson.
- 462 4. In a similar way, calculate the efficiency of the hadronic W candidate  $W \rightarrow q\bar{q}'$  using  
 463 the values in Table 19 ( $\varepsilon_{W_{\text{had}}}$ ) for a W longitudinally polarized. If the W is transversely  
 464 polarized, multiply the values in Table 19 by 0.85 (the motivation is described later in  
 465 Section 8.3.4).
- 466 5. Consider the efficiency for the additional event-veto requirements applied in the analysis,  
 467  $\varepsilon_{\text{vetoes}} = 90.0\%$ , and discussed in Section 8.3.2.
- 468 6. Weight each event passing the acceptance cuts applied at point 2 with the following over-  
 469 all efficiency value:  $\varepsilon_{W_{\text{lep}}}(p_T, \eta) \times \varepsilon_{W_{\text{had}}}(p_T, \eta) \times \varepsilon_{\text{vetoes}}$ .
- 470 7. The resulting sum of weights divided by the total number of events generated at point  
 471 1 provides a reasonable approximation to the total signal efficiency  $\times$  acceptance for the  
 472 given model.

473 We checked the self-consistency of the method by applying this procedure to some of the same  
 474 Bulk Graviton MC samples used in the generation of the efficiency tables. We compare the  
 475 selection efficiency derived from this procedure with the actual signal efficiencies reported in  
 476 Table 9 obtained by running the full selection on the MC samples. The results of this com-  
 477 parison are shown in Table 20 and show that the efficiency parameterization provides results  
 478 consistent with the actual efficiencies within a relative  $\sim 10\%$ .

Electron HP Category		
Resonance Mass [GeV]	Exact efficiency	Parametrized efficiency
800	0.1100	0.0988
1000	0.1245	0.1181
1500	0.1432	0.1369
2000	0.1380	0.1290
2500	0.1097	0.1121
Muon HP Category		
Resonance Mass [GeV]	Exact efficiency	Parametrized efficiency
800	0.1403	0.1303
1000	0.1488	0.1481
1500	0.1510	0.1513
2000	0.1355	0.1388
2500	0.1015	0.1131

Table 20: Comparison between the nominal selection efficiencies and efficiencies obtained by applying the parameterized efficiency tables for narrow-width Bulk Graviton MC samples.

#### 479 8.3.4 Dependence of Efficiencies on W Polarization

480 Special care must be given to cases where the W boson is transversely polarized. The numbers  
 481 in Table 17, 18, and 19 refer to longitudinally polarized Ws, as those produced in the reference  
 482 bulk Graviton model ( $> 99\%$  of the cases). The efficiency of the W-tagging selections depend  
 483 significantly on the degree of polarization of the vector boson [19]. We investigated this using  
 484 MC samples of RS1 Graviton produced with the Pythia6 and MadGraph5 generators reported  
 485 in Table 3.

486 The Ws coming from the decays of RS1 Gravitons are transversely polarized in about 90% of  
 487 the cases. The model in MadGraph5 generates RS1 events with the correct kinematics and  
 488 angular distributions but the available sample has limited statistics. The sample generated  
 489 with Pythia6 is larger, but it suffers from the trivial and inaccurate kinematics of the decays  
 490 (for both the spin-2 graviton and the spin-1 W bosons) and from older detector parameters and  
 491 conditions used in the simulation. Because of this we trust more the predictions obtained with  
 492 Madgraph to provide the final efficiencies for transverse polarized Ws (despite of the small  
 493 statistics of the sample). Still we use the Pythia with large statistics for checking the stability  
 494 of the results over a larger kinematic range and to perform a closure test of the method.

495 Figure 37 shows the ratio of reconstruction efficiencies RS1Madgraph / BulkGraviton (i.e.  
 496  $\varepsilon_{W_T}/\varepsilon_{W_L}$ , where T and L indicated, respectively, transverse and longitudinal polarization of  
 497 the W bosons), for the W in the different decay modes. For the leptonic W, we verify that there  
 498 is no dependence of the polarization on the efficiency. This was expected because the generator-  
 499 level selection on the individual charged leptons and neutrinos (see Table 16) guarantees that  
 500 this effect is included in the acceptance. It was also expected from [19] that the efficiency of  
 501 the jet substructure selection for is lower for transversely polarized  $W \rightarrow q\bar{q}'$  (this is because  
 502 the jet pruning algorithm applied at reconstruction level in the W-tagging includes angular  
 503 and  $p_T$  requirements on the subjets which have different efficiency for different polarizations;  
 504 these requirements, which are applied on the reconstructed jet constituents, cannot be included  
 505 in the gen-level acceptance cuts). However, a good description of the transversely polarized  
 506 case does not need an ad-hoc table of efficiencies; rather it is a good enough approximation to  
 507 rescale the efficiencies for longitudinally polarized Ws (derived from the Bulk Graviton sam-  
 508 ple) by a factor 0.85, independently of the  $\eta$  and  $p_T$  of the  $W \rightarrow q\bar{q}'$  candidate, as shown in the

509 bottom plot of Figure 37.

510 The fact that i) the W leptonic efficiencies are almost independent on the W polarization and ii)  
 511 there is a mild dependency on W polarization of the RS/Bulk rescaling factor for W hadronic  
 512 efficiency, is confirmed by looking at the same table using the larger RS1 sample generated  
 513 with Pythia in Figure 38. The rescaling factor for the hadronic candidate (bottom plot) tends  
 514 to be a bit lower (0.8 instead of 0.85) than the case of Madgraph. This is attributed to the  
 515 different detector conditions used for simulating this older RS1 Pythia sample and to the  
 516 different (wrong) kinematic and angular distributions of W hadronic decays in the Pythia  
 517 sample. However, the general trend is very stable also in this case.

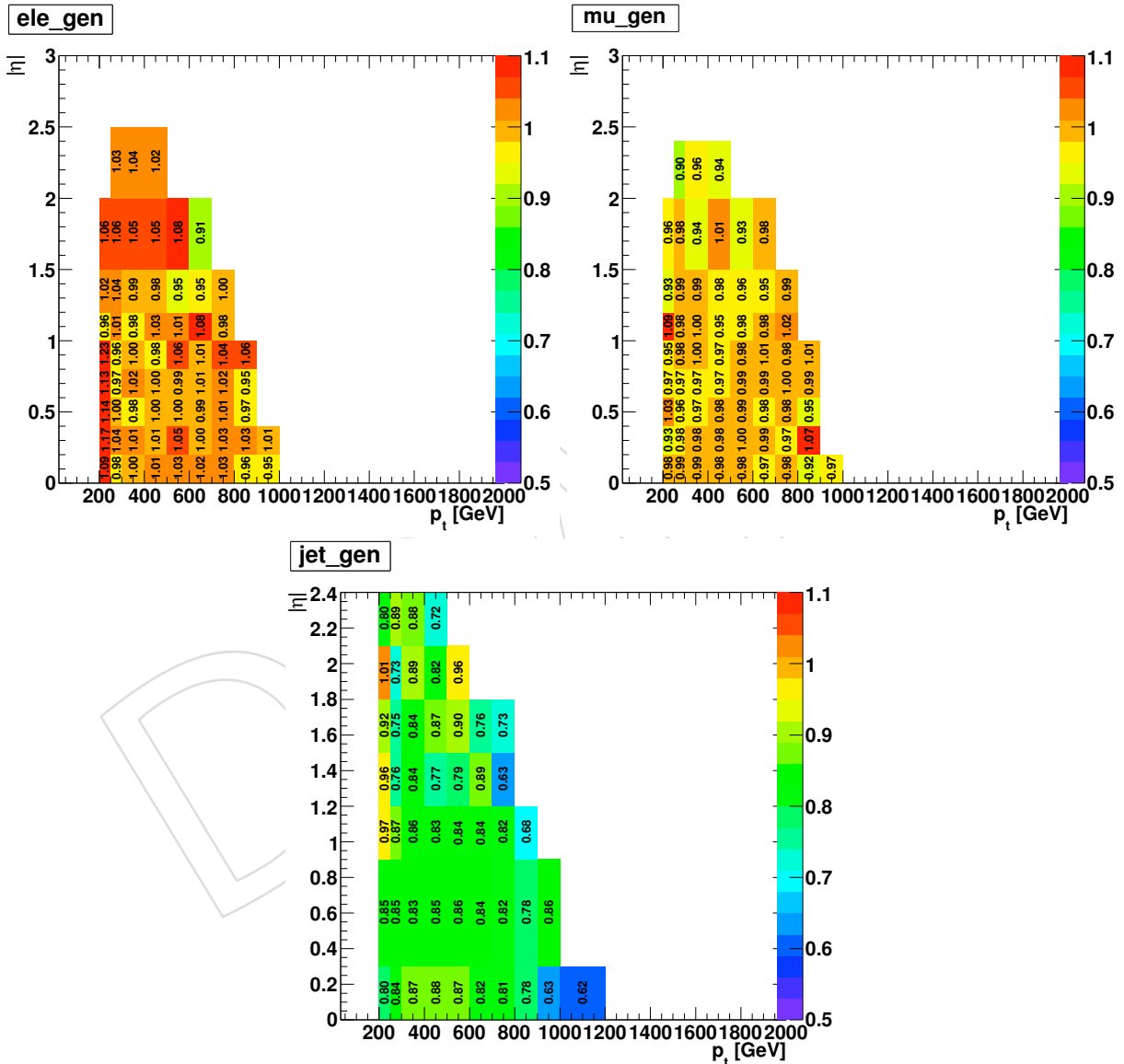


Figure 37: Ratio of reconstruction and identification efficiencies between transversely polarized (RS1 Graviton sample, Madgraph) and longitudinally polarized (Bulk Graviton sample, JHUGen) W bosons, with leptonic and hadronic decays: (top-left:  $W \rightarrow e\nu$  plus  $W \rightarrow \tau\nu \rightarrow e\nu\nu$ , top-right:  $W \rightarrow \mu\nu$  plus  $W \rightarrow \tau\nu \rightarrow \mu\nu\nu$ , and bottom:  $W \rightarrow q\bar{q}'$ ) as function of  $p_{T,W}$  and  $\eta_W$ .

518 To validate the correctness of this procedure, we compare the resulting parameterized signal

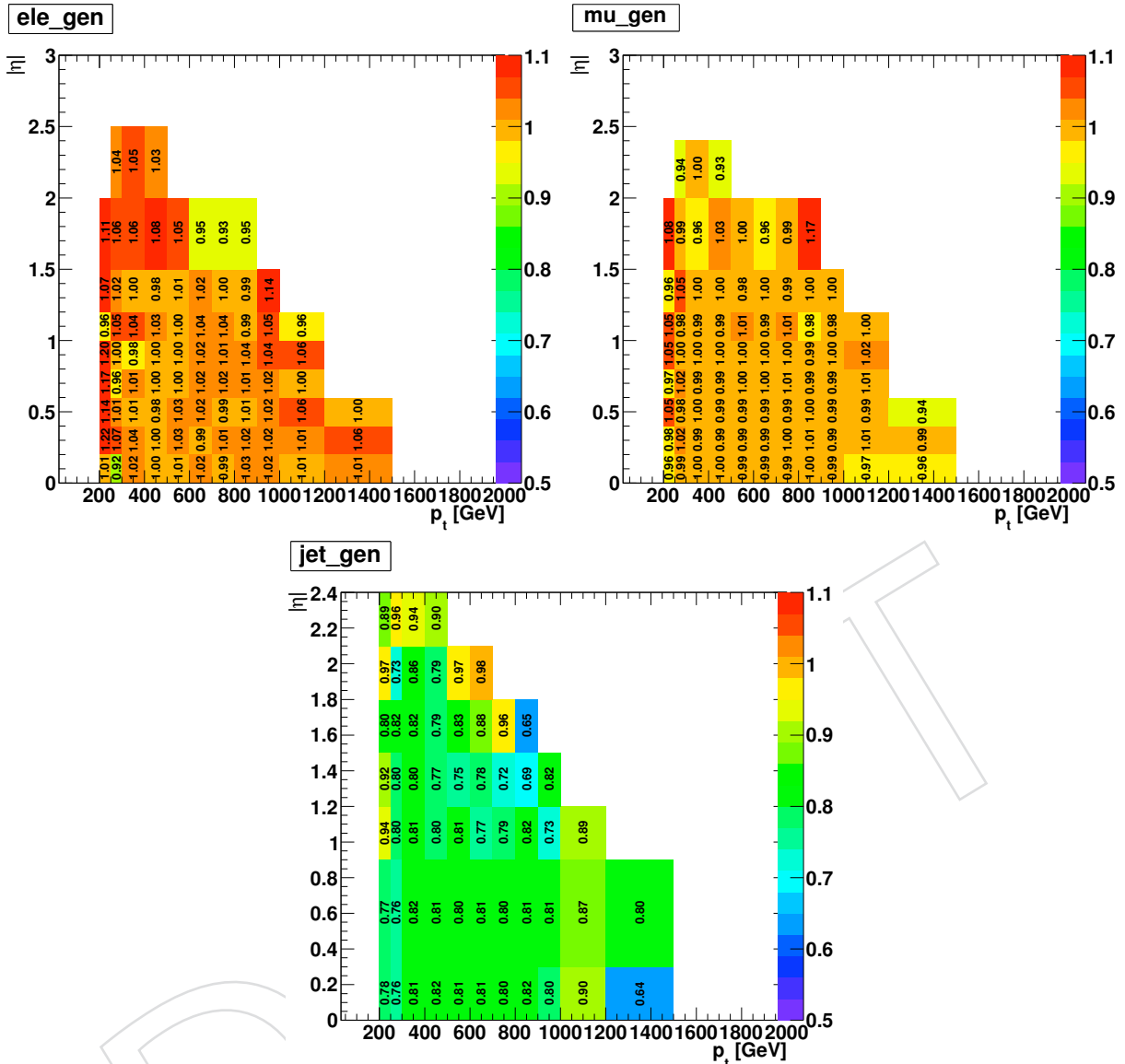


Figure 38: Ratio of reconstruction and identification efficiencies between RS1 Graviton sample (`Pythia`) and longitudinally polarized (Bulk Graviton sample, JHUGen)  $W$  bosons, with leptonic and hadronic decays: (top-left:  $W \rightarrow e\nu$  plus  $W \rightarrow \tau\nu \rightarrow e\nu\nu$ , top-right:  $W \rightarrow \mu\nu$  plus  $W \rightarrow \tau\nu \rightarrow \mu\nu\nu$ , and bottom:  $W \rightarrow q\bar{q}'$ ) as function of  $p_{T,W}$  and  $\eta_W$ .

519 efficiencies (obtained using the method described in Section 8.3.3) to those calculated from an  
 520 RS1 MC sample (i.e. running the full analysis on MC). Because of the different underlying  
 521 dynamics, the RS1 sample has different kinematic distributions than those used for calculating  
 522 the efficiency tables (i.e. Bulk Graviton samples); so, differently from the simple sanity-check  
 523 done in Section 8.3.3, this study represents a real closure test of the method. We decided to use  
 524 the RS1 `Pythia` sample for this closure test since it has a larger statistics. The parameterized  
 525 efficiencies for the closure test are obtained from the Bulk Graviton sample, with the exception  
 526 of the hadronic  $W$  efficiencies which are multiplied by 0.8, accordingly with what observed in  
 527 Figure 38. The result of the closure test is presented in Table 21. The agreement between the  
 528 nominal and parametrized efficiencies is of the order of 10%.

Electron HP Category		
Resonance Mass [GeV]	Exact efficiency	Parametrized efficiency
1000	0.0698	0.0620
1500	0.0847	0.0778
2000	0.0785	0.0800
Muon HP Category		
Resonance Mass [GeV]	Exact efficiency	Parametrized efficiency
1000	0.0900	0.0823
1500	0.1015	0.0957
2000	0.0879	0.0923

Table 21: Result of the closure test. Comparison of the exact signal efficiencies from RS1 `Graイトn Pythia` MC sample, with those obtained from the efficiency parameterization method. The parameterized efficiencies are derived from the Bulk Graviton sample in Tables 17, 18, and 19, with the only change that the W hadronic efficiencies from Table 19 are multiplied by a factor 0.8 (derived from Figure 38).

### 529 8.3.5 Extension to WZ resonances

530 While the analysis is optimized for WW final states, it is also sensitive to resonances decaying to  
 531 WZ with a hadronically decaying Z ( $Z \rightarrow qq$  or  $Z \rightarrow b\bar{b}$ ), as the V-jet mass window requirement  
 532 for selecting hadronic boson is rather loose compared to the V-jet mass resolution.

533 To allow an interpretation of the limits also for such models (for example  $W' \rightarrow WZ$  resonances)  
 534 we check the efficiency for hadronic Z decays to be reconstructed as W-jets in this analysis.  
 535 The parameterized efficiencies are derived with same method as discussed above, but using  
 536 the Bulk Graviton sample with ZZ decays (taken from the complementary search [9]). The  
 537 efficiencies are shown in Figure 39 and Table 22.

538 The b-tag veto efficiency in  $WZ \rightarrow \ell\nu qq$  events is reduced compared to the  $WW \rightarrow \ell\nu qq$  case  
 539 from 91.5% to 82.6%, because of the presence of  $Z \rightarrow b\bar{b}$  decays (in the former case) which can  
 540 be rejected by the veto. The lepton veto efficiency, instead, does not change significantly (and  
 541 we use the same value of WW case, 98.3%). Therefore the combined efficiency of the two vetos  
 542 is 81.2% for WZ resonances.

543 The closure test is then performed with  $W'$  samples generated with `pythia` (see Table 4), where  
 544 V bosons are expected to have mainly longitudinal polarization. The closure test is shown in  
 545 Table 23. A shift of about 15%, still within the quoted systematic uncertainty (Section 8.4), is  
 546 observed in all the mass points considered (actual efficiency higher than predicted).

547 A possible explanation of actual efficiencies being higher than predicted is that the  $W'$  sample  
 548 used to compute the actual efficiencies is inclusive, while for the predicted efficiencies only  
 549 semi-leptonic decays are considered; in fact, some other decays (such as  $WZ \rightarrow q\bar{q}\ell\ell$  with a lost  
 550 lepton) in addition to  $WZ \rightarrow \ell\nu qq$  might contribute at the level of 10-15% to the total efficiency.  
 551 Parametrizing these additional decays is more complex than the simple approach used here  
 552 and beyond the scope of this analysis which is focused on the  $\ell\nu qq$  final state. For simplicity,  
 553 we do not try to further parametrize these extra decays but just accept the current level of  
 554 agreement in this closure test, also considering that the disagreement is still within the quoted  
 555 systematic uncertainty.

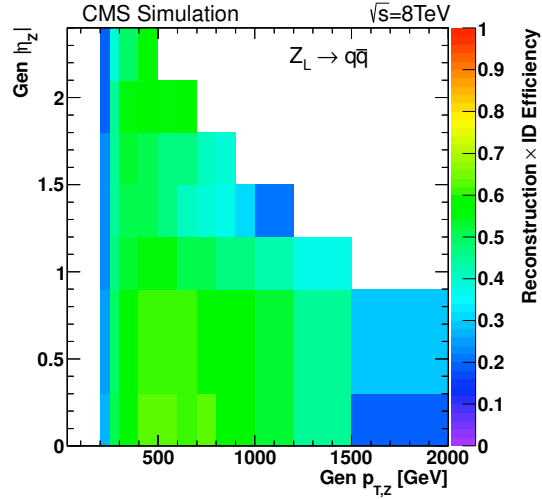


Figure 39: Reconstruction and identification efficiencies for the  $Z \rightarrow qq$  boson decays using  $W$ -tag criteria as function of generated  $p_{T,Z}$  and  $\eta_Z$ .

$p_T$ range in GeV	$\eta$ range						
	0.0 – 0.3	0.3 – 0.9	0.9 – 1.2	1.2 – 1.5	1.5 – 1.8	1.8 – 2.1	2.1 – 2.4
200 – 250	0.27	0.25	0.23	0.23	0.24	0.20	0.19
250 – 300	0.51	0.50	0.46	0.45	0.46	0.45	0.39
300 – 400	0.59	0.58	0.53	0.51	0.52	0.55	0.50
400 – 500	0.62	0.61	0.55	0.51	0.51	0.57	0.58
500 – 600	0.63	0.62	0.55	0.47	0.48	0.56	-
600 – 700	0.61	0.60	0.51	0.41	0.47	0.57	-
700 – 800	0.62	0.60	0.51	0.38	0.41	-	-
800 – 900	0.60	0.58	0.48	0.37	0.38	-	-
900 – 1000	0.57	0.56	0.47	0.31	-	-	-
1000 – 1200	0.54	0.53	0.42	0.21	-	-	-
1200 – 1500	0.46	0.46	0.38	-	-	-	-
1500 – 2000	0.19	0.29	-	-	-	-	-

Table 22: Reconstruction and identification efficiencies for the  $Z \rightarrow qq$  boson decays using  $W$ -tag criteria as function of generated  $p_{T,Z}$  and  $\eta_Z$ .

Electron HP Category		
Resonance Mass [GeV]	Exact efficiency	Parametrized efficiency
1000	0.1089	0.0939
1500	0.1305	0.1083
2000	0.1223	0.1052
2500	0.1065	0.0900

Muon HP Category		
Resonance Mass [GeV]	Exact efficiency	Parametrized efficiency
1000	0.1247	0.1097
1500	0.1410	0.1216
2000	0.1368	0.1166
2500	0.1080	0.0976

Table 23: Result of the closure test. Comparison of the exact signal efficiencies from  $W' \rightarrow WZ$  Pythia MC sample, with those obtained from the efficiency parameterization method. The parameterized efficiencies are derived from the Bulk Graviton sample in Tables 17, 18, and 22. The b-tag veto efficiency used is derived from  $W'$  sample and is equal to 82.6%.

## 556 8.4 Summary of Parameterized Efficiencies and Related Uncertainties

557 To summarize, this is the method we propose to estimate the signal efficiency for a generic WW  
 558 or WZ resonance:

- 559 • Generator-level acceptance cuts from Table 16. If considering a WZ resonance the  
 560 cuts on the hadronic Ws should be applied instead on the hadronic Zs.
- 561 •  $W \rightarrow e\nu$  plus  $W \rightarrow \tau\nu \rightarrow e\nu\nu$  efficiencies taken from Table 17, for both  $W_L$  or  $W_T$ .
- 562 •  $W \rightarrow \mu\nu$  plus  $W \rightarrow \tau\nu \rightarrow \mu\nu\nu$  efficiencies taken from Table 18, for both  $W_L$  or  $W_T$ .
- 563 •  $W_L \rightarrow q\bar{q}'$  efficiencies taken from Table 19.
- 564 •  $Z_L \rightarrow q\bar{q}$  efficiencies taken from Table 22.
- 565 •  $W_T \rightarrow q\bar{q}'$  efficiencies taken from Table 19  $\times$  a constant scale factor of 0.85.
- 566 •  $Z_T \rightarrow q\bar{q}$  efficiencies taken from Table 22  $\times$  a constant scale factor of 0.85.
- 567 • For WW resonances, combined efficiency for b-tag veto and second lepton veto,  
 568  $\varepsilon_{\text{vetoes}} = 90.0\%$ , constant value independent on W boson kinematics.
- 569 • For WZ resonances, combined efficiency for b-tag veto and second lepton veto,  
 570  $\varepsilon_{\text{vetoes}} = 81.2\%$ , constant value independent on W/Z boson kinematics.
- 571 • The method to calculate the total selection efficiency for a generic model is described  
 572 in the 7 points of Section 8.3.3.

573 As the parameterization is not perfect, an uncertainty on the efficiency is assigned that corre-  
 574 sponds to the deviation between the parameterized and true total signal efficiencies observed  
 575 in the cross-checks and closure tests discussed above. In addition, some assumptions were  
 576 made (assuming a constant scale factor for  $W_T$  efficiencies, assuming a flat efficiency for b-tag  
 577 and second lepton vetoes, etc.). When all these consideration are included, we are confident  
 578 that the method proposed is accurate to 15% and we suggest that this number should be used  
 579 as overall uncertainty on the **total signal efficiency** (including both W leptonic and W hadronic  
 580 legs and veto selections) by non-CMS members using the procedure highlighted above.

## 581 8.5 Results

582 We present limits as function of the mass and width of a generic BSM resonance (denoted by  
 583 the symbol “X”). The reconstructed line shape of the resonance is assumed to be a Breit-Wigner  
 584 function (BW) convoluted with a DoubleCrystalBall resolution function, as described in Sec-  
 585 tion 8.2. The intrinsic width of the resonance is defined as the  $\Gamma$  parameter of the BW. The  
 586 exclusion is quoted on the number of events, in order to allow a direct comparison with a  
 587 generic model, once the yields predicted by the theory have been corrected for the reconstruc-  
 588 tion efficiency as described in Sect. 8.4.

589 The limits are calculated with the Asymptotic CL<sub>s</sub> method (CMSSW\_6\_1\_1). The scan over  
 590 mass and width would be too expensive in terms of CPU and time to be run with the full  
 591 CL<sub>s</sub> technique while. On the other hand, in Appendix C.4 of [5] it is shown how the central  
 592 values of both observed and expected upper limits are very well calculated under the asymp-  
 593 totic approximation (few% variations). This is also verified in the ZZ semi-leptonic search, see  
 594 Sect.5.2 of [9]. All the systematics used for the nominal analysis are included in the extraction  
 595 of the limits. Following the comment on the additional uncertainties on the parametrized ef-  
 596 ficiency in Sect. 8.4, we included an additional 15% systematic uncertainty when calculating  
 597 these model-independent limits. This will allow the theorist to compare the expected yield cal-  
 598 culated with the given tables directly to the limits, since the additional uncertainty is already  
 599 taken into account.

Figures 40 and 41 show the expected and observed limits for different values of mass and widths. The 1D limits as function of the mass are presented in the left plot for different values of the relative width,  $\Gamma / M_X$ . The same information is compiled in a two-dimensional plot in the right-hand panel of Figures 40 and 41. One can notice how the limit on the number of events degrades as a function of the width. The relative deterioration slows down with increasing width, at the point of “saturating” for very wide resonances. This was investigated and related to the fact that already at relative widths of 0.25, the signal line shape is spread over a very large range and further enlargements cannot harm the performances further.

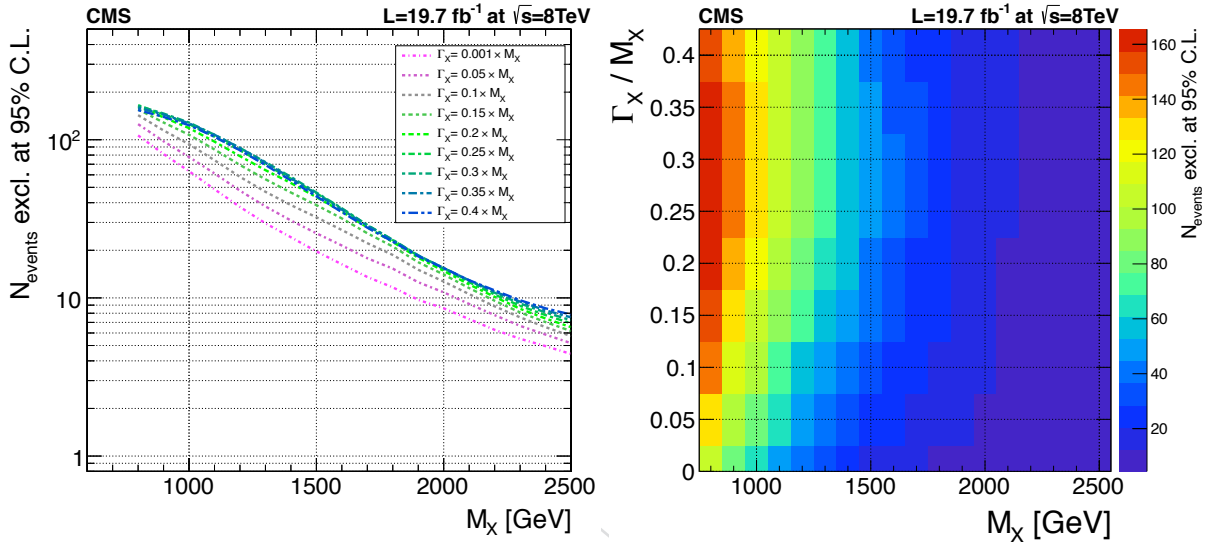


Figure 40: Expected exclusion limits at 95% C.L. on the number of events for a WW resonance, as a function of its mass and natural width. The width is expressed in units of the nominal mass. The left-hand plot shows the limits as a function of the mass for the different values of relative widths considered in the scan. The right-hand plot shows the same limits in the 2D plan, mass vs relative width.

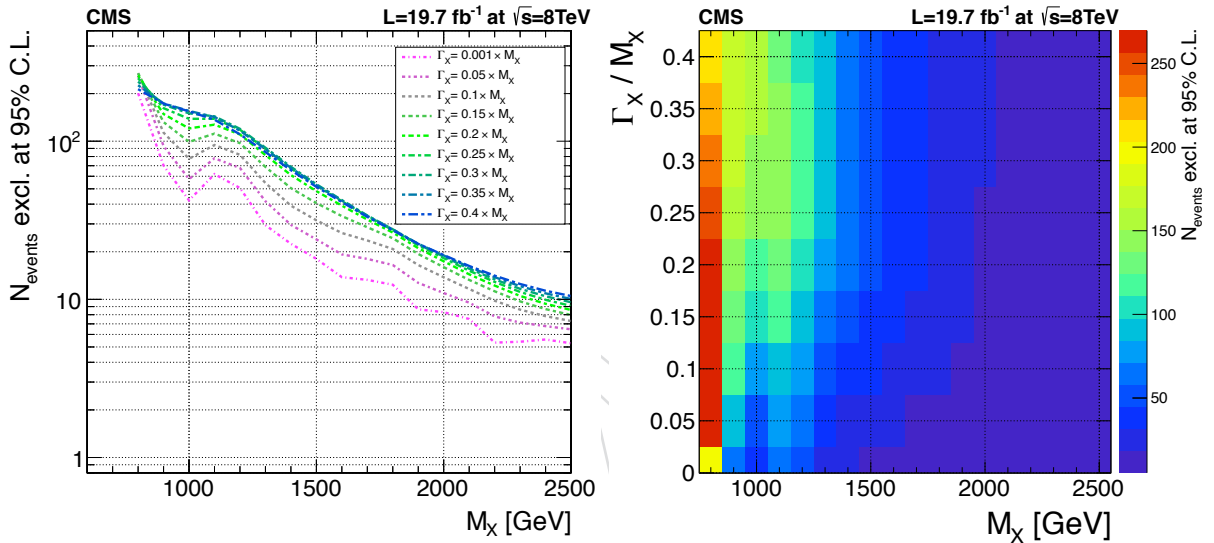


Figure 41: Observed exclusion limits at 95% C.L. on the number of events for a WW resonance, as a function of its mass and natural width. The width is expressed in units of the nominal mass. The left-hand plot shows the limits as a function of the mass for the different values of relative widths considered in the scan. The right-hand plot shows the same limits in the 2D plan, mass vs relative width.

---

## 608 9 Conclusions

609 Compared to the approved preliminary results, we improve and extend the analysis in several  
 610 aspects. We used the latest reprocessed datasets (22Jan2013) and jet energy scale corrections  
 611 recommended for legacy 8 TeV analyses. The muon reconstruction is updated to the latest  
 612 recommendation. Additionally we update the scale factor for the W-tagging efficiency to follow  
 613 the same method used in the past, approved by the JETMET POG. These changes have small  
 614 effects and do not change the overall picture of the approved preliminary result. We have  
 615 also added  $W \rightarrow \tau\nu$  decays in the WW signal samples which provides a 10% increase in the  
 616 efficiency for the bulk graviton model.

617 We also import several features from the corresponding ZZ search, to present a more coherent  
 618 analysis in the combined paper. We use the same function to fit the W+jet background, the  
 619 Double Crystal Ball modeling for the signal shape in the narrow resonance case, and the same  
 620  $\Delta R$  cut between the jet and the leptons.

621 An additionally study on the uncertainty on our results due to parton showering effects was  
 622 performed by the ZZ search by comparing different shower simulations. The outcome of the  
 623 study is that this represents a small effect and can be neglected also for the WW search.

624 Exclusion limits are set on a BSM scenario with a narrow-width bulk graviton over a range of  
 625 masses  $M_{G_*} \in [800, 2500]$  GeV. No large excesses with respect to the background are observed  
 626 over the entire mass range.

627 To present a more general result to the public we also produce model independent limits. This  
 628 includes the reduction of the analysis categories to compute a model-independent limit, as  
 629 well as a limit as function of resonance mass and width. To allow for the interpretation of  
 630 the resulting generic limits by non-CMS members we provide parameterized efficiencies as a  
 631 function of the W boson  $p_T$  and  $\eta$  values. We also include a way to set mass limits on WZ  
 632 resonances.

## 633 References

- 634 [1] CMS Collaboration, ““Search for new resonances decaying to WW to lv qq in the final  
635 state with a lepton, missing transverse energy, and single reconstructed jet””, CMS  
636 Physics Analysis Summary CMS-PAS-EXO-12-021, (2013).
- 637 [2] CMS Collaboration, ““Search for a narrow spin-2 resonance decaying to Z bosons in the  
638 semileptonic final state””, CMS Physics Analysis Summary CMS-PAS-EXO-12-022,  
639 (2013).
- 640 [3] CMS Collaboration, ““Search for heavy resonances in the W/Z-tagged dijet mass  
641 spectrum in pp collisions at 8 TeV””, CMS Physics Analysis Summary  
642 CMS-PAS-EXO-12-024, (2013).
- 643 [4] CMS Collaboration, ““Search for a BSM resonance decaying to W vector bosons in the  
644 semileptonic final state””, CMS Analysis Note CMS-AN-2013/045, (2013).
- 645 [5] CMS Collaboration, ““Search for high mass exotic resonances decaying to WW in the  
646 semi-leptonic channel””, CMS Analysis Note CMS AN-13/139, (2013).
- 647 [6] K. Agashe, H. Davoudiasl, G. Perez, and A. Soni, “Warped Gravitons at the LHC and  
648 Beyond”, *Phys. Rev. D* **76** (2007) 036006, doi:10.1103/PhysRevD.76.036006,  
649 arXiv:hep-ph/0701186.
- 650 [7] L. Randall and R. Sundrum, “A large mass hierarchy from a small extra dimension”,  
651 *Phys. Rev. Lett.* **83** (1999) 3370, doi:10.1103/PhysRevLett.83.3370,  
652 arXiv:hep-ph/9905221.
- 653 [8] L. Randall and R. Sundrum, “An alternative to compactification”, *Phys. Rev. Lett.* **83**  
654 (1999) 4690, doi:10.1103/PhysRevLett.83.4690, arXiv:hep-th/9906064.
- 655 [9] CMS Collaboration, ““Search for a BSM resonance decaying to Z vector bosons in the  
656 semileptonic final state””, CMS Analysis Note CMS AN-13/393, (2013).
- 657 [10] Raffaele Gerosa, ““Update on t̄t studies (consider the first 6 slide only)””, technical  
658 report. <https://indico.cern.ch/getFile.py/access?contribId=0&resId=1&materialId=slides&confId=279718>.
- 660 [11] Raffaele Gerosa, ““Bias study for WW analysis””, technical report.  
661 <https://indico.cern.ch/getFile.py/access?contribId=0&resId=2&materialId=slides&confId=280767>.
- 663 [12] Raffaele Gerosa, ““Comparison of WW fits with two different parameterizations for  
664 W+jets background””, technical report. <https://indico.cern.ch/getFile.py/>  
665 access?contribId=0&resId=1&materialId=slides&confId=280767.
- 666 [13] A. L. Read, “Presentation of search results: The CL(s) technique”, *J. Phys. G* **28** (2002)  
667 2693–2704, doi:10.1088/0954-3899/28/10/313.
- 668 [14] A. L. Read, “Modified frequentist analysis of search results (the CLs method)”, technical  
669 report, (2000).
- 670 [15] G. Cowan, K. Cranmer, E. Gross, O. Vitells, “Asymptotic formulae for likelihood based  
671 tests of new physics”, *Eur. Phys. J. C* **71** (2011) 1554, arXiv:physics/1007.1727v2.

- 672 [16] CMS Collaboration, ““Combined results of searches for the standard model Higgs boson  
673 in pp collisions at  $\sqrt{s} = 7 \text{ TeV}””, *Phys. Lett. B* (2012), no. 710, arXiv:1202.1488.$
- 674 [17] CMS Collaboration, ““Combined results of searches for a Higgs boson in the context of  
675 the standard model and beyond-standard models””, CMS Physics Analysis Summary  
676 CMS-PAS-HIG-12-008, (2013).
- 677 [18] CMS Collaboration, ““Measurements of the properties of the new boson with a mass  
678 near 125 GeV””, CMS Physics Analysis Summary CMS-PAS-HIG-13-005, (2013).
- 679 [19] CMS Collaboration, ““Identifying Hadronically Decaying W Bosons Merged into a Single  
680 Jet””, CMS Physics Analysis Summary CMS-PAS-JME-13-006, (2013).

DRAFT